Investigating the Clinical Utility of Circulating Tumor Cells via Nanomaterial Based Microfluidic Platforms

by

Yang Wang

A dissertation submitted in partial fulfillment
of the requirements for the degree of
Doctorate of Philosophy
(Chemical Engineering)
in the University of Michigan
2017

Doctoral Committee:

Associate Professor Sunitha Nagrath, Chair
Professor Mark A. Burns
Professor Joerg Lahann
Assistant Professor James J. Moon

Yang Wang

wyangela@umich.edu

ORCID iD: 0000-0002-2104-8017

DEDICATION

I dedicate this thesis to my parents Tingming and Li, who have nurtured and loved me unconditionally. They teach me the most fundamental lessons of life since I was little and have supported me to pursue my ambition as I grow up; to my cousins Na and Kehui whose constant encouragement, love and accompany made the journey all the more bearable and enjoyable; to all of my siblings and their families who have brought me unceasing joy throughout the journey; to my advisor Prof. Sunitha Nagrath who has believed in me and mentored me with deep kindness and great patience. She did not give up on me when I got stuck and became frustrated. She offered me great opportunities and support to explore science in ways that really spurred my curiosity and innovativeness.

ACKNOWLEDGEMENTS

Without the help, guidance and collaborative input of a number of individuals, this work would not be possible. Firstly, I acknowledge my advisor Prof. Sunitha Nagrath whose insight, knowledge and unmitigating conviction in the true value of the research we do have been a constant source of energy and inspiration for me. My labmates have also been a tremendous source of encouragement and support to me. Their ingenuity, intellectual curiosity and their remarkable work ethics have shaped and impacted me in many ways. I want to specifically acknowledge Dr. Hyeun Joong Yoon, a past group member who trained me initially, Dr. Tae Hyun Kim and Molly Kozminsky, who are part of the "GO team" with me and closely worked with me on several projects.

I am immensely thankful to my committee members Dr. Mark Burns, Dr. Joerg Lahann, and Dr. James Moon for their valuable feedback and guidance throughout my research. I am deeply grateful to Dr. Kyle Cuneo, Dr. Meredith Morgan, and Dr. Theodore Lawrence for our remarkable collaboration for providing all of the patient samples described in the work and their expertise in pancreatic cancer. Also, I would like to acknowledge Dr. Nithya Ramnath for her immensely useful insights and feedback on the lung cancer project. I am truly grateful to our collaborators Dr. Max Wicha, Dr. Ebrahim Azizi and Shamileh Fouladdel for their help with RNA analysis and their inputs and feedback on cancer biology and molecular analysis. I am thankful to Dr Jinsang Kim and Dr. Apoorv Shanker our collaborations in developing thermal-sensitive polymer-graphene oxide composite for CTC isolation. To the SURE and UROP program and the undergraduate students I mentored, I can't say thank you enough. Additionally,

I am deeply grateful to the experts and staff at the Lurie Nanofabrication Facility (LNF) at the University of Michigan. To the members of OTCC, ICF, and HCC who all made my time at Michigan a happier and more fulfilling experience, I say thank you from the bottom of my heart. I could not have done it without your love and support.

TABLE OF CONTENTS

LIST OF FIGURES

LIST OF TABLES

ABSTRACT

To realize personalized treatment for cancer patients, it is crucial to identify and monitor the molecular drivers of tumors. Currently, the molecular analysis of tumors is mostly performed on tissue biopsies. However, due to the invasiveness of the procedure, biopsies typically cannot be obtained repeatedly during the course of treatment and thus cannot reveal the dynamic evolution of tumors on both the genetic and epigenetic levels. There is a pressing need to monitor tumor evolution and to predict the treatment response to guide the clinical decision-making in the practice of personalized therapy. Circulating tumor cells (CTCs) shed from the primary tumor, travel through the blood, and have the potential to cause metastases. As CTCs can be frequently sampled from peripheral blood, CTC isolation and analysis hold great potential as a biomarker in real-time monitoring of tumor status.

This work highlights the clinical utility of CTCs for providing prognostic and predictive information for specific treatments in cancer patients. First, dynamic changes of PD-L1(+) CTCs during radio(chemo)therapy were investigated in NSCLC. The real-time monitoring of PD-L1 expression in tumor microenvironment is crucial in guiding the therapeutic management of anti-PD-1/PD-L1 immunotherapy. CTCs were isolated using a nanomaterial based microfluidic device, the GO chip. PD-L1 (+) CTCs were detected in 25 out of 36 (69%) samples from 12 NSCLC patients undergoing radiation or radiochemotherapy. After the initiation of radiation, the proportion of PD-L1 (+) CTCs in total CTCs increased significantly (median 4% vs 24%, P=0.018). Furthermore, patients who were PD-L1 positive (5% of CTCs stained with PD-L1) at

baseline had shorter PFS, suggesting the prognostic value of PD-L1 (+) CTCs (6.7 months vs 14.75 months, P = 0.017)

Secondly, CTC number and the molecular features of CTCs were monitored at different time points during the course of treatment for locally advanced pancreatic patients. The reduction of CTC numbers after chemotherapy correlated with shorter progressed free survival (PFS), indicating that changes of CTC numbers may be an early indicator for treatment failure (6.5 months vs 13.5 months, P value= 0.002). Furthermore, in the mRNA profiling of CTCs, the expression levels of three genes that have been shown to play a role in drug resistance, BAX, CHK1 and EZH2, are associated with poor prognosis, which could act as makers to predict and monitor the treatment response.

Thirdly, this work presents two technical advances of CTC technologies. A highly sensitive microfluidic device to capture and release circulating tumor cells from whole blood of cancer patients is developed. Graphene oxide is embeded into a thermoresponsive polymer film to serve as the first step of an antibody functionalization chemistry. As the temperature decreases to around 5 °C, the polymer film dissolves and detaches from the device and captured cells are released. Over 90% capture efficiency and release efficiency have been achieved. Released CTCs were viable and structurally intact, enabling subsequent analysis such as standard clinical cytopathological and genetic testing. Finally, to develop a high throughput CTC isolation technology, a herringbone mixer is incorporated into the previously developed GO chip and optimized the structure of the herringbone mixer and the channel geometry to maximize the

throughput while achieving high capture efficiency (> 80%) and cell viability (> 90%). The time required to process a 1-mL blood sample is reduced to 10 minutes, 6 times faster than in the previous design.

CHAPTER 1

1 Introduction

1.1 Circulating Tumor Cells as 'Liquid Biopsy'

Distant metastases are the cause of about 90% of deaths of cancer patients[1]. Cancer metastasis is an exceedingly complex process, which consists of five sequential steps: (a) Detachment from primary tumor, (b) Invasion into blood circulation, (c) Survival in circulation, (d) Extravasation into distant organs, (e) Proliferation at the secondary site (Figure 1.1). Circulating tumor cells (CTCs) are tumor cells that are shed from the primary tumor and travel through the blood to distant anatomic sites. With the potential to initiate metastases, CTCs provide a unique opportunity to study the biology of tumor metastasis [2]. Moreover, because CTCs can be easily sampled at various time points during the treatment, the isolation and analysis of CTCs provides a strategy for monitoring the molecular features of tumor tissues to provide predictive and prognostic information for the selection of personalized treatment [3].

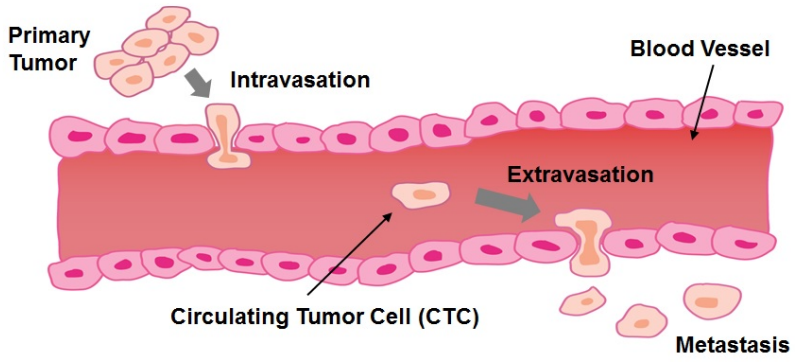

Figure 1.1 Tumor metastasis and circulating tumor cells

1.2 Microfluidic Application in Circulating Tumor Cell Isolation

These circulating tumor cells (CTCs) are incredibly rare and may be present at a frequency as low as one CTC per one billion normal blood cells. Engineers have accelerated the development of technologies that achieve this goal based on exploiting differences between tumor cells and surrounding blood cells such as varying expression patterns of membrane proteins or physical characteristics [4]. Collaboration with biologists and clinicians has allowed additional analysis and will lead to the use of these rare cells to their full potential in the fight against cancer. There have been several macroscale attempts to isolate CTCs based on how they differ from the surrounding blood cells, including the FDA approved CellSearch system [5] and Isolation by Size of Tumor cells [ISET]) platform. However, these technologies suffered from drawbacks such as the low yield and sensitivity, fixation requirements, and high white blood cell (WBC) contamination [6]-[9]. The successful sensitive selection of viable cells was greatly advanced through the introduction of the CTC Chip [10], a microfluidic technology that also marked the entry of engineers into this field. Microfluidic systems offer the advantages of low footprint, small sample volume, low reagent usage, pre-established inexpensive rapid

prototyping methods, diffusion dominated transport, and a length scale on par with cellular systems [11], making them a natural fit for use in CTC research.

Engineers continue to play an integral role in the further optimization of CTC isolation, aiming for increased sample throughput, target cell sensitivity and purity, and viability to ultimately allow the complete interrogation of this useful cell population. As the interest and publication of CTC technologies continues to increase [12], engineers working with teams of clinical collaborators are using varied principles and techniques within microfluidic capture devices (Figure 1.2). Exploitation of expression of cell surface markers, size variation, and other differences have allowed some success and will be covered below, in addition to applications of such devices and potential future directions and challenges.

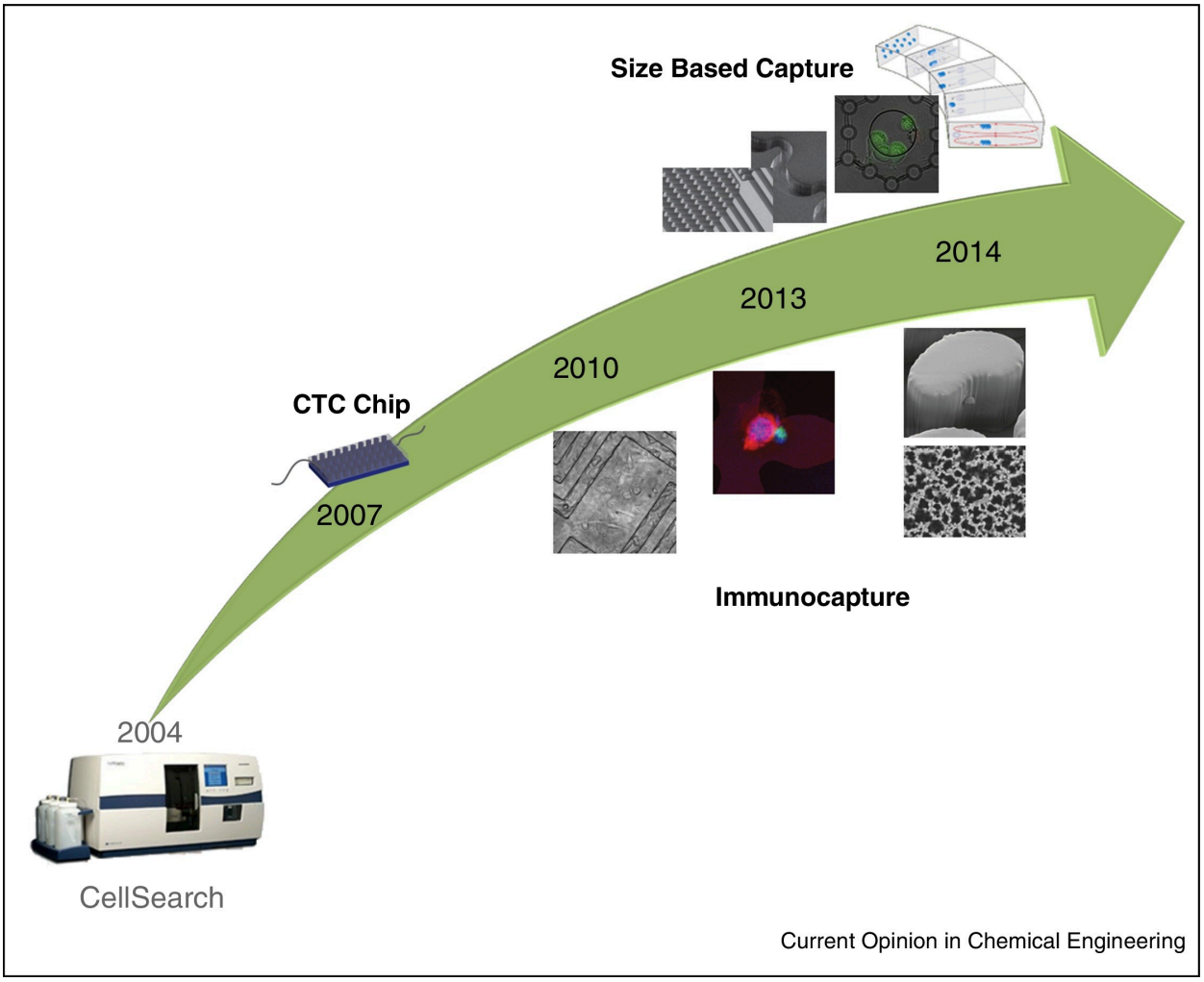

Figure 1.2 Circulating tumor cell (CTC) isolation technologies.
A brief history of CTC isolation technologies beginning with the first FDA approved technique, CellSearch. Microfluidics was introduced in 2007 with the CTC Chip. Subsequent developments have occurred in the areas of immunocapture and size based isolation [4].

1.2.1 Immunocapture of CTCs: a biomarker dependent but highly specific technique

Immunocapture, which is used by CellSearch, the CTC Chip, and many subsequent devices (Figure 1.3), takes advantage of the variety in proteins expressed on the cell membrane of CTCs but not of WBCs, such as the epithelial cellular adhesion molecule (EpCAM), that may be targeted by antibodies against such moieties that are tethered to a surface or feature. The CTC

Chip consisted of 780,000 microposts etched in silicon which were then functionalized with antibodies against EpCAM (anti-EpCAM) and was validated with blood samples from lung, prostate, pancreatic, breast and colon cancer patients. This device viably detected cells in a greater percentage of patients and at lower levels and with higher purity than shown by the CellSearch system. This enabled the molecular characterization of CTCs demonstrating tumor specific genetic alterations present in CTCs [13]. However the need for higher throughput, sensitivity, and the ability to further characterize and study these cells beyond enumeration prompted further developments.

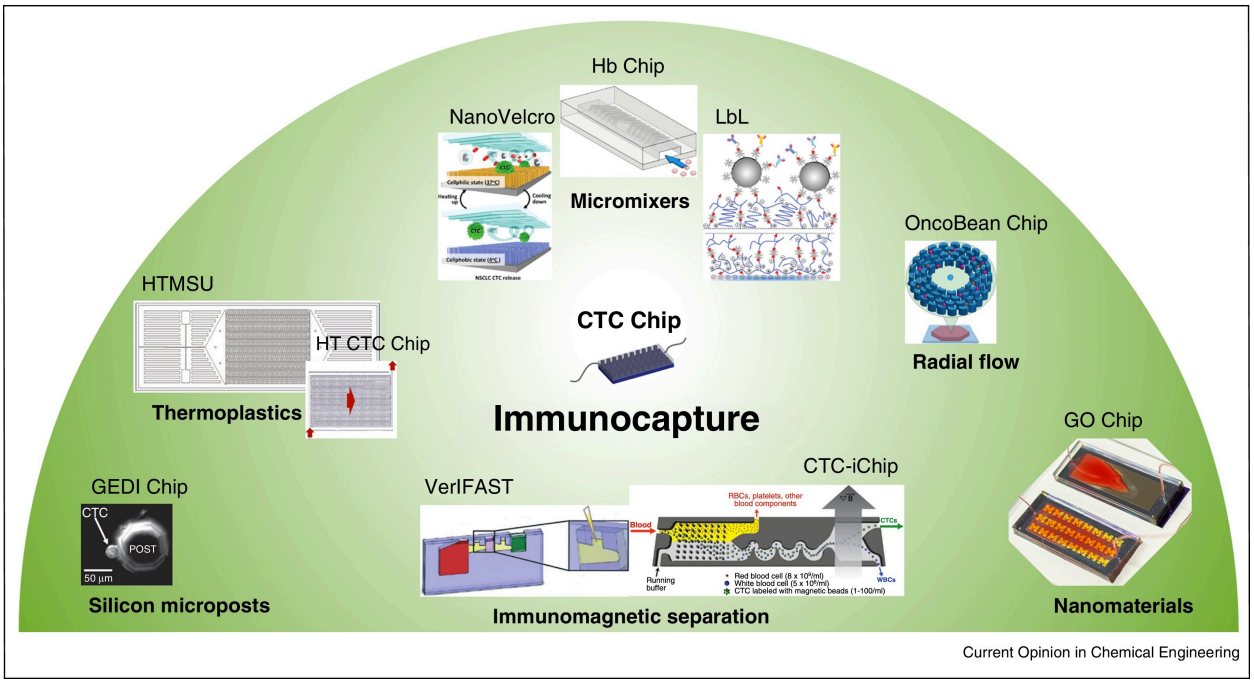

Figure 1.3 Immunocapture methods for microfluidic circulating tumor cell (CTC) isolation. Examples of a number of techniques used to improve metrics such as sensitivity, purity, throughput, and ease of use or fabrication of immunocapture devices include the use of silicon microposts, thermoplastics, micromixers, radial flow, nanomaterials, and immunomagnetic separation [4].

Computational fluid dynamics simulation assisted the redesign of micropost shape and layout in the geometrically enhanced differential immunocapture (GEDI) octagonal micropost

device that has been functionalized with anti-prostate specific membrane antigen (PSMA) [14] or anti-HER2 to target breast and gastric cancers as validated with patient samples [15]. In contrast to micropost devices, high aspect ratio serpentine thermoplastic microchannels maximize collisions between anti-EpCAM functionalized channel walls and CTCs. By using 51 parallel microchannels embossed in polymethylmethacrylate (PMMA), the high throughput microsampling unit (HTMSU) enabled efficient sample processing followed by immediate enumeration of captured CTCs via platinum conductivity sensor [16]. Modifications to the inlet and outlet design as well as the substrate material, now cyclic olefin copolymer (COC), yielded the high-throughput (HT) CTC device [17]. In the NanoVelcro system, cells were released using a thermoresponsive polymer following capture on high surface area silicon nanopillars within a microfluidic chip capped with a chaotic micromixer to increase contact between cells and antibody functionalized surfaces [18].

The chaotic micromixer chamber was first used in the Herringbone (HB) Chip, a follow up to the CTC Chip [19]. Consisting of several parallel functionalized channels in polydimethylsiloxane (PDMS), this device detected CTCs in 14/15 prostate cancer patient samples. Subsequently, the herringbone chamber was integrated with a degradable layer-by-layer (LbL) assembled coating consisting of gelatin and functionalized nanoparticles to increase antibody presentation and allow both single cell and bulk release [20]. Utility was verified with breast and lung patient samples.

Besides multiplexing to increase throughput, a radial flow strategy was used to increase flow rate while decreasing the linear velocity and therefore shear stress exerted on the cells. This OncoBean Chip [20] also featured a redesigned functionalized micropost structure to minimize flow separation, increasing the area on the post utilized in capture.

In contrast to the aforementioned 3D features, the GO Chip incorporated the nanomaterial graphene oxide (GO) for the first time to capture CTCs. GO allowed highly specific and selective capture of CTCs on an effectively 2D surface through a functionalization chemistry that presented the antibody on a high surface area material [21]. The device was verified by capturing CTCs from breast, lung, and pancreatic patient samples.

An alternative to a functionalized surface is magnetic beads functionalized with antibodies that adhere to cells, which may then be separated using an external magnet. In the CTC-iChip, cells in blood samples were magnetically labeled in a preprocessing step, followed by the initial separation of small cells through deterministic lateral displacement (DLD) and alignment by inertial focusing (to be further discussed in 'Size based capture') and ultimate separation through magnetic sorting of the prelabeled cells [23]. In 'positive selection' mode, magnetic beads were functionalized to target CTCs, while in 'negative selection' mode, magnetic beads were functionalized against WBC markers, allowing those cells to be removed, leaving any remaining cells, including EpCAM negative cells, for further analysis. That the cells are not bound to a surface facilitated further study.

Other immunomagnetic systems prioritize ease-of-use. The VerIFAST (Immiscible Filtration Assisted by Surface Tension) system [22] processed small volumes of peripheral mononuclear blood cells that have been prelabeled with functionalized magnetic beads. Using a handheld magnet, labeled cells are then dragged through successive chambers machined in polystyrene that are gated by oil trapezoids to separate CTCs from non-target cells and guide them into a staining well. This allowed for analysis of both blood and mini-bronchoalveolar lavage samples from lung cancer patients.

Immunoaffinity microfluidic separation has turned to a variety of materials and structures to improve in areas where isolation technologies are still lacking. Each device balances added functionality of various features and materials with the associated necessary expertise or increased fabrication logistics and costs. Downstream analysis is hindered when cells remain attached to the capture substrate, although the nascent field of cell release and immunomagnetic capture may counter this. A commonality among these devices is that a specific population is assumed to be the entirety of the target CTC population based on the choice of capture antibody, missing cells in transformations such as the epithelial to mesenchymal transition (EMT). Some of these drawbacks have been addressed through the incorporation of nanomaterials [23]. Another category of CTC isolation techniques prioritizes label free capture and often has the added advantage of high throughput, although this strategy has its own drawbacks.

1.2.2 Size based capture

CTCs also differ from blood cells in size and deformability, offering molecular marker-independent, high-throughput, and inexpensive options for isolation (Figure 1.4). CTCs are generally larger and stiffer than WBCs, leading to the early use of commercial filters [24], [25]. To solve problems with earlier filters including fixation requirements, non-uniform pore sizes, and low pore density, the separable bilayer (SB) microfilter was microfabricated by etching parylene polymer via reactive ion etching to precisely control pore sizes and density [26]. Parylene is ideal for this application because it is mechanically strong while still malleable, with good biocompatibility and low membrane fouling. The bilayer design consisted of a bottom layer with 8 μm pores and a top layer with 40 μm pores, trapping CTCs between the two layers that could be separated easily, leaving CTCs accessible. A flexible micro spring array (FMSA) was designed as a high-porosity filter [27] capable of processing 7.5 mL whole blood without

clogging while still preserving viability. CTCs were detected in 76% of clinical samples from breast, colorectal, and lung cancer patients. Microclusters and multinucleated CTCs were enriched from patients from all three cancers.

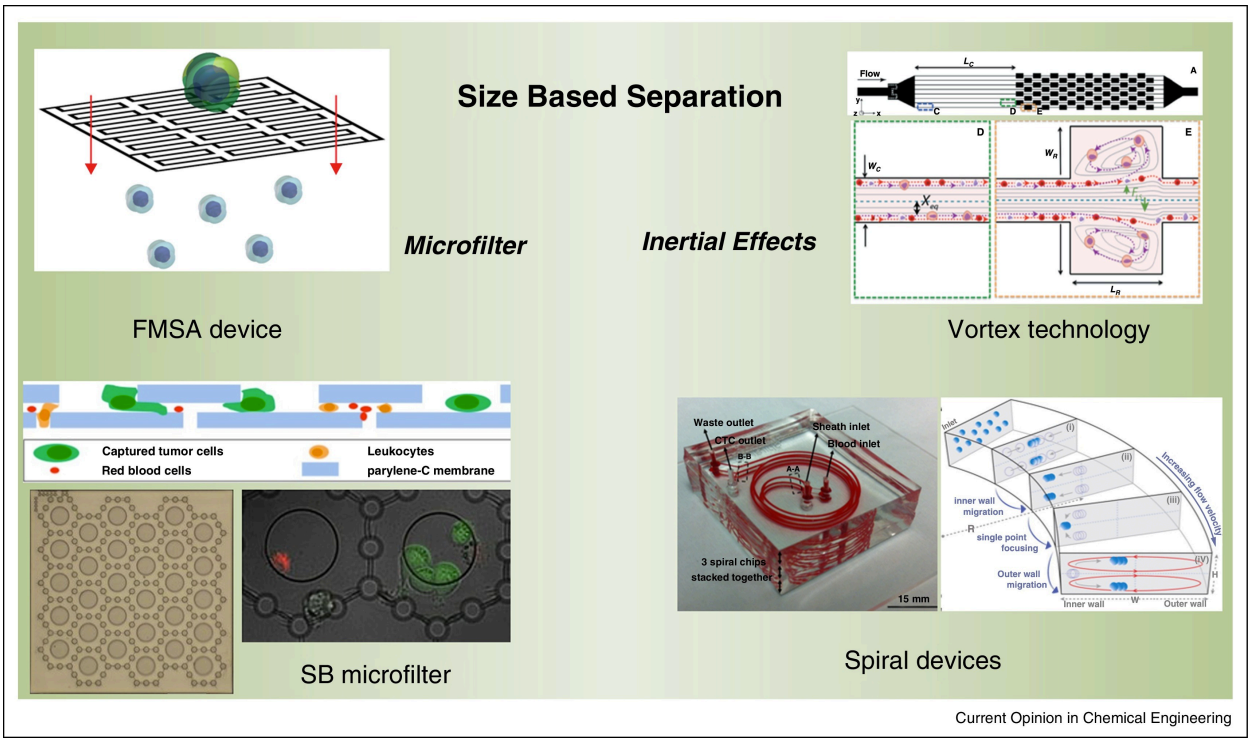

Figure 1.4 Size based technologies for circulating tumor cell (CTC) separation.
On the basis of differences in size between CTCs and white blood cells, microfilters and inertial sorting techniques have been incorporated into microfluidic CTC isolation [4].

An alternative approach to separation exploited unique properties of particles moving in microchannels. Under laminar flow, deterministic lateral displacement (DLD) within an array of microposts has been used to separate particles of different sizes [28]. Depending on the geometry of the microarrays, particles above and below a certain size follow different and predetermined migration paths. The CTC-iChip (also mentioned in the Immunocapture section) utilized DLD to first separate nucleated cells (CTCs and WBCs) from red blood cells (RBCs) using an array of microposts with 32-μm gaps [31]. When flowing through the device, small cells like RBCs

remained along their original streamlines, whereas larger cells like CTCs and most WBCs were fully deflected into the coincident running buffer stream by the end of the array.

Other separation approaches exploited inertial forces. Within microchannels, particles of different sizes can migrate across streamlines to focus at different positions due to the shear induced lift force and the wall induced lift force. In vortex technology, cells of various sizes are aligned by size in different streamlines in straight channels by inertial focusing followed by multiple expansion-contraction reservoirs to create laminar microvortices that can trap large cells within reservoirs [29]. As cells entered the expanding regions, wall lift forces were diminished and cells mainly experienced lateral lift forces, which are proportional to the cell volume. The larger lift forces on CTCs pulled them into the vortices while other blood cells experiencing smaller forces passed through the vortex and remained in the main stream.

Curvature in microchannels causes particles to experience an additional lateral Dean drag force because fluids in curved channels develop a secondary lateral flow. The combination of the inertial lift force and the Dean force leads to particle migration which can result in high resolution separation. Single spiral, double spiral, cascaded spiral, and slanted spiral structures have been designed and optimized to maximize separation efficiency for various parameters including channel length, height, width, radius of curvature, and flow rate [29]-[33] . Generally, near the outlet of spiral devices, larger CTCs focus near the inner wall due to the combination of the inertial lift force and the Dean drag force. To this end, Hou *et al.* designed a multiplexed spiral device that detected CTCs in clinical samples from breast and lung cancer patients [34].

CTC enrichment by size offers a fast, inexpensive, and label-free way to harvest CTCs. However, as there is a wide range of CTCs sizes, sized based separation often suffers from low purity and the risk of losing smaller CTCs. Additionally, size based separation often requires

preprocessing of blood, like RBCs removal and further, dilution or runs the risk of device clogging. To date, size based technologies have shown proof-of-concept clinical validation but have not been applied in large scale clinical or biological investigation.

Other separation methods based on physical properties include the interplay of dielectrophoresis (DEP) forces and inertial forces in microfluidic devices to lead to different patterns of cell migration to viably separate cells [35]. Similarly, acoustophoresis causes particles within the fluid to move toward regions with minimal acoustic radiation forces in distinct migration patterns [36], [37]. Although promising, approaches like DEP and acoustophoresis have the disadvantages of low throughput, low sensitivity and purity, and additional required steps like RBC lysis and may require further clinical validation.

1.3 The biology of circulating tumor cells

1.3.1 Epithelial–mesenchymal transition

Occurrence of the epithelial-to-mesenchymal transition (EMT) process is observed in various types of human cancer and may play an important role in tumor metastasis and resistance to standard treatment [38]. During EMT, epithelial cells lose cell-cell contacts and their apical–basal polarity and become spindle-shaped mesenchymal cells. These changes lead to the detachment of tumor cells from the extracellular matrix (ECM) and increase their ability to invade into the surrounding stroma and intravasate into the bloodstream, initiating the metastatic process [39].

The functions of EMT may vary greatly depending on the cancer types. In squamous cell carcinoma, EMT driven by the activation of Akt is associated with enhanced motility and invasiveness [40]. In pancreatic cancer, EMT induces chemoresistance but has little effect on

increasing invasiveness or metastasis [41]. In breast cancer, Mani et al. observed that after the induction of EMT, cells acquire stem cell properties such as self-renewal [42].

At the molecular level, the expressions of many epithelial junction proteins such as E-Cadherin and α-catenin are down-regulated or lost during EMT [43], [44]. Furthermore, intermediate filaments are rearranged, typically switching from cytokeratins to vimentin. EMT can be induced by both intrinsic and extrinsic factors including multiple transcription factors (e.g. Snail, Twist, Slug, ZEB1, FOXC2), growth factors (e.g. epidermal growth factor (EGF), transforming growth factor β (TGF-β)), and small non-coding RNAs (micro-RNAs, e.g. miR-200 or miR-155). Several signaling pathways play an important role during EMT, e.g. Ras/MAPK, PI3 K/Akt/GSK, and Wnt/β-catenin.

The loss of epithelial markers (e.g. E-Cadherin), the up-regulation of mesenchymal markers (e.g. Vimentin and N-Cadherin) and the activation of EMT regulator (e.g. Snail, Twist, Slug and ZEB1) have been use to characterize EMT process in cancer cells [38]. Molecular analysis of tumor specimens revealed that the expression of EMT markers have emerged as independent prognostic markers in various cancer types such as breast cancer [45], lung cancer [46], gastric cancer [45], and oral squamous cell carcinoma [50].

The analysis of EMT markers in CTCs is another exciting research area. CTCs undergoing EMT may not be captured by many CTC isolation assays relying on the expression of epithelial marker like EpCAM. This could be resolved by applying a cocktail of antibodies targeting both epithelial and mesenchymal markers or by using physical property based separation. These approaches identified a population of mesenchymal like CTCs in various cancer types such as breast, lung, and prostate cancer [47]-[50]. In these studies, the expression of EMT markers in CTCs was found to be heterogeneous and CTCs were classified into different

subgroups using EMT markers, including epithelial CTCs, intermediate CTCs and mesenchymal CTCs.

The expression of EMT markers in CTCs could undergo dynamic changes throughout the treatment course. Yu et al studied the changes of EMT characteristics of CTCs after chemotherapy using RNA–in situ hybridization (ISH) assay among breast cancer patients [51]. Using a panel of epithelial and mesenchymal genes they identified a spectrum of CTCs ranging from exclusively epithelial to intermediate and exclusively mesenchymal. The comparison of CTC features in samples before and after chemotherapy showed that the increase of mesenchymal like CTCs after treatment were associated with disease progression. After analyzing CTCs by RNA sequencing, the authors reported that 170 transcripts were enriched in CTCs captured at a mesenchymal predominant time point, and suggested that aberrant expression of FOXC1, along with TGF-β activation, may be a contributor to EMT in human breast cancer. This result suggested that the expression of EMT markers in CTCs could be used as a potential biomarker of therapeutic resistance and cancer progression. Furthermore, studying the mechanism of EMT regulation in CTCs could bring insights into developing potential drug targets for cancer treatment.

1.3.2 Circulating tumor microemboli

Circulating tumor microemboli (CTM), or CTC cluster, are clusters formed by more than two CTCs. In addition, CTCs have been observed to associate with leukocytes, platelets, and stromal cells such as fibroblasts to form clusters [52], [53]. CTM have been detected by various CTC technologies in different cancer types such as breast, lung, prostate, and pancreatic cancer [54]-[56]. The presence of CTM is associated with poor prognosis in pancreatic and small cell lung cancer [57], [58]. Change et al demonstrated that in pancreatic cancer patients CTM were

abundantly present in 81% of patients and that the number of CTM is an independent prognostic marker of overall survival (OS) and progression free survival (PFS) [57].

CTC clusters have been proposed to have higher metastatic potential compared to single CTCs [56]. Possible explanations for this phenomenon include resistance to anoikis, presence of stromal cells providing a permissive microenvironment and presence of blood cells for immune escape [59].

Cells generally undergo apoptosis after they lose contact with neighboring cells or with extracellular matrix (ECM), in a process named 'anoikis'. The ability to resist anoikis is essential for CTCs to initiate cancer metastases. The avoidance of anoikis can be attributed to the cell junctions preserved by CTMs [56]. In metastatic breast cancer, the expression level of cell–cell junction marker plakoglobin in CTM is found to have a 200-fold increase than that of single CTC [56]. Plakoglobin knockdown triggered the dissociation of CTM and resulted in a reduced number of lung metastases in mouse models. Therefore, while epithelial tumor cells that are shed into the blood circulation and lose cell-cell contact generally undergo anoikis, CTMs still preserve some level of cell junction and could survive in the circulation.

Several blood cell types, such as platelets, leukocytes, and myeloid-derived suppressor cells (MDSC), have been proposed to shield tumor cells escape from immune surveillance, facilitating the formation of distant metastases [60]-[62]. Additionally, platelets adhere to CTCs has been shown to induce EMT activation in tumor cells and promote metastasis. Bastid et al suggested that CTCs can enter the vasculature as epithelial tumor cells and upon stimulation by platelets-derived TGF-β can change into mesenchymal tumor cells [63]. This work showed that the co-culture with platelets resulted in an increased number of metastatic foci generated by

tumor cells injected into the tail-vein of the examined mice. In contrast, selective knock-out of TGF-β in platelets and megakaryocytes led to the reduction of metastatic events.

The effect of stromal cell presence in CTM has been studied in mouse models [64]. It is demonstrated that CTCs can attach to cancer-associated fibroblast (CAF), which results in higher viability of cancer cells in circulation and the increased early growth of metastatic colonies in lung. By bringing its own soil (stromal cells), tumor cells can gain a favorable traveling and seeding niche to form metastatic colonies.

1.4 Clinical use of CTCs — non–small-cell lung cancer (NSCLC)

Lung cancer is the leading cause of cancer-related death in US and worldwide, with non–small-cell lung cancer (NSCLC) accounting for more than 80% of those cases[65]. CTC analysis provides opportunities in early diagnosis, prognosis, evaluation of curative efficacy, and molecular analysis of lung cancer for targeted therapies [66], [67].

1.4.1 CTCs as prognostic and predictive markers

Many studies have shown that the presence of CTCs is associated with shorter PFS or OS time using different technologies and thresholds. Krebs et al used CellSearch Assay to isolate CTCs from 101 untreated stage III/IV NSCLC patients. Stage IV patients were found to have higher CTC counts than stage III patients. Patients with >5 CTCs at baseline had shorter PFS (2.4 vs. 6.8 months) and OS (4.3 vs. 8.1 months) than those with <5 CTCs at baseline ($P<0.001$). Additionally, CTCs were measured after one cycle of chemotherapy, and the reductions of CTCs after chemotherapy were associated with improved PFS (5.4 vs. 1.9 months; $P < 0.001$) and OS (8.3 vs. 3.3 months; $P < 0.009$). Using another CTC isolation technology ISET, Hofman et al identified CTCs in 49%(102 out of 208) of patients by morphological examination [68]. The

presence of 50 or more CTCs was associated with worse disease free survival (DFS) for both early-stage I + II- and later-stage III + IV-resectable NSCLCs (P = 0.05, and P < 0.0001, respectively).

To compare these two commercialized CTC isolation methods, Hofman et al conducted another study isolating CTCs by the CellSearch Assay™ and by ISET from 210 patients undergoing radical surgery for NSCLC [68]. CTCs were detected in 104 of 210 (50%) and 82 of 210 (39%) patients using ISET and CellSearch, respectively. Patients with CTCs detected by CellSearch alone or by ISET alone had worse DFS than patients without CTCs ($p < 0.0001$). However, no correlation between the presence of CTCs and disease stage, or other clinicopathologic parameters was observed in this study.

CTCs are typically isolated from peripheral blood of cancer patients. To increase the likelihood of CTC enrichment, Hashimoto et al. sampled pulmonary vein (PV) blood to isolate CTCs from in patients undergoing surgery. CTCs were more frequently observed in PV blood than in peripheral blood (73.3% vs 6.7%). Interestingly, CTC number increased significantly after surgical manipulation and the increase of CTCs in PV blood was significantly associated with lymphatic invasion (P = 0.043). Another phenomenon observed in PV blood by Funaki et al was the presence of CTC clusters (present in 33% of the patients) . The existence of CTC clusters was correlated to worse disease-free survival rate (P<0.001). This is consistent with other reports about the prognostic value of CTC clusters [57], [58], [69].

The predictive value of CTCs for assessing treatment response was examined by a study investigating the correlation between CTC enumeration and radiographic appearance [70]. Treatment response to chemotherapy agents is generally assessed by comparing baseline and post-treatment positron emission tomographic (PET) imaging and computed tomographic

(CT) scans. Punnoose et al correlated the changes in CTC levels with CT scans, which is evaluated via Response Evaluation Criteria in Solid Tumors (RECIST), and fluorodeoxyglucose-PET (FDG-PET) imaging. The authors showed that patients with partial or complete responses tend to have higher baseline CTC counts than patients with stable disease or progressive disease. Meanwhile, the reductions of CTC counts after chemotherapy were associated with FDG-PET and RECIST response ($P = 0.014$ and $P = 0.019$) and longer PFS ($P = 0.050$), suggesting that monitoring of the changes in CTC numbers could be used as an early indication of response. Similarly, additional studies showed that the decreases in CTC number were associated with shorter PFS and OS, indicating that CTCs could be used as surrogate biomarker for evaluating the effectiveness of chemotherapy [71], [72].

1.4.2 CTCs as a biomarker for early detection and diagnosis

Because of the low cost and the minimal invasiveness of CTC isolation, CTCs have the potential to offer a cost efficient way to screen patients with a high risk of lung cancer. Ilie et al examined the presence of CTCs among 168 patients with Chronic obstructive pulmonary disease (COPD)[73]. Within 1 to 4 years after CTC detection, the 5 CTC-positive patients were detected with lung nodules by CT scan, which led to prompt surgical resection and the diagnosis of early-stage lung cancer. This result indicated that CTCs could be used to monitor COPD patients for the early detection of lung cancer.

To study the diagnostic value of CTCs, Fiorelli et al conducted a study using CTCs to differentiate benign from malignant lung lesions [74]. Malignant circulating cells (their term for CTCs) were detected in 54 of 60 (90%) malignant patients and in 1 of 17 (5%) benign patients whereas benign circulating cells were detected in 1 of 60 (1%) malignant patients and in 15 of 17 (88%) benign patients. CTCs shared morphological features similar to those of the corresponding

primary tumor and lead to the same histologic diagnosis in 72% cases. Although promising, the early detection and diagnosis of CTCs still need to be validated in large-scale clinical studies. However, the low abundance of CTCs present in early stage cancer may hinder the detection rate, thus more sensitive technologies are needed to allow the advances in this area.

1.4.3 CTCs as a biomarker for early detection and diagnosis markers

Due to the low cost and the minimal invasiveness of CTC isolation, CTCs have the potential to offer a cost efficient way to screen patients with high risk of lung cancer. Ilie et al examined the presence of CTCs among 168 patients with Chronic obstructive pulmonary disease (COPD) [73]. Within 1 to 4 years after CTC detection, the 5 CTC-positive patients were detected with lung nodules by CT scan, which leads to prompt surgical resection and the diagnosis of early-stage lung cancer. This result indicated that CTCs could be used to monitor in COPD patients for the early detection of lung cancer.

To study the diagnostic value of CTCs, Fiorelli et al conducted a study to use CTCs to differentiate benign from malignant lung lesions [74]. Malignant circulating cells *or CTCs* were detected in 54 of 60 (90%) malignant patients and in 1 of 17 (5%) benign patients whereas benign circulating cells *CTCs* were detected in 1 of 60 (1%) malignant patients and in 15 of 17 (88%) benign patients. CTCs shared similar morphological features and lead to the same histologic diagnosis of the corresponding primary tumor in 72% cases. Although promising, the early detection and diagnosis of CTCs still need to be validated in large scale clinical studies. Besides, the low abundance of CTCs present in early stage cancer may hinder the detection rate and thus more sensitive technologies are needed to allow the advances in this area.

1.4.4 CTCs used for the molecular analysis in targeted therapy

Nearly two thirds of the patients with advanced lung cancer acquire at least one of the recognized “driver mutations”, which are specific gene mutations that are involved in driving the development of lung cancer [75]. The most common driver mutations are mutations in epidermal growth factor receptor (EGFR) and the rearrangement of ALK gene. Other genomic aberrations such as HER2, KRAS, PIK3CA, AKT and BRAF mutation and amplification have also been extensively studied. The development of targeted agents, such as EGFR inhibitors and ALK inhibitors has changed paradigms of management of patients with these mutations. Biopsies may not provide enough samples for mutation analysis at the time of diagnosis and cannot be sampled frequently during treatment. Thus CTCs may provide an additional way of assessing and monitoring the tumor genotypes.

Maheswaran et al conducted the first study to monitor EGFR mutations in CTCs isolated by CTC chip during targeted therapy among metastatic NSCLC patients [76]. EGFR mutation was detected in CTCs from 11 of 12 patients (92%). Furthermore, the emergence of a treatment resistance mutation, T790M, was found in CTCs samples during the treatment and was associated with tumor progression. These findings indicated that CTCs could monitor the mutation status of tumor tissue and might predict the treatment outcomes. Using an RT-PCR assay, Breitenbuecher et al. were able to detect EGFR mutations in CTCs among all 8 EGFR mutant patients [77]. After following the patients through the treatment, they demonstrated that patients without *EGFR*-mutant CTCs during treatment were more likely to respond to therapy than those with persisting EGFR-mutant CTCs.

Several other studies have investigated the detection of ALK rearrangement in CTCs. Pailler et al examined the ALK status in CTCs via a filtration enrichment technique and filter-adapted fluorescent in situ hybridization (FA-FISH) [78]. All ALK-positive patients had four or

more ALK-rearranged CTCs per 1 mL of blood whereas no or one ALK-rearranged CTC was detected in ALK-negative patients. Furthermore, they detected the changes of ALK-rearranged CTC levels in patients being treated with a tyrosine kinase inhibitor of ALK, crizotinib. Similar results are reported in a study using a microfluidic platform, NanoVelcro chip[79]. The ALK status detected in CTCs accurately matched the status of tumor samples when applying a cutoff of 3 ALK-rearranged CTCs. Overall, these studies using different isolation technologies suggested that CTCs could be used for ALK-gene status pre-screening on a routine basis for patients with lung cancer and open new opportunities for real-time monitoring of targeted therapies.

1.5 Clinical use of CTCs — Pancreatic cancer

1.5.1 CTCs as a biomarker for diagnosis and staging

Pancreatic cancer is a very aggressive cancer type; the five year survival rate is only 8% [80]. It is usually diagnosed at an advanced stage and is resistant to treatment. Even when patients are diagnosed with small primary tumors (<2 cm) and have no clinical evidence of metastatic disease, 5-year survival after surgery is less than 18% because of metastatic disease [81]. More interestingly, some patients undergoing surgery for chronic pancreatitis will develop disseminated pancreatic adenocarcinoma (PDAC), although only precancerous lesions of pancreas, but no tumors, are found locally [82]. These observations suggest that tumor dissemination may occur before the formation of large primary tumors or the diagnosis of the tumor.

Rhim et al showed that circulating pancreatic cells were detected in liver before the formation of pancreatic tumor in a lineage-labeled genetic model of pancreatic cancer,

suggesting that metastatic seeding could occur before tumor formation[83]. To validate this finding in a clinical setting, Rhim et al reported that more than 3 circulating pancreas epithelial cells/mL were detected via GEDI chip in 7 of 21 (33%) patients with cystic lesions and no clinical diagnosis of cancer [84]. This result indicates that circulating pancreas epithelial cells could be useful as a biomarker for risk assessment in patients with high risk of pancreatic cancer or even for early detection of pancreatic cancer.

Clinical staging of pancreatic cancer based on multi-section CT or MRI imaging may not be sensitive enough to detect small-volume metastatic lesion, which causes under-staging. Approximately 80% of patients who undergo successful surgery will experience metastatic recurrence, indicating that distant metastases may be present at the time of surgery [85]. In these cases, surgery may not be the proper initial treatment. Thus a biomarker that could improve the accuracy of staging is needed to assist the selection of frontline therapy. Ankeny et al processed blood samples from 100 pancreatic cancer patients using the microfluidic NanoVelcro CTC chip and demonstrated that a cut off of ≥ 3 CTC in 4 ml blood could discriminate between local/regional and metastatic disease [86]. In addition, they performed mutational analysis of KRAS codon 12 in CTCs and achieved 100% concordance of KRAS mutation subtype between CTCs and primary tumor tissue in five patients tested. This study showed that CTCs could be used as an adjunct biomarker for molecular diagnosis and staging of PDAC at the time of disease presentation.

1.5.2 CTCs as a biomarker for prognosis

Han et al conducted a meta-analysis to evaluate the prognostic value of CTCs in pancreatic cancer [87]. In this meta- analysis, nine cohort studies were included with a total of 623 pancreatic cancer patients consisting of 268 CTC-positive patients and 355 CTC- negative

patients. Four studies used CellSearch technology to enumerate CTCs while the other four studies use RT-PCR to detect the expression of CTC specific genes. The meta-analysis revealed that patients in the CTC-positive group were significantly associated with poor progression-free survival (PFS) and overall survival (OS) ($P<0.001$, $P<0.001$) [87].

Furthermore, as most cancer deaths are associated with metastases and CTCs can potentially initiate metastatic spread, CTCs can be used to identify specific genes to serve as prognostic markers in patients with pancreatic cancer. Sergeant et al studied the gene-expression profiles of CTCs isolated by FACS-based negative depletion among patients who underwent surgery for PDAC [92]. Based gene expression analysis and pathway analysis, they developed a CTC gene signature consisting of TGF-β1 involved in the p38 MAPK pathway and 9 other genes associated with both p38 MAPK signaling and cell motility. They validated the prognostic value of this CTC gene signature in 78 primary tumor tissue samples and revealed that high co-expression of TGF-β1 and the cell motility panel in primary pancreatic cancer was an independent predictor of disease-free (DFS) and overall survival (OS) ($p=0.041$, $p=0.047$).

Recently, the prognostic value of CTM in pancreatic cancer was investigated by Chang et al [57]. They detected CTM in 81% (51 of 63) of patients with mean (SD) 29.7 (1101.4). With a cutoff of 30 CTMs per 2 ml, patients are categorized into favorable and unfavorable CTM group. Compared to the favorable CTM group, the unfavorable CTM group had much shorter PFS (2.7 vs 12.1 months; $P <0.0001$) and OS (6.4 vs 19.8 months; $P <0.0001$).

CHAPTER 2

2 Monitoring Dynamic Changes of PD-L1 (+) CTCs in Non-Small Cell Lung Cancer During Radio(chemo)therapy

2.1 Abstract

The development of immune checkpoint inhibitors such as anti-PD-1/PD-L1 marks a new era in treating cancer with immunotherapies. Preclinical studies demonstrated that radiation up-regulates PD-L1 expression in tumor cells, which provides the primary rationale for combining PD-1/PD-L1 inhibitors with radiation. These results haven't been validated among non-small cell lung cancer (NSCLC) patients because it is difficult to obtain serial biopsy samples to monitor the PD-L1 expression in NSCLC. Measuring the PD-L1 expression of circulating tumor cells (CTCs), which could be sampled repeatedly with minimal invasiveness, enables the real-time monitoring of immune activation in tumor. Using a nanomaterial based microfluidic device (the GO chip), we obtained serial blood samples from 12 non-metastatic NSCLC patients undergoing radiation or radiochemotherapy. CTCs were detected in all 36 samples with the average of 20.8 CTCs/ml (range 4-72) and PD-L1 (+) CTCs were detected in 24/36 samples (66.7%) with an average number of 4.7/ml (range 0-43). After the initiation of radiation, the proportion of PD-L1 (+) CTCs among total CTCs increased significantly (median 0.7% vs 24.7%, $P < 0.01$), indicating the upregulation of PD-L1 expression in tumor cells during radiation. In addition,

patients who were PD-L1 positive (5% of CTCs stained positive for PD-L1) at baseline had shorter PFS time (6.7 months vs 14.75 months, $P < 0.05$), while the total CTC number is not associated with poor prognosis. The mRNA levels of PD-L1 were significantly higher in the samples from patients with poor prognosis (PFS < 9 months) than in those from good prognosis patients (PFS > 9 months). Therefore, PD-L1 expression in CTCs may have prognostic value and may serve as a biomarker to monitor tumor immunity among non-metastatic NSCLC patients.

2.2 Introduction

Lung cancer is the leading cause of cancer-related death in the US and worldwide, with non–small cell lung cancer (NSCLC) accounting for over 80% of those cases [65], [80]. Non-metastatic NSCLC patients who are medically inoperable or unresectable are generally offered radiotherapy with or without concurrent chemotherapy which yields 5-year overall survival rates ranging from 10–35% [88]-[90]. New treatment options are urgently needed for these patients.

Recent development in checkpoint immunotherapy draws the beginning of a new era in NSCLC treatment. Programmed death 1 (PD-1) receptor and its ligand (PD-L1) are key checkpoint molecules for regulating antitumor immune responses [91]. The binding of PD-L1 to PD-1 can inhibit T cell function and proliferation and result in immune tolerance. As PD-L1 expression has been found in various tumors including NSCLC [92], the blockage of PD-1/PD-L1 has emerged as a new therapeutic approach that can restore the antitumor immunity.

Exciting results from clinical trials of PD-1/PD-L1 inhibitors have shown improved overall survival with low toxicity among NSCLC patients [93]-[95]. Based on data from the recent phase 3 trial, the PD-1 inhibitor pembrolizumab was approved by the US Food and Drug Administration (FDA) for the first-line treatment of metastatic NSCLC whose tumors have 50 percent or more PD-L1 expression with no EGFR or ALK genomic tumor aberration [96]. To

further improve the response rate and duration and to extend the benefit to additional patients, the idea of combining anti–PD-1/PD-L1 therapies with radiation or radiochemotherapy has been proposed and tested in clinical trials among non-metastatic NSCLC patients [97]-[99]. Growing evidence demonstrates that radiation can elicit adaptive immune response, but this immunogenic effect of radiation could be undermined by the upregulation of PD-L1 in tumor microenvironment. This provides the primary rationale for combining PD-1/PD-L1 inhibitors with radiation [100], [101]. However, the upregulation of PD-L1 expression during radiation has not been validated among NSCLC patients because it is difficult to obtain serial biopsy samples to monitor the PD-L1 expression in solid tumors due to the invasiveness of biopsies.

Alternately, isolation of circulating tumor cells (CTCs), as a mean of liquid biopsy, provides a minimally invasive method to repeatedly sample tumor cells from the patient's blood and to monitor PDL-1 expression on tumor cells over time. The potential of CTCs as a prognostic and surrogate biomarker for NSCLC has been investigated using the FDA approved CellSearch System [67], [70], [72], [102]. However, due to the low detection sensitivity of this assay, the CellSearch system has been reported to undercount CTCs and has a limited ability to detect CTCs in non-metastatic NSCLC patients, which largely limits its clinical utility [71].

Microfluidic based CTC isolation technologies have emerged as an approach to capture CTCs with high sensitivity and have demonstrated the capacity to characterize the molecular traits of tumors, such as EGFR mutations [4], [13], [22], [67], [79]. Previously we developed a nanomaterial based microfluidic platform for CTC isolation, the GO chip, which consists of a microfluidic chamber and a substrate coated with graphene oxide (GO) nanosheets where the antibodies are tethered [21]. This technology takes advantage of the increased surface area

afforded by graphene oxide to achieve higher antibody coating density, and thus improved sensitivity for CTC capture.

In this study, to investigate whether radiation therapy can increase PD-L1 expression in CTCs, we monitored the dynamic changes of PD-L1 expression in CTCs via the GO chip among 12 non-metastatic NSCLC patients who received radiation alone or with concurrent chemotherapy (Figure 2.1). Furthermore, we evaluated whether PD-L1 (+) CTC counts and PD-L1 mRNA expression level have correlation with disease progression.

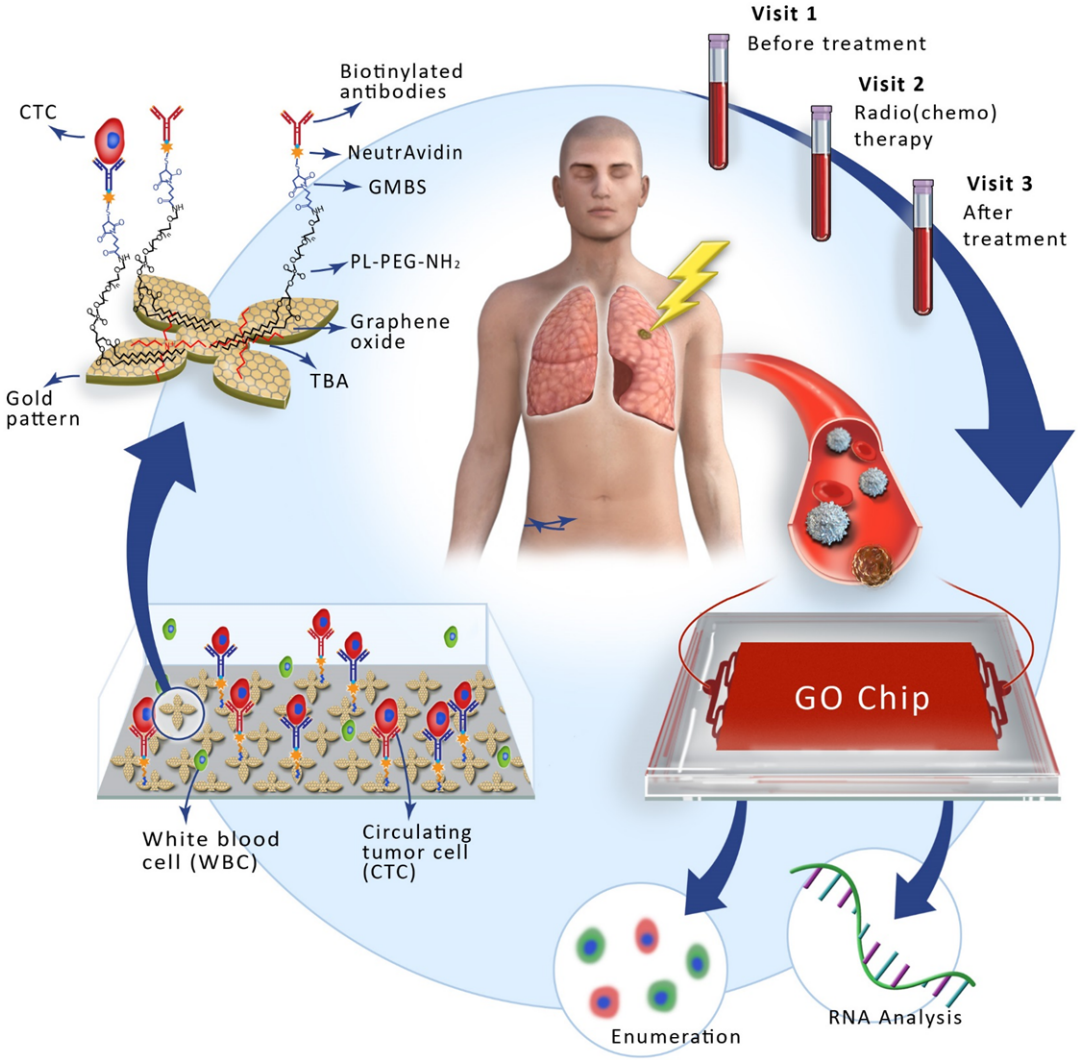

Figure 2.1 An overview of this study
An overview of this study, with sample collection and circulating tumor cell (CTC) isolation before treatment, during treatment and months after treatment (follow up). The GO chip configuration and work mechanism is also shown by the schematic representations of CTC isolation within the microfluidic chamber and of antibody conjugation chemistry.

2.3 Materials and Methods

2.3.1 GO Chip production and surface functionalization

The GO Chip is made of a gold patterned silicon substrate and a PDMS top layer. Chips were fabricated and functionalized as previously described [21]. In brief, PDMS top layer was fabricated using standard soft lithography. Master molds were fabricated using SU8-2025

photoresist (Microchem Corp.). A 10:1 ratio of polydimethylsiloxane (PDMS) polymer to curing agent (Dow-Corning) was well mixed and de-bubbled prior to pouring over the SU8 molds. After curing at 65^0C for over 6 hours, PDMS were manually cut from the mold, trimmed to size, and inlet/outlet holes were punched. Cr and Au films were deposited onto a silicon oxide coated silicon wafer by evaporation and were patterned by conventional photolithography. Patterned silicon substrates were dipped in a GO suspension for 10 minutes and rinsed with DI water and isopropanol. Then a silicon substrate and a PDMS chamber were bonded by corona discharge treatment to form a microfluidic chamber. The device was infused with N-γ-maleimidobutyryl-oxysuccinimide ester (GMBS) in ethanol. After 30-minute incubation, the excess GMBS solution was washed out by ethanol. NeutrAvidin in phosphate buffered saline (PBS, Gibco) was flowed through the chip and incubated for 50 minutes. Afterwards, the excess NeutrAvidin was washed out by PBS. A biotinylated antibody cocktail (anti-EpCAM, anti-CD133 and anti-EGFR at a concentration of 10μg/mL) was flowed through the chip and incubated for 30 minutes. After washing with PBS, 3% bovine serum albumin (BSA, Sigma-Aldrich) blocking solution was injected and incubated for 30 minutes.

2.3.2 Cell preparation

Cell culture reagents were purchased from ThermoFisher Scientific unless otherwise specified. H1440 (provided by David Beer lab) and H1650 cells (purchased??) were cultured in RPMI medium containing 10% fetal bovine serum and 1% penicillin–streptomycin solution. When cells reached 70–80% confluence, they were collected. To perform the capture efficiency experiments, cells were labeled with a green cell tracking dye (Invitrogen, CellTracker Green CMFDA, C7025).

2.3.3 Human Blood Sample Collection and Processing

Blood samples were drawn from NSCLC patients and healthy donors after obtaining informed consent under an IRB-approved protocol. All samples were collected in EDTA tubes and were processed within 3 hours. 1 ml blood was flowed through each device at 1 mL/hr by a syringe pump. After flowing blood, the captured cells were washed with PBS, fixed with 4% paraformaldehyde (PFA), and stored at 4°C until immunofluorescent staining.

2.3.4 Immunofluorescence Staining of Isolated CTCs

Cells were permeabilized with 0.2% Triton-X (Sigma-Aldrich) and incubated for 30 min followed by a PBS wash. The device was incubated for 30 min with blocking buffer containing 2% normal goat serum and 3% BSA. Anti-cytokeratin(Pan) (Bio Rad), anti-CD45 (Bio Rad) and anti-PD-L1 (BioLegend) were antibodies were flowed through the graphene oxide chip, incubated for 1 h, and washed with PBS. Anti-cytokeratin(Pan), anti-CD45 and anti-PD-L1 were probed respectively with Alexa Fluor 546 IgG1 (Invitrogen), Alexa Fluor 488 IgG2a (Invitrogen), and Alexa Fluor 647 IgG2b (Invitrogen). These secondary antibodies were flowed through the graphene oxide chip, incubated for 1 h, and washed with PBS. To stain the nuclei of the captured cells, DAPI (4',6-Diamidino-2-Phenylindole, Dihydrochloride) (Invitrogen) was flowed through the device. The device was incubated for 15 min and washed with PBS. The device was imaged using Nikon Eclipse Ti fluorescence microscope.

2.3.5 RNA extraction and RT-qPCR

Arcturus PicoPure RNA Extraction buffer (Life Technologies) was flowed through the chip to lyse the captured cells immediately after PBS wash. After incubation at 42 °C for 30 min,

the device was washed with water and the effluent were collected. The effluents, which were the total RNA samples, were stored at -80 °C until cDNA preparation. The cDNAs were synthesized from the total RNA samples and then pre-amplified for the selected 96 genes using the corresponding pool of 96 TaqMan gene expression assays (Life technologies). The expression patterns of preamplified cDNAs for each sample were determined by qPCR using the same TaqMan gene expression assays and the BioMark HD system (Fluidigm).

2.3.6 Statistical analysis

Paired sample test the CTC counts and the proportion of PD-L1 (+) CTCs between different visits was compared by the Wilcoxon rank sum test using paired observations. The Wilcoxon rank sum test was done between the patients with disease progression and those with stable disease on the number of PD-L1 (+) CTCs. Differences were considered significant, if p value was less than 0.05. To analyze expression levels of selected genes between different patient groups, each transcript was normalized to the average of three house-keeping genes (HKGs: GAPDH, ACTB, and UBB), and reported as $-\Delta C_T$, where $\Delta C_T = C_{T\ gene} - C_{T\ (HKGs)}$. The Ct values equal or above 35 was considered as no expression [104]. All data analysis was performed using R software.

2.4 Results

2.4.1 Isolation of lung cancer cells from model blood samples

The performance of the GO chip for CTC isolation has been previously tested using breast and prostate cancer cell line[21]. To validate the performance of the GO chip for lung cancer, fluorescence labeled human lung cancer cell lines H1650 and H441 (1000 cells/mL) were

spiked into blood obtained from healthy donors and flowed through the GO chip at 1mL/hr. The capture efficiency of H441 and H1650 was 91% and 97% respectively (Figure 2.2A).

The specificity of the PD-L1 antibody was tested by immunofluorescent staining of lung cancer cell lines. After capture on the chip, cells were stained for anti-Pan cytokeratin (CK) (tumor marker), anti-CD45 (leukocyte marker), anti-PD-L1 and DAPI (nuclear stain) and respective secondary antibodies. White blood cells were identified as positive for DAPI and CD45, while cancer cells were identified as positive for DAPI and CK, but negative for CD45. PD-L1 positive cell line H441 stained positive for PD-L1 (Figure 2.2C) while no PD-L1 expression was detected in PD-L1 negative cell line H1650 (Figure 2.2B).

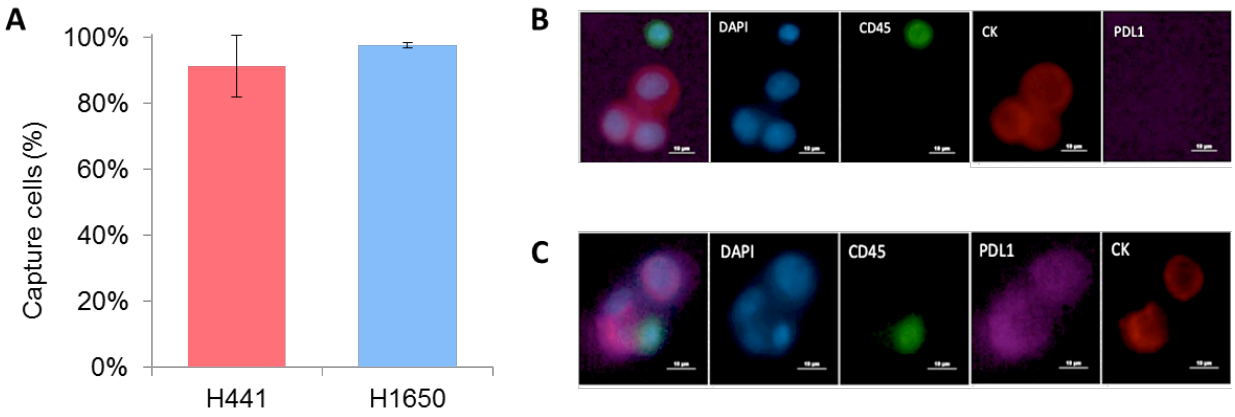

Figure 2.2 Capture efficiency and fluorescence images of lung cancer cell lines
(A) Capture efficiency of lung cancer cell lines H441 (n=3) and H1650 (n=3). (B) Representative images of immunofluorescence staining of H1650 lung cancer cells along with WBCs captured on the chip. (C) Representative images of immunofluorescence staining of H441 lung cancer cells along with WBCs captured on the chip

2.4.2 Isolation of CTCs in non-metastatic NSCLC patients undergoing radiation or radiochemotherapy

Demographics of 12 NSCLC patients enrolled in this study are shown in Table 2.1. We collected serial blood samples from 12 patients with non-metastatic NSCLC who received radiation alone (n=4) or radiochemotherapy (n=8) (Table 2.1). Serial blood samples from the patients enrolled in

the study were collected at the following time points: before the initiation of treatment (visit 1), during treatment (visit 2), and at follow up at least one month after treatment (visit 3). The flowchart in Figure 1 provides an overview of the recruitment process and the method of CTC isolation. Depending on the length of the treatment, we might receive multiple samples during treatment. In these cases, we reported here the averaged CTC number for visit 2.

Table 2.1 Demographics of patients

Patient	Age	Sex	Histology	T	N	M	RT dose	RT fraction size	Concurr-ent chemo	Concurrent chemo drugs	Adjuva-nt chemo
Patient 1	60	Male	Adenocarcin-oma	2a	1	0	60	2	No	N/A	No
Patient 2	79	Male	Carcinoma	2	0	0	70	2	No	N/A	No
Patient 3	64	Male	Adenocarcin-oma	1	0	0	50	10	No	N/A	No
Patient 4	73	Male	Squamous	1a	3	0	50	5	No	N/A	No
Patient 5	72	Male	Squamous	2a	1	0	60	2	Yes	Carboplatin/ Taxol	No
Patient 6	67	Male	Sarcomatoid - carcinoma	3	2	0	60	2	Yes	Carboplatin/ Taxol	No
Patient 7	65	Male	Squamous	4	3	0	60	2	Yes	Carboplatin/ Taxol	No
Patient 8	63	Male	Squamous	2b	0	0	60	2	Yes	Carboplatin/ Taxol	No
Patient 9	82	Male	Squamous	3	2	0	60	2	Yes	Carboplatin/ Taxol	No
Patient 10	60	Male	Adenocarcin-oma	4	3	0	60	2	Yes	Carboplatin/ Taxol	Yes
Patient 11	57	Male	Squamous	1b	3	0	60	2	Yes	Carboplatin/ Taxol	No
Patient 12	67	Male	Squamous	2b	2	0	60	2	Yes	Cisplatin/ Etoposide	No

After cells were captured on the chips, GO chips were stained and imaged, and CTCs were identified as CK+/CD45−/DAPI+ cells. Figure 2.3A and Figure 2.3B shows representative micrographs of PD-L1 (+) CTC and PD-L1(-) CTC. While the majority of captured CTCs were single cells, clusters of 2- 4 CTCs were observed in most patients (10/12) (Figure 2.3C). Blood

samples from healthy donors gave a counting of 2 or 3 CTCs/ml and thus a threshold of ≥ 3 CTCs /ml was used for CTC detection in patient samples (Figure 2.3D).

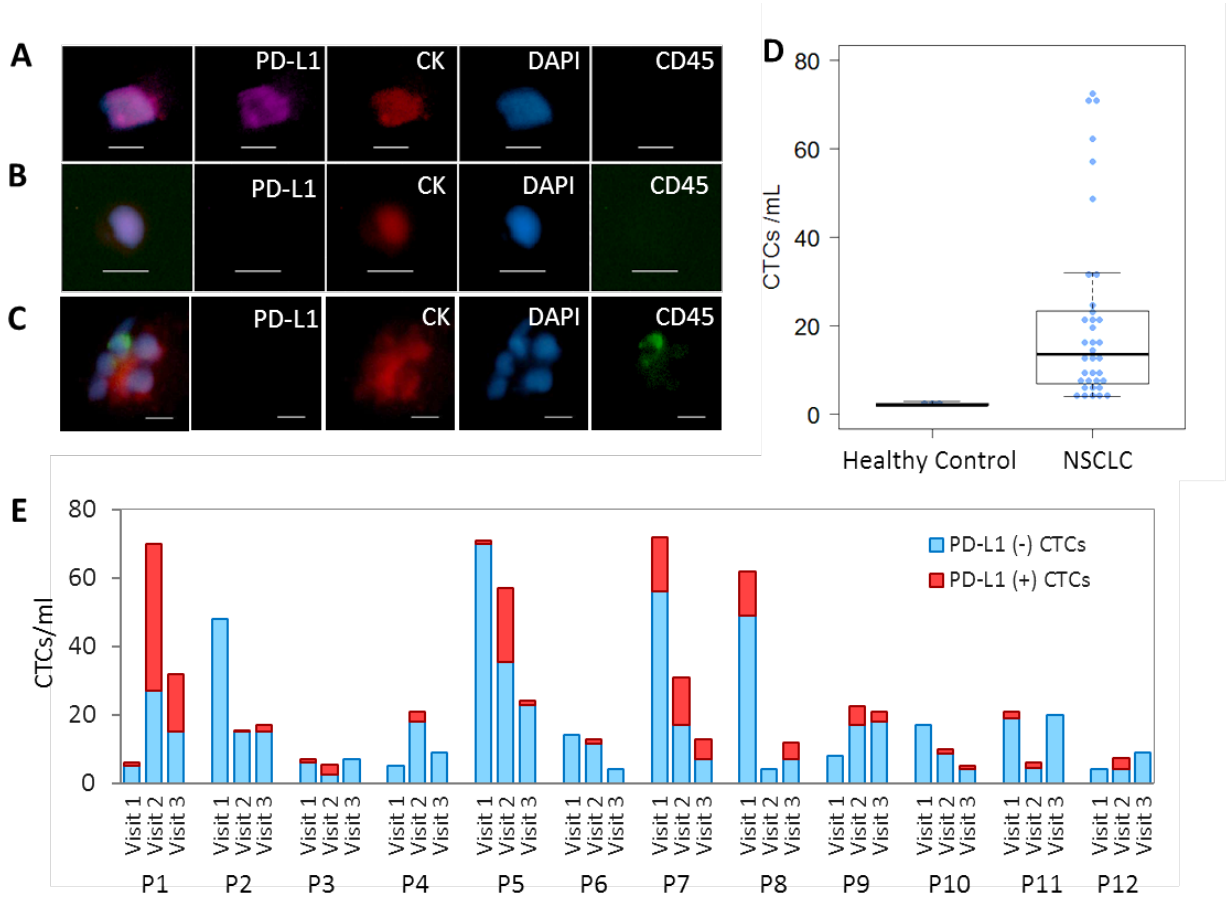

Figure 2.3 CTC counts and images isolated by GO chip from different visits of 12 NSCLC patients
(A) – (C) Representative images of CTCs isolated from NSCLC patients stained by antibodies against cytokeratin (red), a leukocyte marker CD45 (green), and a nuclear stain (DAPI). (A) CK+/PD-L1+ CTC, (B) CK+/PD-L1- CTC, (C) CTC cluster. Scale bar is 10 µm. (D) CTC enumeration from blood samples of healthy donors (n=3) and from blood samples of NSCLC patients (n=36). (E) Number of CTCs isolated by GO chip from blood samples from different visits of 12 NSCLC patients (P1 through P12). P1 stands for 'patient 1'. Blue bar represents the number of CK+/PD-L1- CTCs. Red bar represents the number of CK+/PD-L1+ CTCs.

CTCs were detected in all samples with the average of 20.8 CTCs/ml (range 4-72) (Figure 2.3D, Table 2.2). The average number of CTCs for visit 1, visit 2, and visit 3 were 29.2 CTCs/ml, 20.3 CTCs/mL, and 14.6 CTCs/mL respectively (Table 2.2). For the eight patients

receiving radiochemotherapy (patient 5-12), a decrease in CTC numbers was observed in visit 2 and visit 3 compared to visit 1 among 6 patients (75%) although it was not statistically significant (Figure 2.3D). Among the rest of the four patients who received radiation therapy only (patient 1-4), CTC numbers increased 10 folds and 3 folds during radiation in patient 1 and patient 4 respectively (Figure 2.3D, Table 2.3).

Table 2.2 Statistics of total CTC number and PD-L1 (+) CTC number at different visits
(Unit, cells per mL; SD: standard deviation)

	CTC range	Average CTC	SD for CTC	Median CTC	PD-L1 (+) CTC range	Average PD-L1 (+) CTC	SD for PD-L1 (+) CTC	Median PD-L1 (+) CTC
Total	5 – 79	21.3	20.3	13.5	0 - 32	4.1	6.8	1.5
Visit 1	5 – 79	29.2	27.1	18.5	0 - 14	2.6	4.2	1
Visit 2	3.5-68	20.3	20.7	14.3	0 - 32	6.7	9.5	3
Visit 3	5 - 32	14.6	8.5	12.5	0 - 17	3	4.7	1

Table 2.3 A list of total CTC number, PD-L1 (+) CTC number and the fraction of PD-L1 (+) CTCs at different visits for 12 patients

Patient	Visit 1			Visit 2			Visit 3		
	CTCs (/mL)	PD-L1 (+) CTCs (/mL)	Proportion of PD-L1 (+) CTCs	CTCs (/mL)	PD-L1 (+) CTCs (/mL)	Proportion of PD-L1 (+) CTCs	CTCs (/mL)	PD-L1 (+) CTCs (/mL)	Proportion of PD-L1 (+) CTCs
Patient 1	6	1	17%	68	32	47%	32	17	53%
Patient 2	50	0	0%	15.5	0.5	3%	17	2	12%
Patient 3	7	1	14%	5.5	3	55%	7	0	0%
Patient 4	5	0	0%	21	3	14%	9	0	0%
Patient 5	79	3	4%	57	21.5	38%	24	1	4%
Patient 6	14	0	0%	13	1.5	12%	5	0	0%
Patient 7	73	9	12%	21	8.5	40%	13	6	46%

Patient 8	50	14	28%	3.5	0	0%	12	5	42%
Patient 9	9	0	0%	15.5	3.5	23%	22	4	18%
Patient 10	23	0	0%	10	1.5	15%	5	1	20%
Patient 11	28	1	4%	6	1.5	25%	20	0	0%
Patient 12	6	2	33%	7.5	3.5	47%	9	0	0%

2.4.3 CTCs and PD-L1 expression of CTCs in non-metastatic NSCLC patients undergoing radiation or radiochemotherapy

PD-L1 (+) CTCs were detected in 24 samples (66.7%) with an average number of 4.7/ml (range 0-43) (Figure 2.3D, Table 2.3). The average number of PD-L1 (+) CTCs for visit 1, visit 2, and visit 3 were 2.7 CTCs/ml, 6.7 CTCs/mL, and 3 CTCs/mL respectively (Table 2.2). The PD-L1 (+) CTCs number in visit 2 sample is significantly high compared to that in visit 3 ($P = 0.037$) (Figure 2.4A). The proportion of PD-L1 (+) CTCs to total CTCs ranged from 0 to 61.4% with an average of 17.1% (Table 2.2). Compared to the proportion of PD-L1 (+) CTCs isolated before treatment (mean 7.1%, SD 8.6%), the proportion of PD-L1 (+) CTCs during treatment increased in 11 out of 12 patients (mean 28.3%, SD 24.7%) . This difference reached statistical significance ($P = 0.0068$) (Figure 2.4B), suggesting that radiotherapy or radiochemotherapy induces PD-L1 expression in CTCs.

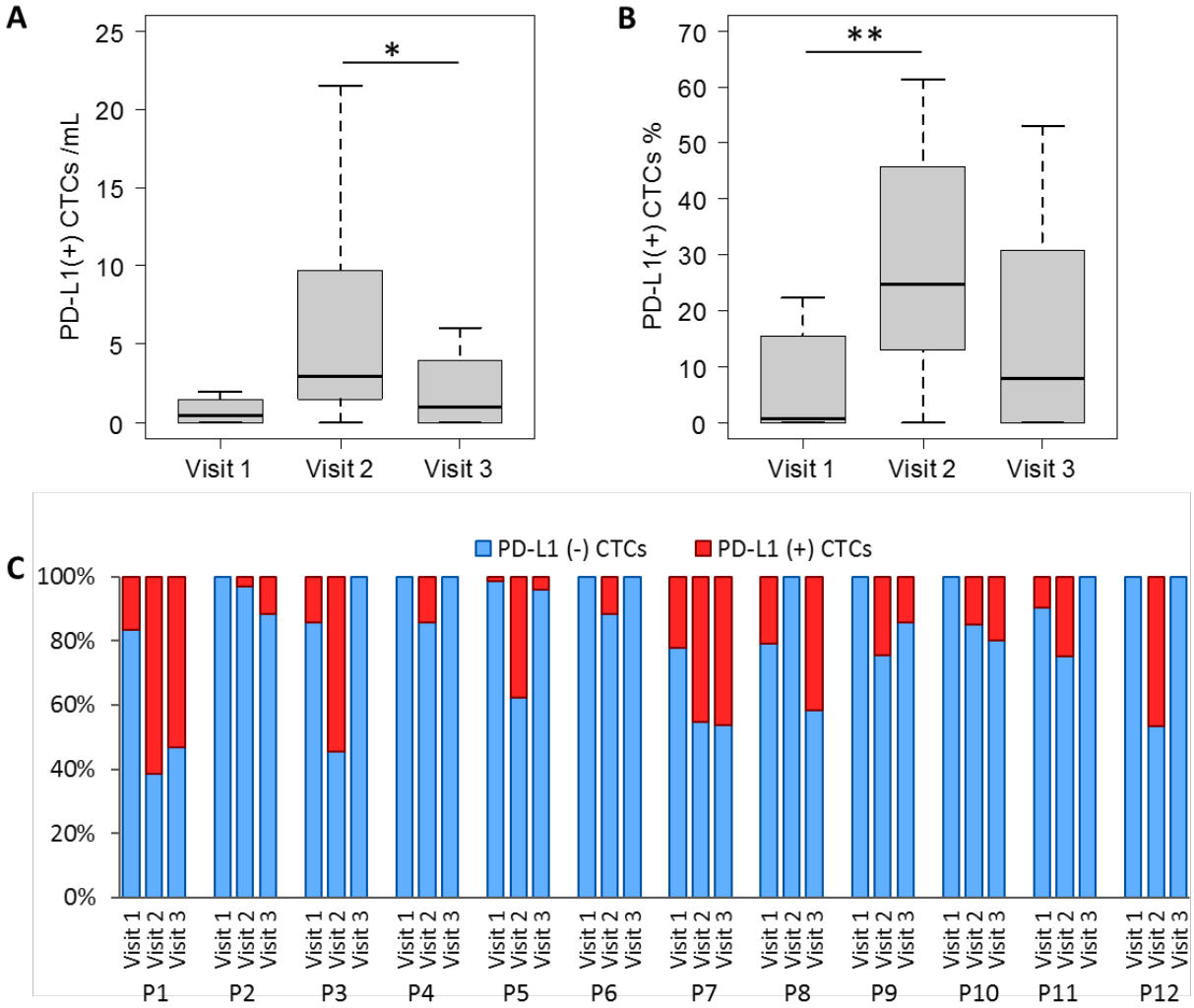

Figure 2.4 Dynamic changes of PD-L1 (+) CTC proportions at different visits
(A) Dynamic changes of PD-L1 (+) CTC proportions at visit 1, visit 2, and visit 3 for 12 patients. P1 stands for 'patient 1'. Red bar represents the percentage of PD-L1 (+) CTC number in total CTC number. Blue bar represents the percentage of PD-L1(-) CTCs in total CTCs. (B) The fraction of PD-L1 (+) CTCs out of total CTCs in different visits (n=12).

2.4.4 Prognostic significance of PD-L1 status in CTCs at baseline

Patient 3 were lost to follow-up after 3 months. For the rest 11 patients, progression-free survival (PFS) was analyzed according to the baseline CTC number and PD-L1 (+) CTC

number. No significant difference in PFS was found in the patients with high CTC number (CTCs≥20 /ml) (median 9.9 months) compared to those with low CTC number (CTCs < 20/ml) (median 6.95 months). The commonly used cutoff value for assessing PD-L1 positivity in tissue biopsy staining is 5% [105], which is close to the mean value of PD-L1 (+) CTC% (7.1%) at baseline. If ≥5% of PD-L1 (+) staining among CTCs is used as cutoff for PD-L1 positivity, PD-L1 positive patients have much shorter PFS as compared with PD-L1 negative patients (median 6.7 months, range 5.7 – 9.9 month vs median ≥14.75 months, range 7.5 - 18.9 months: P=0.016) (Figure 2.5B). Notably, patient 1 who had high PD-L1 (+) CTC counts at visit 2 and visit 3 was put on therapy with PD-1 inhibitor pembrolizumab after initial progression and has had stable disease for 7 months.

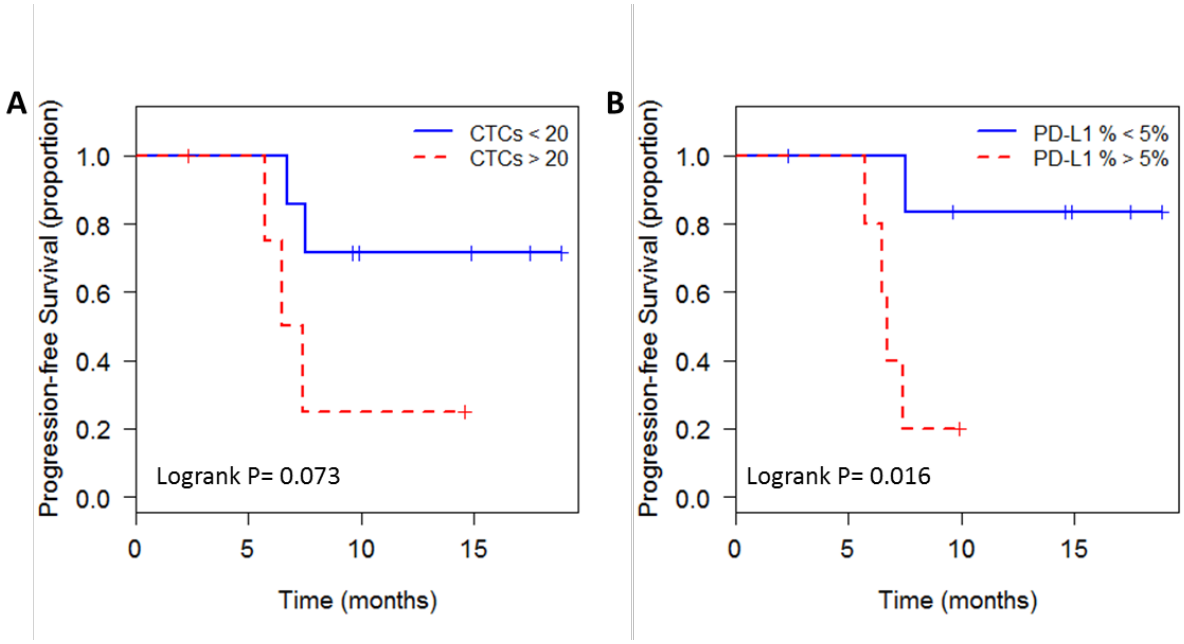

Figure 2.5 Kaplan–Meier life-table analysis of the PFS time in all patients.
Kaplan–Meier life-table analysis of the PFS time in all patients. Grouping was done according to (A) CTC number more or less than 20/ml (B) PD-L1 (+) CTC% more or less than 5%.

Table 2.4 Progression-free survival (PFS) of Patient.
("NED" stands for "no evidence of disease")

Patient	Status	PFS (months)	PFS censor
Patient 1	Alive, Progressed	6.7	0
Patient 2	Alive, NED	2.3	1
Patient 3	Alive, NED	9.9	1
Patient 4	Alive, NED	9.6	1
Patient 5	Alive, NED	14.6	1
Patient 6	Alive, NED	18.9	1
Patient 7	Dead	6.5	0
Patient 8	Dead	5.7	0
Patient 9	Alive, NED	14.9	1
Patient 10	Alive, NED	17.5	1
Patient 11	Dead	7.4	0
Patient 12	Alive, Progressed	7.5	0

2.4.5 Gene expression profiling of CTCs

To further investigate the molecular signature of CTCs from patients and study the association with treatment outcomes, mRNA profiling of the captured CTCs was carried out by performing quantitative RT-PCR for selected panel of 96 genes consisting of lung cancer related genes, epithelial and mesenchymal genes and immune checkpoint-related genes (Table 2.5). After normalization to average of internal house-keeping genes (HKGs: GAPDH, ACTB, and UBB) using the ΔCt method, the PD-L1 mRNA expression at different visits were compared. Among visit 1 samples, 30% of the samples had detectable levels of PD-L1 mRNA expression. Whereas, 70% of visit 2 samples and 25% of visit 3 samples showed detectable PDL-1 gene expression (Figure 2.6A). The expression level of PD-L1 in visit 2 samples are significantly higher than those in visit 1 and visit 3 samples ($P = 0.043$ and $P = 0.026$, respectively), which is consistent with the results of PD-L1 (+) CTC number. To investigate the prognostic value of

CTC gene expression, patients were classified into poor prognosis (PP group) and good prognosis (GP group) based on a cutoff at 9 month PFS. This cutoff is chosen based on the median PFS time of patients. Five patients had disease progression within 9 months while the other seven patients had stable disease in a time period of 9 months or more. The mRNA levels of PD-L1 is detected in 9 out of 12 samples in PP group while the mRNA levels of PD-L1 is detected in 3 out of 14 samples in the GP group. The mRNA levels of PD-L1 were significantly higher in the samples from PP group than that of GP group (P = 0.025) (Figure 2.6B). Similarly, from the results of IF staining, samples from PP group tend to have higher proportion of PD-L1 (+) CTCs than those from GP group, although not reaching statistical significance (median 22% vs 7.8%, P=0.063, Figure 2.6C). MTOR gene which is related to PD-L1 upregulation in tumor cells [106] also displayed increased level of expression in PP samples(Figure 6D). In addition, Ki67 and CD33 were highly expressed in the samples from PP group (P = 0.042 and 0.042 respectively) (Figure 2.6E and F).

Table 2.5 The 96 gene panel for CTCs in NSCLC

GAPDH	TGFB1	CD20	BCL-xL	CTNND1	FOXC2	MTOR	SNAI1
ACTB	EMP2	CD45	BMi1	CXCL16	IGFBP5	MUC1	SNAI2
UBB	TROP2	EGFR	CASP3	CXCR1	IL6	NFKB1	SPARC
ALDH1A1	KRT5	KRAS	CCND1	DSP	IL8	NTRK2	STAT3
ALDH1A3	KRT7	MKI67	CD146	ELF3	JUP	PIK3CA	TIMP1
CD24	KRT8	AR	CD33	ERCC1	KLF4	PKP2	TIMP2
CD44	KRT14	PD-1	CD34	ERG	KLK3	PSME3	TMPRSS2
CD44v6	CDH1	PDL-1	CHP1	ETV1	LGALS3BP	PTCH1	TP53
CD133	CDH2	XIST	COL1A2	EVPL	MAPK1	PTEN	XBP1
EPCAM	CDH11	HOTAIR	COL3A1	FGF18	MLPH	PTPRN2	XIAP
ERBB2	CD3D	ABCG2	CTNNA1	FOLH1	MMP2	RB1	ZEB1
VIMENTIN	CD11B	ALK	CTNNB1	FOXC1	MMP9	SERPINB6	ZEB2

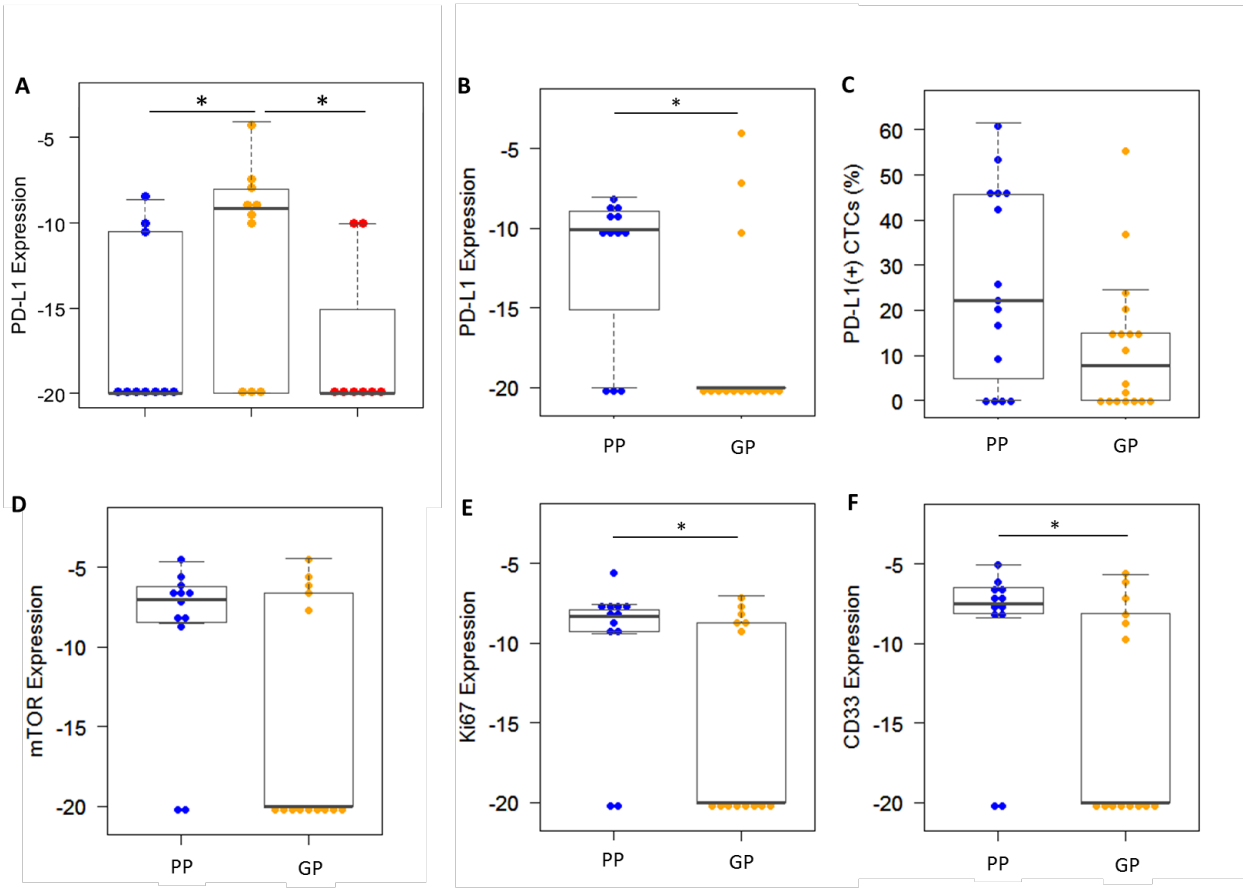

Figure 2.6 mRNA profiling of CTCs.
(A) mRNA level ($-\Delta C_t$) of PD-L1 in visit 1 samples(n=10), visit 2 samples(n=10) and visit 3 samples (n=8); (B),(D)-(E) mRNA level ($-\Delta C_t$) of differentially expressed genes PD-L1 (B), mTOR (D), Ki67(D), and CD33 (E) in PP samples (n=12) versus GP samples (n=14). P-value < 0.05 (*); (C) PD-L1 (+) CTC proportion in PP samples (n=15) versus GP samples (n=21).

2.5 Discussion

Preclinical studies have demonstrated that the combination of radiotherapy and PD-1/PD-L1 checkpoint blockade synergistically enhances antitumor immune activity and increase the treatment efficacy of either therapy alone [100], [101]. A suggested mechanism is that the inflammatory response after radiation up-regulates the PD-L1 expression in tumor cells and surrounding cells, resulting in an immune-suppressive microenvironment [100], [101]. These

findings, however promising, have not been validated in clinical settings for NSCLC. CTC isolation provides a noninvasive way to monitor PDL-1 expression in tumor cells over time. The feasibility of analyzing PD-L1 (+) CTCs has been demonstrated in breast cancer and NSCLC [107], [108]. In a recent study, the persistence of PD-L1 (+) CTCs detected by CellSearch System was shown to be correlated with immunotherapy resistance in 14 metastatic NSCLC patients treated with PD-1 inhibitor Nivolumab, indicating that PD-L1 (+) CTCs may be a marker of immunotherapy escape [108]. However, the small number of PD-L1 (+) CTCs detected cannot reflect the dynamic changes of PD-L1 expression. In this study, we were able to detect sufficient number of CTCs via the GO chip at different time points to monitor changes of PD-L1 expression. Several features of the GO chip contribute to the improved sensitivity of CTC isolation compared to conventional methods: 1) graphene oxide increases the surface area on which the tumor specific capture antibody was present, 2) microfluidic structure obtains optimized flow pattern for cell capture, 3) an antibody cocktail of anti-EpCAM, anti-EGFR and anti-CD133 enables the isolation of CTCs expressing variable levels of epithelial and mesenchymal markers. Furthermore, as the white blood cell contamination within the GO chip is very low, the captured CTCs maintained high purity and thus enabled downstream gene analysis [21].

In this study, we demonstrated for the first time that PD-L1 expression in CTCs is up-regulated through the course of radio(chemo)therapy in non-metastatic NSCLC patients. At baseline, 42.9% of samples showed PD-L1 staining in CTCs if a 5% threshold for positivity is used. This is in line with previous studies reporting that a range of 20% to 57.5% of solid biopsy samples from stage I-III NSCLC patients express PD-L1 [109]-[111]. During radiation, the PD-L1 expression in CTCs increased significantly (P=0.018). This finding is consistent with the

results of preclinical studies and might represent a mechanism of tumor immune escape. However, it is still unclear whether PD-L1 expression is obtained in primary tumor before intravasation or could be acquired within the blood circulation. Future studies that compare the PD-L1 expression of tissue biopsies or surgical specimens with that of CTCs will be very helpful to investigate the mechanism of PD-L1 expression in CTCs and to understand the significance of PD-L1 (+) CTCs.

Furthermore, we revealed that PD-L1 positivity in CTCs may serve as a prognostic marker among non-metastatic NSCLC patients receiving radiation or radiochemotherapy. If more than 5% CTCs showing PD-L1 staining is considered to be PD-L1 positive, PD-L1 positive patients have much shorter PFS compared with PD-L1 negative patients. A possible explanation is that these PD-L1 (+) CTCs reflect immunosuppressive tumor microenvironment which promotes tumor relapse. In addition, with the capacity of evading immune response in a foreign environment, PD-L1 (+) CTCs may have higher metastatic potential. Indeed, two patients who later developed metastases showed PD-L1 positivity at baseline. However, the current study is limited due to the small patient cohort and the limited follow-up interval. Future studies in a large cohort would be valuable to investigate the potential of PD-L1 (+) CTCs for predicting disease progression for this subgroup of patients. Notably, patient 1 with high PD-L1 expression (>50% CTCs expressing PD-L1) at follow-up time point (visit 3) was treated with PD-1 inhibitor pembrolizumab one month after the follow-up visit and the tumor has been stable till now for 7 months. As 50 percent or more PD-L1 expression in tissue samples has been used as a predictive biomarker for pembrolizumab, PD-L1 expression in CTCs could serve as a biomarker for selecting and monitoring patients for pembrolizumab therapy.

Furthermore, as we examined the mRNA expression pattern of CTCs for a 96-gene panel, PD-L1, Ki67 and CD33 was found to be highly expressed in patients who had disease progression within 9 months compared to patients who had stable disease for 9 months or more. The differences of PD-L1 mRNA expression levels between different visits are similar to that of the PD-L1 (+) CTC counts via the immunofluorescent staining, further confirming our findings in the upregulation of PD-L1 during radiation. The high expression of PD-L1 mRNA in poor prognosis group also supports the prognostic value of PD-L1. The expression of Ki67, a proliferation marker, has been associated with chemoresistance and poor prognosis [112], [113]. Ki67+ CTCs were detected in various cancer types including NSCLC and is associated with shorter overall survival [55], [114]. CD33, a myeloid cell marker, has been shown to be upregulated in the adenocarcinoma of NSCLC compared to the adjacent non-neoplastic lung tissue because of the infiltrated myeloid cells in tumor tissue [115]. Furthermore, myeloid-derived suppressor cells (MDSC), an immune-suppressive population of myeloid cells, can form clusters with CTCs to protect CTCs from immune surveillance and may facilitate the formation of distant metastases [62]. Thus CD33 mRNA signal we detected may come from myeloid cells adhering to CTCs. Indeed, we frequently observed clusters of CTC and CD45+ blood cells captured in the chip. It is also possible that this signal comes from the non-specific binding of CD33+ blood cells on the chip, as the overexpression of CD33+ MDSC is observed in the peripheral blood of advanced stage NSCLC and is associated with immune suppression [116].

The high purity of captured CTCs within the GO chip enabled downstream gene analysis such as qPCR. However, as it is unrealistic to achieve 100% purity, mRNA was extracted from a mixed population of CTCs and WBCs captured in the GO chip. Thus the mRNA levels detected here contained signals from both CTCs and the blood cells. This limitation could be overcome by

developing single cell gene analysis technique to differentiate the CTC population with the contaminating blood cells.

To create successful combinations of immunotherapy, radiation, and chemotherapy, many concerns need to be addressed such as how to select patients and how to choose the optimal treament regimen and sequence when combined with PD-1/PD-L1 inhibitors. CTC enumeration and molecular characterization can be a useful tool to help in this decision making process as CTCs can be sampled frequently without an invasive procedure. As we demonstrated the feasibility of monitoring PD-L1 (+) CTCs in this study, this CTC subgroup could potentially act as a biomarker to monitor the tumor immunity to facilitate treatment selection for combinational immunotherapies. Future efforts should incorporate dynamic monitoring of PD-L1(+)CTC for the timed administration of PD-1/PD-L1 inhibitors such as pembrolizumab in patients with locally advanced NSCLC.

CHAPTER 3

3 Investigating the Potential of CTCs for Monitoring Tumor Status and Predicting Treatment Response in Locally Advanced Pancreatic Cancer

3.1 Abstract

The median overall survival of locally advanced pancreatic cancer patients ranges only from 9 to 10 months. For those patients, treatment options range from chemotherapy alone to combination of radiation therapy and chemotherapy. To improve the treatment outcome, there is a pressing need to develop biomarkers to monitor treatment response and to provide valuable information for treatment selection and adaption. CTCs can be isolated from peripheral blood of patients and hold the promise of being a real time biomarker for cancer detection and management. In this study, CTCs were isolated via the GO chip from blood samples taken at different time points during the course of chemotherapy and subsequent radiation therapy from 26 patients with the locally advanced pancreatic cancer. Patients with decreased number of CTCs after chemotherapy had longer progression free survival (PFS) than patients with increase or no change in CTC counts prognosis (13.5 months vs 6.5 months, P value= 0.002), indicating that changes of CTC numbers may be an early indicator for treatment failure. Furthermore, the persistence of high expression of Vimentin, an epithelial-mesenchymal transition (EMT) marker, in CTCs is correlated with shorter PFS (7.55 vs 14 months, P=0.019). In mRNA profiling of

CTCs, the mRNA expression levels of three genes, BAX, CHK1 and EZH2 are associated with poor prognosis, which is in line with previous preclinical studies that these genes are involved in drug resistance.

3.2 Introduction

Pancreatic cancer is the 4th leading cause of death in the United States with a five-year survival rate of only up to 8% [80]. Approximately 30% of patients with pancreatic cancer are being diagnosed with locally advanced disease [122]. For these patients, systemic chemotherapy or any combined forms of radiation therapy and chemotherapy are typically the treatment options available. Although no evidence of metastasis is observed at the time of diagnosis, the median overall survival rate of those patients only range from 9 to 10 months. Pancreatic cancer is highly resistant to chemotherapy drugs, which leads to the failure of chemotherapy and thus contributes to the high mortality rate [123].

Several mechanisms and signaling pathways involved in the drug resistance process of pancreatic cancer have been proposed. For instance, it has been found that the cell cycle checkpoint proteins can help tumor cells escape the cytotoxic effects of the drugs by inducing cell cycle arrest for the repair of DNA damage caused by chemotherapy [124]. Therefore, the inhibition of cell cycle checkpoints such as Wee1 and CHK1 can sensitize the tumor cells to chemotherapy and enhance the treatment efficacy. Moreover, many recent studies have demonstrated that cancer cells with EMT phenotypes and stem cell properties play pivotal roles in treatment resistance [125]. Thus, analyzing the molecular signature of drug resistance in tumor samples from pancreatic cancer patients can assist the investigation of the resistance mechanism and the discovery of new therapeutic targets. Furthermore, in clinical practice, characterizing and monitoring the molecular feature of tumor cells for drug resistance markers is particularly

important for the prediction of treatment outcome in order to select the most effective therapy and limit the toxicity to patients.

Currently, serial sampling of tumor tissues for molecular analysis during the course of treatment is impractical. Circulating tumor cells (CTCs) are tumor cells that are shed from tumor and enter the blood circulation and hold the potential to provide an alternative to biopsy for the real-time monitoring of tumor status. As CTCs can be easily sampled at various time points, the isolation and analysis of CTCs can substitute biopsies for monitoring the molecular features of pancreatic cancer to provide predictive and prognostic information for the selection of personalized treatment for patients. Evidence from recent studies showed that the presence of CTCs are associated with poor outcome [87], but relatively low levels of CTCs can be detected in most pancreatic cancer patients compared to other types of malignancies [5], [117].The limitation of current widely used technologies to detect CTCs in sufficient number in pancreatic cancer patients poses as a potential barrier for their use as an effective biomarker.

Microfluidic technologies have emerged as a solution to isolate CTCs with high sensitivity and purity[4]. Previously we developed a nanomaterial based microfluidic chip, the GO chip, for capture and proteomic analysis of CTC [21]. The GO Chip consists of a microfluidic chamber and a substrate coated with graphene oxide (GO) nanosheets where the antibodies are tethered. This technology takes advantage of the increased surface area afforded by graphene oxide to achieve higher antibody coating density, thus improving sensitivity for CTC capture. Furthermore, antibodies are specifically patterned onto the flower patterns rather than the entire surface (as shown in Figure 1), which results in high purity of captured cells.

In this study, we isolated CTCs using the GO chip from locally advanced pancreatic cancer patients and monitored the changes of CTC numbers over the course of treatment. Also

we characterized the captured CTCs using a DNA damage marker (H2AX) and an EMT marker (Vimentin) (Figure 3.1). Furthermore, mRNA expression of CTCs was analyzed using RT-PCR using a panel of genes specific to pancreatic cancer and resistance. Finally, we investigated the correlation between the numbers and the molecular features of CTCs and the patients' clinical outcome to assess treatment outcome and disease progression among patients with locally advanced pancreatic cancer.

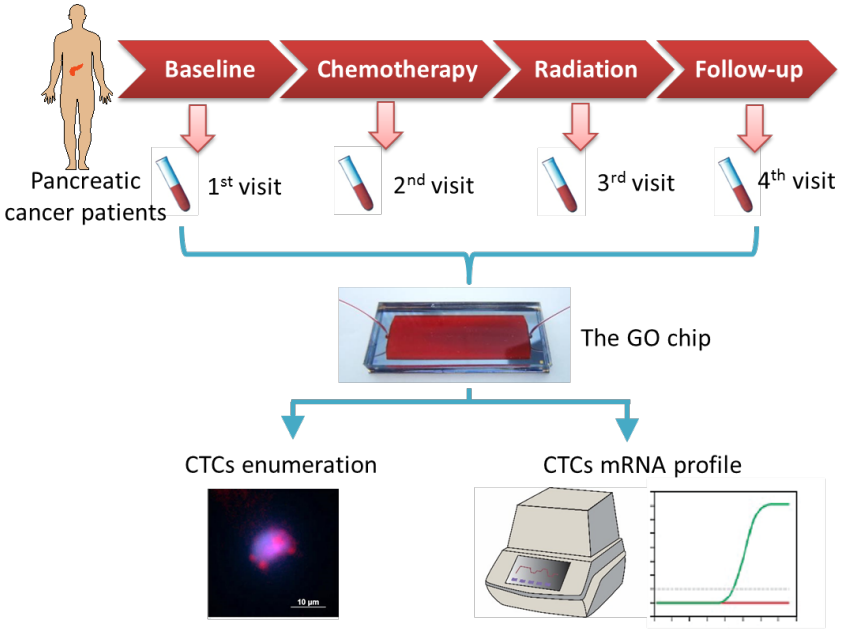

Figure 3.1 An overview of this study.
An overview of this study, with sample collection and circulating tumor cell (CTC) isolation at baseline, after chemotherapy and during radiation and months after treatment (follow up)

3.3 Materials and Methods

3.3.1 Patient selection and sampling

We selected patients with histologic or cytologic proof of pancreatic cancer, for whom the treatment plan at the time of enrollment is chemotherapy and radiation therapy. Patients may be enrolled on other clinical trials. The target population of this study is locally advanced,

unresectable patients with no evidence of metastatic disease. A total of 50 patients were planned to be enrolled for the study. Patients signed an informed consent indicating that they were aware of the investigational nature of this study, in keeping with the policies of UM hospital.

Selected patients had blood samples drawn at the following time points:

(1) At baseline, prior to the start of chemotherapy or radiation therapy for pancreatic cancer (if the patient already received chemotherapy for pancreatic cancer then this time point will be omitted).

(2) After the first 3 weeks of induction chemotherapy are complete and prior to the start of radiation therapy. Note: For patients receiving more than three weeks of induction chemotherapy an additional sample will be obtained after induction chemotherapy has been completed (and prior to the start of radiation therapy).

(3) After completion of approximately 60% of the planned radiation dose (e.g. if 25 fractions of radiation are planned the sample would be obtained no earlier than the 14th fraction and no later than the 19th).

(4) After completion of radiation therapy and adjuvant chemotherapy. Typically, this will occur one to two weeks after completing adjuvant chemotherapy.

3.3.2 GO device Fabrication

The fabrication and functionalization of GO chip has been previously described[9]. Briefly, gold films were deposited onto a silicon oxide coated silicon wafer by evaporation and were patterned by conventional photolithography. Graphene oxide nanosheets are absorbed onto gold patterns on the silicon substrate, then chemically functionalized with EpCAM antibodies. A polydimethylsiloxane (PDMS) layer were bonded with silicon substrate to forms a microfluidic chamber with a height of 50 μm and total volume of 45 μl.

3.3.3 Patient Sample Processing

Patient blood samples were obtained according to the schedule described above. Most of the patients had 3 or 4 blood draws over the course of the study depending on the length of their induction chemotherapy. Within 3 hours of collection, blood samples were processed by GO chips at a flow rate of 1 mL/hr.

3.3.4 CTC enumeration and characterization

After sample processing, one chip containing bound CTCs were used for CTC enumeration and evaluating the expression of certain proteins by immunostaining. To differentiate captured CTCs and white blood cells, immunostaining was performed using anti-cytokeratin(Santa Cruz), and anti-CD45(Bio Rad), where white blood cells were identified as positive for 4′ ,6-diamidino-2-phenylindole (DAPI) (Invitrogen) and CD45, a common leucocyte antigen, while CTCs were identified as positive for DAPI and cytokeratin (CK) or ZEB1, but negative for CD45. An additional marker, a DNA damage marker H2AX (Millipore) or an EMT marker Vimentin (BD), were used for immunostaining.

The other chip were used for RNA analysis. RNA was extracted from captured circulating tumor cells with commercially available extraction kit, Arcturus PicoPure RNA Extraction buffer (Life Technologies). RNA Extraction buffer was flowed through the chip to lyse the captured cells immediately after PBS wash. After incubated at 42 °C for 30 min, the device were washed with water and the effluent were collected. The effluents, which were the total RNA samples, were stored at -80 °C until cDNA preparation. The cDNA was synthesized from the total RNA and then pre-amplified for the selected 96 genes using the corresponding pooled TaqMan gene expression assays (Life technologies). The expression patterns of

preamplified cDNA were analyzed by a quantitative polymerase chain reaction (qPCR) setting using the same TaqMan gene expression assays and the Biomark HD system (Fluidigm).

3.3.5 Statistical analysis

The number of CTCs and CTC subpopulations between different visits was compared by the Wilcoxon rank sum test. Logrank test was done for calculating the P value of Kaplan–Meier survival plot. if p value was equal to or less than 0.05, the differences were considered significant. To analyze expression levels of selected genes between different patient groups, each transcript was normalized to house-keeping gene GAPDH and reported as -ΔCT, where ΔCT = CT gene – CT GAPDH. If the CT values were above 40, which indicates that the amplification was not detected during the 40-cycle qPCR, it is regarded as off-scale data. Therefore, an arbitrary cycle number of CT gene = 40 was assigned for numerical analysis36. All statistical analysis was performed using R software.

3.4 Results

3.4.1 Patient characteristics

A total of 26 patients with locally advanced pancreatic cancer undergoing chemotherapy and subsequent radiation therapy were enrolled in our study for CTC isolation and analysis. The demographics of all patients are summarized in Table 3.1. For each patient, 2 mL of whole blood was processed at the following three time points for analysis (Figure 3.1): a. 3 weeks after completion of chemotherapy prior to the following radiation therapy (after-chemo); b. After an approximate of 60% of the scheduled radiation dosage was applied (during-radio); c. after completion of radiation and adjuvant chemotherapy (follow-up). An additional blood sample was

obtained from 12 patients who were treatment naïve at the time of study enrollment (baseline) to monitor and evaluate changes in CTC counts during treatment.

Table 3.1 Patient information
"Y" stands for "Yes", "N" stands for "No", and "N/A" stands for "Not available".

Study ID	Patient No.	Chemotherapy agents	OS	OS censor	PFS	PFS censor	CTC Enumeration	Vimentin staining	RNA analysis	Treatment Naïve
W117	1	FOLFIRINOX , MK1775	24.1	0	11.7	1	Y	N/A	N/A	Y
W126	2	FOLFIRINOX , MK1775	27.8	0	25.5	0	Y	N/A	N/A	Y
W144	3	FOLFIRINOX , MK1775	11.4	1	11.4	1	Y	N/A	N/A	Y
W153	4	FOLFIRINOX , MK1775	24.5	1	18.8	1	Y	N/A	N/A	Y
W162	5	FOLFIRINOX , MK1775	25.8	0	18.9	1	Y	N/A	Y	Y
W199	6	FOLFIRINOX , MK1775	22.6	1	20.5	1	Y	N/A	N/A	Y
W206	7	FOLFIRINOX , MK1775	16.3	0	15.4	0	Y	Y	N/A	Y
W233	8	FOLFIRINOX , MK1775	17.4	0	9.2	1	Y	Y	N/A	Y
W242	9	FOLFIRINOX , MK1775	7.5	1	3.4	1	Y	Y	Y	Y
W288	10	FOLFIRINOX , MK1775	7.6	1	6.8	1	Y	Y	Y	Y
W395	11	FOLFIRINOX , MK1775	8.3	0	8.3	0	Y	Y	Y	Y
W439	12	FOLFIRINOX , MK1775	6.1	0	6.1	0	Y	Y	Y	Y
W411	13	FOLFIRINOX , MK1775	8	0	8	0	N/A	N/A	Y	N
W297	14	FOLFIRINOX , MK1775	8.3	1	6.1	1	Y	Y	N/A	N
W359	15	FOLFIRINOX , MK1775	11.1	0	8.4	1	Y	Y	Y	N
W368	16	FOLFIRINOX , MK1775	10.6	0	9.5	1	Y	Y	Y	N
W377	17	FOLFIRINOX , MK1775	9	0	9	0	N/A	N/A	Y	N
CTC171	18	N/A	27.4	0	15.4	1	Y	N/A	N/A	N
CTC251	19	FOLFIRINOX	17.4	1	14	1	Y	Y	N/A	N
CTC279	20	Gemcitabine, NAB-paclitaxel	15.8	1	14.7	1	Y	Y	Y	N
CTC304	21	Gemcitabine, cisplatin, veliparib	11.8	1	6.4	1	Y	Y	N/A	N
CTC313	22	Gemcitabine, NAB-paclitaxel	13	1	9.2	1	Y	Y	Y	N
CTC322	23	FOLFIRINOX	15	0	15	0	Y	Y		N
CTC331	24	FOLFIRINOX	17.4	0	16.3	1	Y	Y	Y	N
CTC386	25	Gemcitabine	12.6	0	6.4	1	Y	Y	Y	N
CTC402	26	FOLFIRINOX	10	0	10	1	N/A	N/A	Y	N

3.4.2 Monitoring changes in CTC number during treatment

Each blood samples were processed through individual GO chips to quantify the number of CTCs from patients with pancreatic cancer. CTCs were identified using immunofluorescence staining showing positivity in pan-cytokeratin (pan-CK), DAPI, and negative for CD45. Concurrently, whole blood from healthy donors (n=3) was processed identically for negative

controls. The average CTC counts from healthy individuals were 2.67 /ml, ranges 2 ~ 3 CTCs/mL, thus a 3 CTCs/mL threshold applied for CTC positivity in our analysis. Overall, CTCs were detected in 90.3% of blood samples. The mean number of CTCs for each visit (baseline, after-chemo, during-radio, and follow-up) was 31, 23, 14, and 21 cells/ml respectively (Figure 3.2A). No statistical significance was observed in CTC numbers between samples after-chemo, during-radio and follow-up time points. However, 12 out of 21 patients, for whom we collect blood samples for all four time points (who were treatment naïve at the time of enrollment), resulted in a significant decrease (P= 0.033) in CTC counts after chemotherapy compared to CTC counts prior to chemotherapy (Figure 3.2B). To correlate these results with clinical outcomes including progression free survival (PFS), patients were further divided into two groups depending on whether or not CTCs decreased after chemotherapy. Patients with decreased number of CTCs after chemotherapy experienced a longer PFS–with statistical significance (13.5 months vs 6.5 months, P value= 0.002) than patients with increase or no change in CTC counts (Figure 3.2C), suggesting that CTC counts during the first cycle of chemotherapy may be a surrogate of sensitivity to chemotherapy.

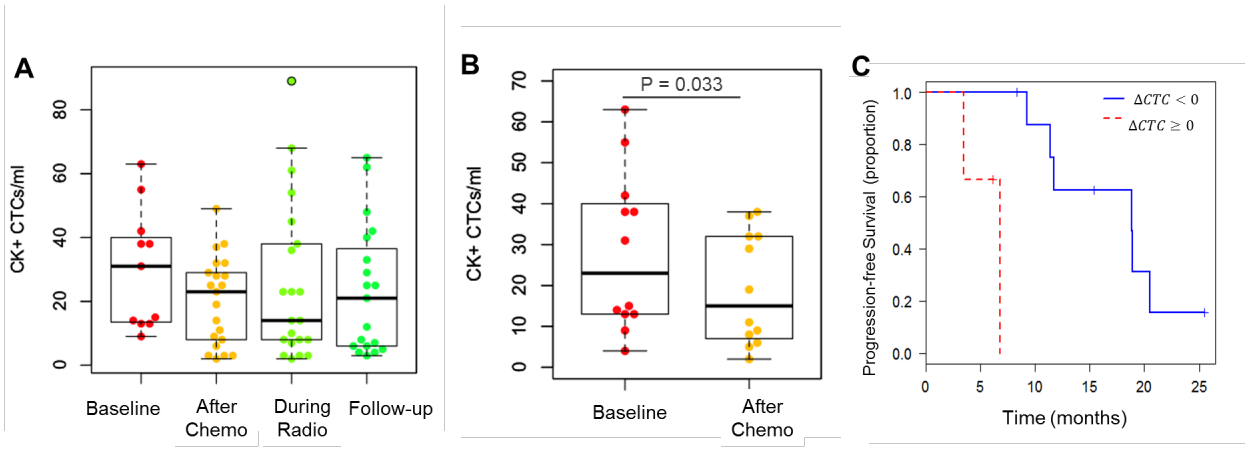

Figure 3.2 Number of CTCs at different visits.
(A) Number of CTCs isolated from blood samples of different visits among 12 treatment naïve patients (n=12). (B) Number of CTCs isolated from blood samples of different visits among 9 patients who have been previously treated (n=8). (C) Kaplan–Meier life-table analysis of the PFS time in 12 patients. Grouping was done according to the change of CTC number in after chemo sample compared to baseline sample. A decrease of CTC number in after chemo sample compared to baseline sample (red, n = 3) and an increase or unchanged CTC number in after chemo sample compared to baseline sample (blue, n = 9).

3.4.3 Molecular characterization of CTCs using H2AX and Vimentin

The phosphorylated histone H2AX, a marker for DNA double stranded breaks (DSBs), has been used for monitoring DNA damage in clinical trials of various chemotherapy agents [118]. To assess the DNA damages during treatment, we studied the H2AX expression of CTCs using IF in 4 patients. H2AX+ CTCs were detected in 10 out of 15 (67.7%) samples with a median number of only 1/ml (Figure 3.3). Interestingly, CK-/H2AX+/CD45- cells were frequently observed which might indicate that CTCs undergoes EMT and have decreased or lost CK expression. If CK-/H2AX+/CD45- cells could be considered as CTCs, patient W126 would have a high proportion of H2AX+ CTCs (92%) at the endpoint of chemotherapy, indicating that severe DNA damage in tumor cells was induced by chemotherapy.

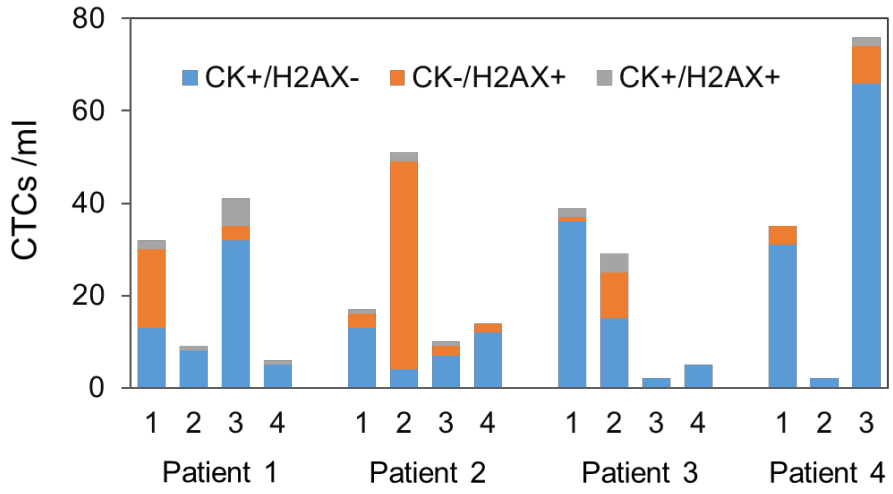

Figure 3.3 CTCs stained with H2AX
Number of CTCs isolated by GO chip from blood samples from different visits of 4 patients. Blue bar represents the number of CK+/H2AX- CTCs. Orange bar represents the number of CK-/H2AX+ CTCs. Grey bar represents the number of CK+/H2AX+ CTCs.'1', '2', '3' and '4' in X axis represents visit 1, visit 2, visit 3, and visit 4 respectively.

To further characterize EMT in CTCs, an additional marker vimentin (Vim) was applied to the captured CTCs using IF staining. Three CTC subtypes were identified including epithelial-like (CK+/Vim-/CD45- cells), intermediate (CK+/Vim+/CD45- cells), and mesenchymal-like CTCs (CK-/Vim+/CD45- cells). Overall, CTCs with epithelial-like or intermediate phenotypes were more abundantly observed in our study population compared to completely mesenchymal-like CTCs (Figure 3.4A). The median numbers of these epithelial, intermediate, and mesenchymal-like CTCs were 11.5, 11.5 and 1 cells/mL respectively. The median percentage of Vim+ CTCs (Vim + %) after-chemo, during-radio and follow-up samples were 63.5, 68.5, and 32.4%, respectively (Figure 3.4B). The proportions of Vim+ CTCs in samples after-chem and after-radio were significantly high compared to that in follow-up samples (P=0.034 and P=0.014, respectively) (Figure 3.4C).

Samples were stratified into high expression (>30%) and low expression of vimentin (≤30%) based on Vim+%. The persistence of high vimentin expression in all three samples correlated with worse PFS (7.55 vs 14 months, P=0.019) (Figure 3.4D).

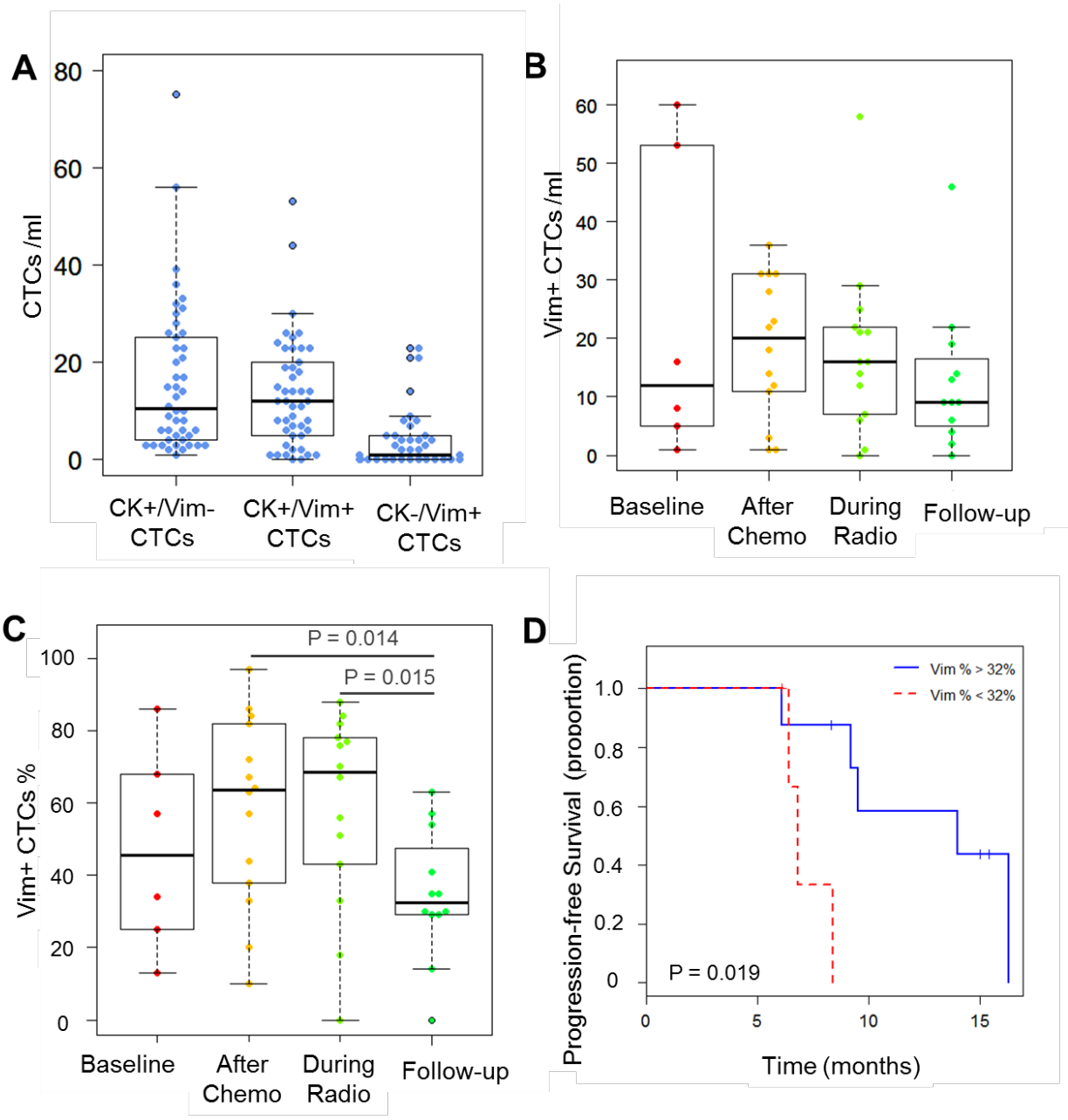

Figure 3.4 CTCs stained with Vimentin

(A).CTC number of three CTC subtypes were identified, epithelial CTCs (CK+/Vim-/CD45- cells), intermediate CTCs (CK+/Vim+/CD45- cells), and mesenchymal CTCs (CK-/Vim+/CD45- cells). (B) Number of Vim+ CTCs from blood samples of different visits among

15 patients; (C) The proportion of Vim+ CTCs in total CTCs from blood samples of different visits among 15. (D) Kaplan–Meier life-table analysis of the PFS time in 12 patients. Grouping was done according to the persistence of high vimentin expression (Vim+% > 30%) in three samples (after chemo, during radio and follow-up sample). Patients with high vimentin expression in these three samples (red, n = 4) and patients with low vimentin expression in one or more samples (blue, n = 8).

3.4.4 mRNA profiling of CTCs

To further investigate the molecular signature of CTCs related to treatment resistance and study their association with treatment outcomes, CTCs were isolated from 13 patient samples for mRNA expression analysis. Using quantitative RT-PCR, a selected panel of 96 genes consisting of pancreatic cancer related genes, DNA damage- and cell cycle-related genes, and EMT related genes were used (Table 3.2). The quality of RNA was verified by the internal control, GAPDH, which was also used as a housekeeping gene for normalization purposes. The RNA expression data was analyzed using the comparative C_t method ($2^{-\Delta\Delta Ct}$) and correlated to PFS of patients with pancreatic cancer.

We evaluated the prognostic value of genes expressed in CTCs at after-chemo visit among 13 patients. Patients with low expression of BAX, a pro-apoptotic gene, had shorter/worse PFS (8.15 vs 14.7, P value= 0.050) (Figure 3.5); whereas the high expression levels of CHK1 and EZH2 are also associated with shorter PFS (7.55 vs 9.2, P = 0.043; 6.8 vs 9.6, P = 0.0023) (Figure 3.5).

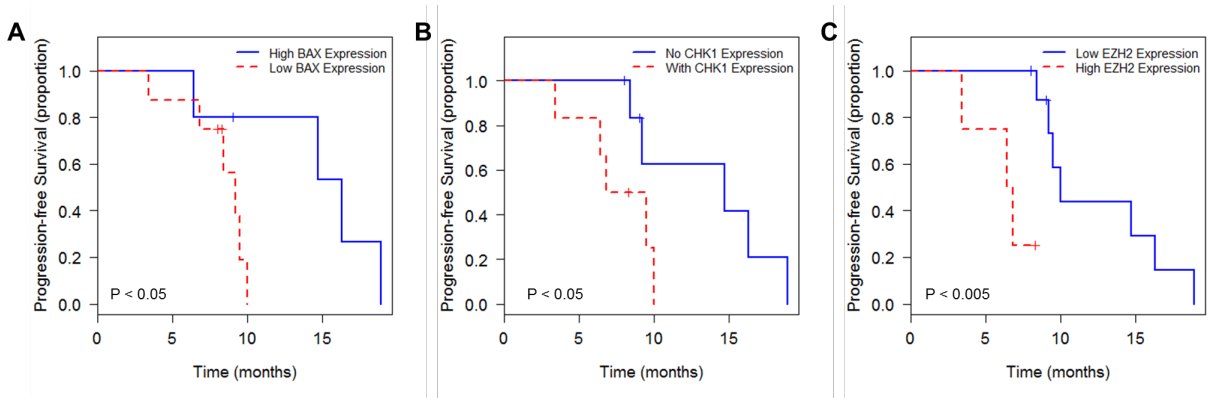

Figure 3.5 Kaplan–Meier life-table analysis of the PFS time for patient subgroups as defined by mRNA expression of different genes.
Kaplan–Meier life-table analysis of the PFS time for patient subgroups as defined by mRNA expression of BAX (A), mRNA expression of CHK1 (B), and mRNA expression of EZH2 (C). The P value is calculated by logrank test.

Table 3.2 The 96 gene panel for pancreatic CTCs.

CDH1	CD20	EZH2	JUN	WEE1	MCM10	PALB2	CDH1
KRT7	CD33	BMi1	MMP2	CCNE1	MYT1	TROP2	KRT7
KRT14	CD34	MUC1	MMP6	CCNE2	PARP1	COL1A2	KRT14
KRT20	CD3D	NES	TIMP1	CDK1	RB1	ANXA2	KRT20
MKI67	CD45	ATDC	KRAS	CDKN1A	FBXW7	ANXA10	MKI67
EPCAM	CD56	TWIST1	BRAF	CDKN2A	HSP27	RRM1	EPCAM
BAX	CD66b	ZEB1	cMYC	CHK1	HSP90	RRM2	BAX
BCL2	CD90	CDH2	CTNNB1	CTNNB1	HEY1	ERCC1	BCL2
BNIP3	PIK3CA	VIMENTIN	JUN	FBXW7	HIF1A	hCNT1	BNIP3
TYMP	MTOR	GLi1	MET	TP53	MSLN	SMAD4	TYMP
TYMS	AKT1	MUC1	STAT1	XRCC1	PDX1	TBX4	TYMS
DPYD	MAPK1	TGFB1	ABL1	ATM	CDA	MYT1	DPYD

3.5 Discussion

Patients with locally advanced pancreatic cancer, which are unresectable, are typically treated with chemotherapy with or without radiotherapy. However, the survival rate beyond 2 years is less than 10%. This poor clinical outcome has been closely associated with drug resistance [129]. Understanding the resistance mechanisms at the molecular level brings new

insights in designing new therapeutic strategies. Because these emerging therapeutic approaches target specific molecular abnormalities, molecular characterization of tumor cells has becomes critical for selecting appropriate therapy. Furthermore, since tumor cells can evolve and acquire resistance during treatment, monitoring tumor cells for the early assessment of treatment response is necessary to adapt therapy and limit toxicity in non-responding patients. The molecular analysis of circulating tumor cells (CTCs) holds potential as a 'real time' biomarker in monitoring treatment response and tumor progression and can potential guide the selection of personalized therapy.

In this study, we quantified the number of CTCs among locally advanced pancreatic cancer patients and analyzed changes in its protein and gene expression levels of specific markers in these CTCs to correlate with the outcome of the patients.

We first demonstrated that the CTC number tends to decrease during chemotherapy and that the reduction of CTC number after chemotherapy is associated with longer PFS. This is in agreement with previous studies in lung cancer showing that the decreases in CTC number were associated with better treatment response and prognosis [71], [72]. These results indicate that change in the number of CTC can be used as surrogate biomarker for evaluating the effectiveness of chemotherapy.

Standard chemotherapeutic drugs for pancreatic cancer such as gemcitabine and 5-fluorouracil (5-FU) eliminate cancer cells because of their DNA damaging properties [130]. γ-H2AX, a double-strand breaks (DSBs) has emerged as a biomarker to monitor the clinical response to DNA targeted therapies such as DNA damaging chemotherapy drugs, ionizing radiation or combinations thereof [118]. To evaluate the DNA damages in the tumors during treatment, we characterized CTCs using DNA damage marker H2AX in four patients. H2AX+

CTCs were detected at a low level (median 1 cell/ml). Interestingly, in the after-chemo sample of patient W126, CK-/H2AX+/CD45- cells were detected at a level of 45 cells/ml. As CK-/H2AX+/CD45- cells may be CTCs undergoing EMT, the elevated level of H2AX+/CD45- cells may indicate severe DNA damage in tumor cells during the treatment with Wee1 inhibitor and 5-FU. Indeed, so far this patient has the longest PFS among all patients (PFS 20.5 months without progression).

Because cytokeratin is down-regulated in mesenchymal cells, we may miss CTCs undergoing EMT if we use cytokeratin as the only marker. Furthermore, as EMT has been shown to induce resistance to treatment in pancreatic cancer [41], CTCs with EMT phenotypes may be important CTC subgroups to study. To investigate the EMT properties of CTCs, we characterized the vimentin expression of CTCs and identified three CTC subtypes: epithelial CTCs, intermediate CTCs, and mesenchymal CTCs. We observed the dynamic changes of the proportion of Vim+ CTCs (intermediate/mesenchymal CTCs), which greatly increased during the treatment. The persistence of high vimentin expression in CTCs in all samples during and after treatment is correlated with poor prognosis. We postulated that the abundance of Vim+ CTCs throughout the treatment might be an indicator of tumors undergoing EMT, which is a significant contributor to therapy resistance and leads to tumor progression.

Furthermore, we profiled the mRNA expression of CTCs using a 96-gene panel to identify additional molecular features with prognostic value in pancreatic cancer. For samples taken at the endpoint of chemotherapy, mRNA expression levels of three genes, BAX, CHK1 and EZH2 are associated with poor prognosis. BAX, a member of Bcl-2 protein family, is a pro-apoptotic gene that induces cell death. BAX expression has been found to be a stronger indicator of survival in pancreatic cancer [132]. As an important regulator of G2/M checkpoint, CHK1

inhibits CDC25 in response to DNA damage and induces cell cycle arrest to allow the repair of damaged DNA before cells enter mitosis [133]. In addition, CHK involves in homologous recombination for DNA repair. Thus due to its role in DNA damage repair, CHK1 have been shown to contribute to therapy resistance of DNA damage agents. EZH2 is a member of the polycomb group (PcG) proteins that involve in the epigenetic control of gene expression. EZH2 has been shown to play an important role in tumor growth, liver metastasis and cancer stem cell self-renewal activity in pancreatic cancer [134], [135]. Inhibitors for EZH2 and CHK1 and the induction of BAX have been shown to sensitize pancreatic cancer cells to chemotherapy agents and/or radiochemotherapy [119]. This is in concordance with our findings that the high expression of EZH2 and CHK1 and the low expression of BAX at the endpoint of chemotherapy correlate with shorter PFS. Thus our data support previous results in preclinical models, indicating that EZH2, CHK1 and BAX may be candidate therapeutic targets in treating pancreatic cancer [119]. Furthermore, because, as we have illustrated, detecting the expression of these genes during treatment is feasible, these genes could act as makers to predict and monitor the treatment response of chemotherapy for pancreatic cancer patients.

The major limitation of the current study is the small sample size. The prognostic value of CTCs should be further validated in a larger cohort. Moreover, a longer follow-up time might allow for better evaluation of the prognostic value of CTCs. We will follow these patients in long term for future analysis.

CHAPTER 4

4 Tunable Thermal-Sensitive Polymer-Graphene Oxide Composite for Efficient Capture and Release of Viable Circulating Tumor Cells

* This chapter was previously published as H. J. Yoon, A. Shanker, Y. Wang, M. Kozminsky, Q. Jin, N. Palanisamy, M. L. Burness, E. Azizi, D. M. Simeone, M. S. Wicha, J. Kim, and S. Nagrath, "Tunable Thermal-Sensitive Polymer-Graphene Oxide Composite for Efficient Capture and Release of Viable Circulating Tumor Cells," *Advanced Materials*, vol. 28, no. 24, pp. 4891–4897, Jun. 2016 [103].

4.1 Abstract

The rarity of CTCs poses huge technical challenges for its isolation and down-stream analysis. Immunoaffinity based technologies can harvest CTCs with high sensitivity and purity, but has the drawback of tethering cells within the device. Overcoming this limitation, a highly sensitive microfluidic system to capture circulating tumor cells from whole blood of cancer patients is developed. The device incorporates graphene oxide into a thermoresponsive polymer film to serve as the first step of an antibody functionalization chemistry. The LCST of around 13 °C for the polymer matrix made it possible to process blood through the device at room temperature. As the temperature decreases to around 5 °C, captured cells can be released for subsequent analysis such as standard clinical cytopathological and genetic testing. Over 90% capture efficiency and release efficiency is achieved. Released CTCs were viable and structurally intact, enabling subsequent analysis such as standard clinical cytopathological and genetic testing. To demonstrate the CTC capture and release in clinical samples, we processed blood samples obtained from 10 metastatic breast cancer patients and 3 pancreatic cancer patients.

CTCs were successfully recovered from 10 out of 13 samples (ranging from 2 to 20 CTCs mL−1). Furthermore, we examined the feasibility of detecting HER2 amplification by fluorescence in situ hybridization (FISH). CTCs released from the chip were made into "cell blocks" to perform FISH analysis and HER2 amplification was detected in CTCs isolated from one breast cancer patient. The downstream analysis facilitated by the efficient release of captured cells highlights the potential for this device's use in basic and clinical cancer investigation.

4.2 Introduction

With over 1600 people dying of cancer in the United States every day [120], the prevention of the second leading cause of death is a clear area of research interest in the medical community. The spread of tumor cells to distant locations in the body, or metastasis, is the cause of 90% of cancer related deaths [143], presenting an impetus for the study of those cells most responsible for cancer mortality. Circulating tumor cells (CTCs) are those cells shed from the primary tumor into the blood circulation, potentially en route to forming a secondary tumor, and are present at the incredibly low frequency of on the order of one in one billion normal blood cells in the peripheral blood of cancer patients [144]**.** CTCs can not only provide biological insight into primary and metastatic tumors but also have the potential to serve as real time biomarkers for making treatment decisions and monitoring drug efficacy [121]. Indeed, over 270 clinical trials have now been proposed using CTCs as surrogate biomarkers [122]. However, to date, CTCs have not been incorporated into clinical practice for management of patients with cancer. The main challenges to this field include: (i) reaching the sensitivity needed to isolate these extremely rare cells from the surrounding blood cells (1 in 1 billion), (ii) minimizing processing to preserve the viability of cells, and (iii) achieving the specificity necessary to acquire pure population to enable meaningful genomic and functional analysis.

Microfluidic technologies have emerged as a solution to isolate live CTCs from small amounts of blood collected from cancer patients. A common separation technique involves immunocapture, the tethering of an antibody against a CTC-specific marker to a surface or structure to bind CTCs but not the normal blood cells. Functionalized microposts have been used in a number of CTC isolation devices [10], [14], [23]. Antibody-functionalized silicon microposts for CTC capture were used in the first microfluidic device designed for this purpose, the CTC Chip [123]. Subsequent microfluidic CTC capture devices also featured microfeatures coated with antibodies, such as the geometrically enhanced differential immunocapture (GEDI) chip [148], chaotic micromixer HB CTC Chip [19], high throughput microsampling unit (HTMSU) [16] and the HD-CTC module of an integrated system [149]. These immunocapture devices included features fabricated from polymers such as polydimethylsiloxane (PDMS), poly(methyl methacrylate) (PMMA), and cyclic olefin copolymer (COC). In order to push the field to realize the opportunities afforded by these cells, which may be captured at early stage as well as mid-metastasis, orthogonal techniques and materials would be necessary to enhance the sensitivity. Nanomaterials provide one such avenue, with advantageous properties such as a high surface area to volume ratio and a length scale on the order of magnitude of extracellular features. Many different classes of nanomaterials have been incorporated into CTC research [23], [124]. One example, graphene oxide (GO) has a number of proven biomedical applications [125]-[127]. We have recently developed a graphene oxide (GO) based device, the GO Chip, that took advantage of the increased surface area afforded by graphene oxide for highly sensitive and selective cell capture [21]. Using this method, we were able to demonstrate the capture of CTCs from peripheral blood samples from pancreatic, breast, and early stage lung cancer patients with low white blood cell contamination. However, this device shares the common drawback across

most immunoaffinity based technologies reliant on antibodies attached to a surface: the limitation of post-capture analysis because of difficulty in releasing viable cells from the capture substrate.

Thermoresponsive polymers, a class of stimuli-responsive polymers that respond to temperature changes by undergoing conformational changes, have found wide applications in drug delivery, tissue engineering [128], controlling cell adhesion [129] and bacterial growth [130], protein encapsulation [131], and the release of captured CTCs from the surface of such capturing devices [132], [133]. Alternative CTC release techniques take advantage of alginate hydrogel [133], [134] or layer-by-layer assembled [161] degradable capture substrates. However, these approaches all feature performance limitations in throughput [134], purity requiring additional processing [18], ability to process blood collected by standard conditions,[133] immense fabrication facility requirements [18], [132], time-consuming chemistry [135], and inconvenient experimental temperature conditions [135].

Graphene- and graphene oxide (GO)-based polymer composites are a new class of materials which combine the excellent properties of graphene, such as high surface-to-volume ratio, high Young's modulus, and high thermal and electrical characteristics [136], with the easy processability of polymers. Such composites have found uses in fields ranging from energy storage [137] and electronic devices [138], [139], to biomedical applications such as drug and gene delivery [140], cancer therapy [141], cell differentiation [142], [143], coating of biomedical implants [144], [145], and bio-imaging [140].

We hypothesized that the combined advantages of a biocompatible functionalized nanomaterial with a thermoresponsive polymer that promotes effective cell release could address the challenge of sensitive capture while simultaneously allowing viable cell release. This could

lead to improvement in downstream analysis such as fluorescence *in situ* hybridization (FISH), molecular analysis, and single cell analysis. We present a new tunable thermal-sensitive polymer-GO Chip for highly efficient capture and subsequent release of CTCs incorporated into a microfluidic device (Figure 4.1A).

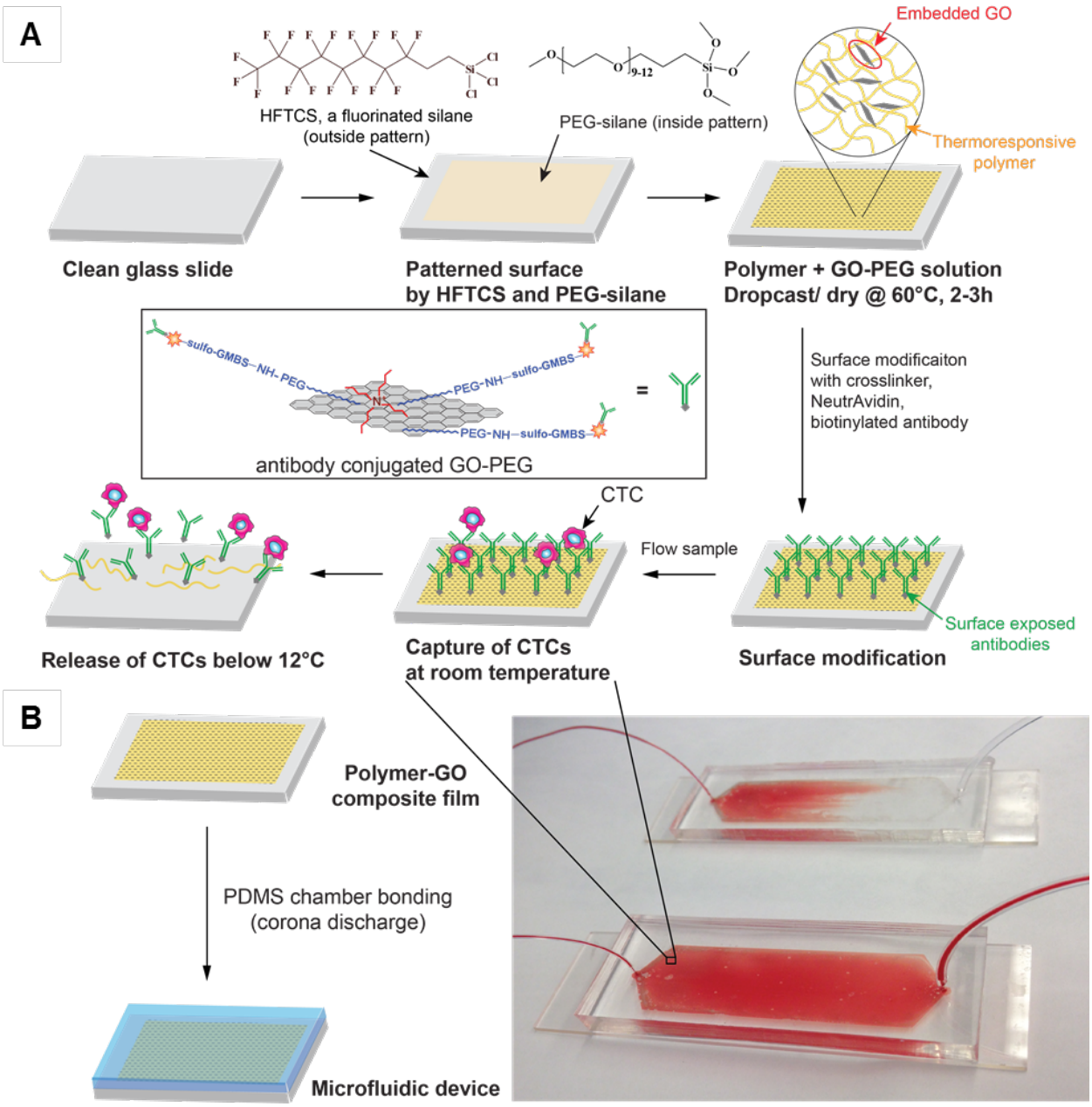

Figure 4.1 Schematic concept of a polymer-GO microfluidic device
(A) Schematic concept of a polymer-GO microfluidic device for the capture/release of CTCs. (B) Enclosure within polydimethylsiloxane chamber and photograph of patient blood samples being processed by the polymer-GO devices.

4.3 Materials and Methods

4.3.1 Polymer Synthesis

N-acryloyl piperidine was synthesized through reaction between acryloyl chloride and piperidine (Figure 4.1A) [146]. In short, 0.11 mol of piperidine and 0.12 mol of triethylamine were dissolved in 100 mL of dichloromethane maintained at 0-5^{o}C. A solution of acryloyl chloride (0.10 mol) in 15 mL of dichloromethane was added drop-wise to the above solution over 2 hours under constant stirring. After complete addition, the reaction mixture was stirred at room temperature for 24 hours and was extracted with water and purified by column chromatography (hexane:ethyl acetate, 1:1) to yield colorless to light yellow liquid. *N,N*-diethylacrylamide was passed through a basic alumina column prior to polymerization. AIBN was recrystallized from methanol before use. In a typical polymerization reaction, the required amount of monomers was dissolved in anisole and 0.3 mol% (of total monomer content) of AIBN was added to the solution. The reaction flask was completely sealed and the solution was purged with Argon for 20 minutes. The reaction was carried out at 65°C for 20 hours. After the reaction, all the solvent was evaporated at high temperature under vacuum to obtain white solid residue. The residue was re-dissolved in chloroform and then twice precipitated in ethyl acetate to obtain white solid mass. The precipitate was recovered and dried at 60°C under vacuum for 2-3 days.

4.3.2 Polymer Characterization

The synthesized polymers were characterized by gel permeation chromatography (GPC, Waters Inc., 1515 Isocratic HPLC pump and 2414 RI detector) using 3 Styragel columns- HR2, HR3 and HR4 in series maintained at 35^{o}C with chloroform as eluent (flow rate- 1 mL/min, total elution time- 40 min). The instrument was calibrated with polystyrene standards. LCST was ascertained by measuring UV-vis transmittance (Varian Cary 50 Bio) of a 0.1 wt.% aqueous solution of polymers as a function of temperature. A thermocouple was used for real-time

measurement of temperature, with the metal junction dipped in the cuvette during the measurement. For effective measurement, the polymer solution was cooled down to 2-3°C along with the metal cuvette holder to slow down the heating up of sample in ambient condition. $CaCl_2$ was placed inside the UV-vis spectrophotometer chamber to ensure humidity-free environment. This was necessary to prevent atmospheric water vapor from condensing on the cold cuvette walls. UV-vis spectrum was measured from 200-800 nm at every 0.2-0.5°C with more frequent measurements near the transition temperature. Transmittance at 400 nm was plotted against temperature and the temperature for 50% transmittance was noted as the LCST. Molecular weights and LCSTs of different polymer batches are noted (Table 4.1).

Table 4.1 Molecular weights, PDI, and LCST of different batches of synthesized polymers used in the study

Polymer	M_n (kDa)	M_w(kDa)	PDI	LCST (^oC)
P1	209.246	308.086	1.47	13.6
P2	151.332	253.380	1.67	12.7
P3	175.085	255.778	1.46	12.0
P4	173.019	303.009	1.75	11.8

Materials Kapton polyimide tape was purchased from Cole Parmer. Ethanol, acetone, chloroform, and isopropanol were solvent grade and were used without further purification. Surface modifying agents – (Heptadecafluoro-1,1,2,2-tetrahydrodecyl)trichlorsilane (HFTCS) and 2-methoxy(polyethyleneoxy)propyltrimethoxysilane (PEG-silane) – were purchased from Gelest Inc. Microscope glass slides were purchased from Fisher.

4.3.3 Device Fabrication

The glass slides were sequentially washed with chloroform, acetone, and isopropanol via sonication for 5 minutes each. The glass slides were then air dried and treated in a UV-ozone generator for 30 minutes to remove any carbon contamination and to obtain a high density of surface hydroxyl groups. The cleaned substrates were patterned using Kapton tape by masking the active device area. Kapton tape was chosen for its impermeability to silane vapors and good stability at high temperatures. The patterned substrates were then cleaned with wipes dipped in ethanol to remove any adhesive residue and treated with HFTCS via vapor phase surface modification at 100°C for 30 minutes. HFTCS treatment results in hydrophobic fluoroalkyl groups on the unmasked peripheral regions of the substrates which prevent the use of any physical confining barrier to pattern the device with polymer-GO film by drop-casting method. After HFTCS treatment, the Kapton tape mask was removed and the glass slides were washed with copious amounts of ethanol to remove any physisorbed silane as well as any adhesive residue. The second surface modification was done in liquid phase by immersing the glass slides in 3.35mM of PEG-silane in ethanol for 12-15 hours. Subsequently, the glass slides were again washed with ethanol to remove any physisorbed silane. A polymer-GO blend solution containing 10 mg/mL of polymer in 975 µL DMF and 25 µL of GO-PEG solution was then drop-casted in requisite amount on the surface modified glass substrates and allowed to dry at 60°C in an oven. The PDMS chamber was assembled on the glass substrate with polymer-GO composite film through corona discharge to produce a microfluidic device (Figure 4.2).

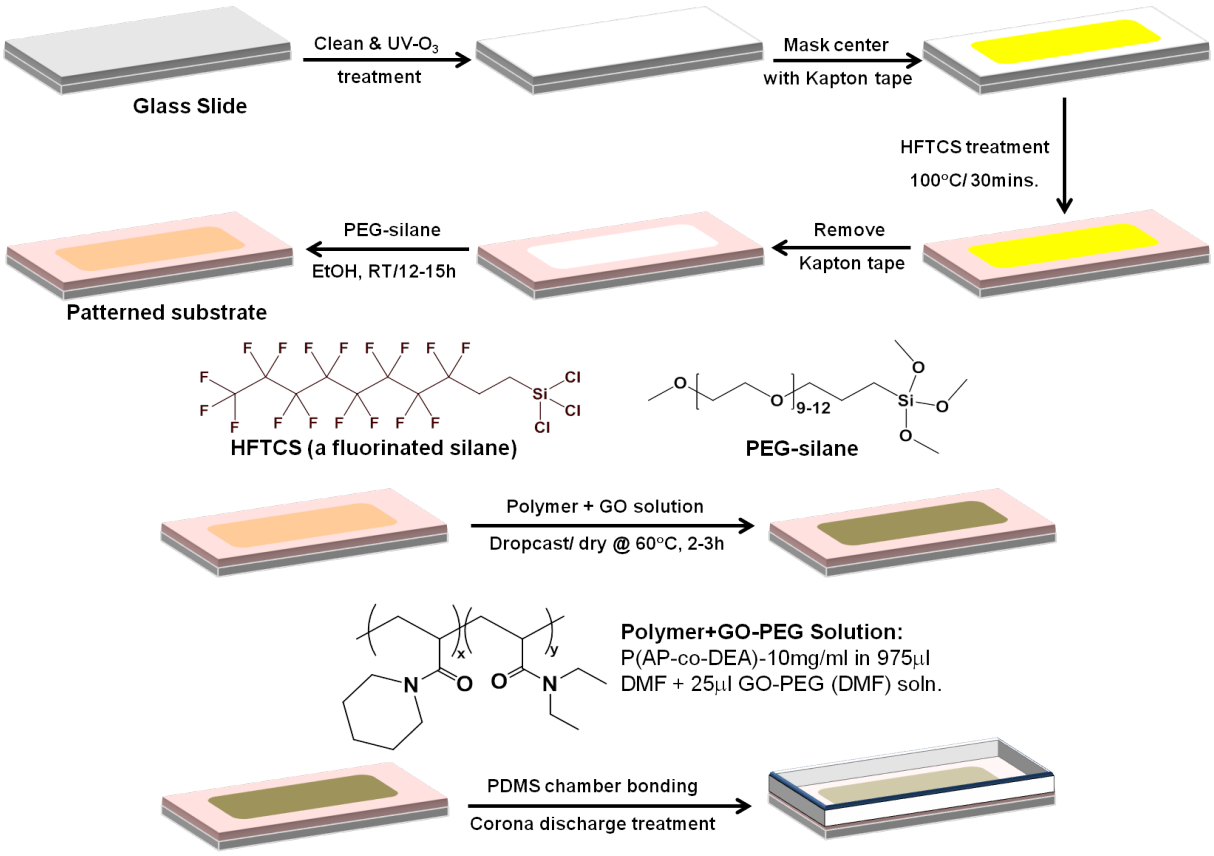

Figure 4.2 Schematic for CTC device fabrication

4.3.4 Fluorescent biotin assay

To verify the ability to immobilize biotinylated antibody to the polymer-GO film surface, surface coverage by a fluorescently labeled biotin (Biotin (5-fluorescein) conjugate, Sigma Aldrich) was assessed (Figure 4.3A). Three polymer-GO films underwent the entirety of the conjugation chemistry (i.e. treatment with the GMBS crosslinker and NeutrAvidin; termed "Condition") with fluorescent biotin addition as the terminal step. To account for non-specific binding, three polymer-GO films were treated only with the fluorescent biotin to serve as a control in an analogous fashion to an isotype control (termed "Control"). ImageJ was used to quantify the fluorescence. This technique showed a statistically significant increase in fluorescence intensity relative to the control (Figure 4.3B).

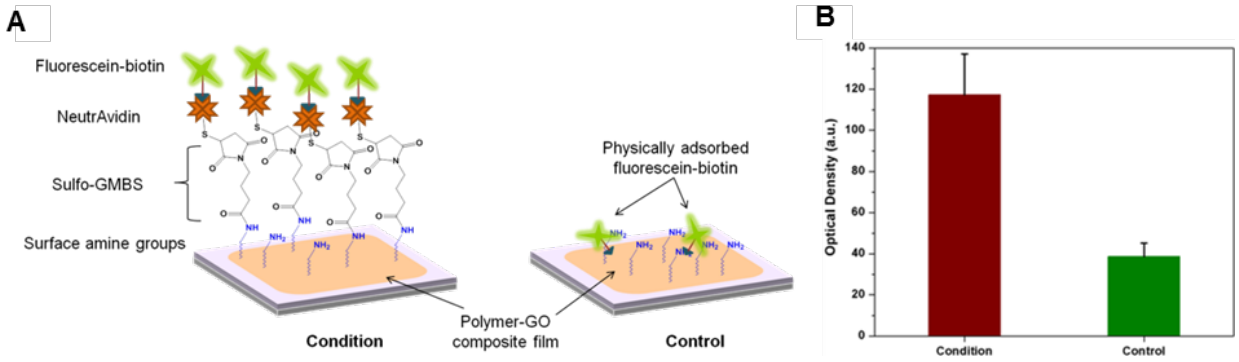

Figure 4.3 Fluorescent biotin assay to verify the immobilization biotinylated antibody. (A) Schematic represents fluorescent biotin assay and negative control. (B) The full conjugation chemistry features statistically higher fluorescence than the negative control as assessed via optical density ($p = 0.019$).

4.3.5 Cell labeling for optimization experiments

Cells were stained with CellTracker™ Green CMFDA Dye (ThermoFisher Scientific) according to the manufacturer's protocol. The staining process takes approximately two hours and was performed in parallel with device preparation.

4.4 Results

4.4.1 Thermal-Sensitive Polymer-Graphene Oxide Composite Synthesis

In the current work, the microfluidic device bottom substrate was coated with a composite film of functionalized GO dispersed in a matrix of thermoresponsive polymer with a lower critical solution temperature (LCST) of 13°C. Surface available functionalized GO (described below) provided anchors for attaching the CTC capture antibody while the polymer matrix provided temperature dependent modulation of capture or release functionality. The microfluidic assembly facilitated the processing of patient blood samples within a simple planar device (Figure 4.1B). Drop-casting the polymer-GO blend on a patterned and surface modified

substrate made such a device cheap and easy to fabricate. Moreover, the LCST of around 13°C for the polymer matrix made it possible to use the device at room temperature as opposed to higher temperatures [18], such that there are no concerns about inadvertently releasing the cells during the capture step. Additionally, cell release occurred under gentle conditions, maximizing the viability of released cells. The consolidation of the advantageous properties of GO-based capture with superior release functionality of the chosen polymer yielded a device that enables the study of these clinically interesting cells without many of the shortcomings of past technologies (Table 4.2), while simultaneously presenting an easy, scalable fabrication method.

Table 4.2 Comparison of CTC isolation technologies
Both commercially available and recently developed CTC isolation technologies are compared across multiple relevant metrics and abilities, showing the high versatility and performance of the technology put forth in this work. [21], [71], [146]-[151]

Table S3. Comparison of CTC Isolation Technologies							
Technology	**Approach**	**Flow rate mL/hr**	**Cell line capture efficiency**	**CTC detection in patient samples**	**Whole blood**	**Live cells**	**Release capability**
CellSearch	Anti-EpCAM coated magnetic beads	NA	>80%	34 out of 92 patients had ≥5 CTCs/7.5 mL in metastatic breast cancer[2], 21 out of 101 patients had ≥2 CTCs/7.5 mL in NSCLC[3]	No	No	NA
Epic Sciences	No enrichment, RBCs lysed blood deposited on slides	NA	NA	57 out of 78 in NSCLC[4], 22 out of 40 in melanoma[5]	No	No	NA
Mag Sweeper	Immunomagnetic capture	NA	62%	17 out of 17 in metastatic breast cancer[6]	Yes, need dilution	Yes	Yes
ISET	Size based filtration	NA	As low as 1 CTC per 1 mL of blood[7]	32 out of 40 in NSCLC[8]	No	No	NA
CTC iChip	Size based separation +ve or –ve selection with mag beads	9.6	>95% for –ve 78%-98% for +ve	37 out of 41 in CRPC[9]	Yes, not a single step	Yes	Yes
FACS Sorting	Surface marker based selection	Very Low	NA	3 out of 8 brain metastatic breast cancer[10]	Yes	Yes	Yes
RosetteSep kit	Depletion of WBCs	NA	NA	NA[11]	multiple steps	Yes	NA
CTC Chip	Positive selection	1	>87%	14 out of 19 in lung cancer[12]	Yes	Yes	No
GO Chip	Nano pillars with Graphene Oxide	1-3	>82.3%	7 out of 7 in breast cancer 8 out of 9 in pancreatic cancer[13]	Yes	Yes	No
Polymer-GO Release Chip	**Thermosensitive polymer-graphene oxide composite**	**1**	**>88.2%**	**8 out of 10 in breast cancer 2 out of 3 in pancreatic cancer**	**Yes**	**Yes**	**Yes**

To create a tunable thermal responsive polymer, copolymer poly(*N*-acryloyl piperidine-*co*-*N,N*-diethyl acrylamide) was synthesized via free radical polymerization using AIBN as an initiator and was characterized for its molecular weight and LCST (Figure 4.4A). LCST was modulated by employing a copolymerization technique using two acrylamide monomers with different degrees of hydrophobicity: *N*-acryloyl piperidine (AP) and *N,N*-diethyl acrylamide (DEA). The homopolymers poly(*N*-acryloyl piperidine) (PAP) and poly(*N,N*-diethyl acrylamide) (PDEA) have LCSTs of 4^{o}C and 25^{o}C respectively [152]. The required capture/release modulation temperature for the CTC device can be achieved by changing the ratio of the two monomers in the copolymer. For example, a copolymer synthesized with 7:3 molar ratio of AP:DEA showed a critical temperature of around 12-13^{o}C, which was used in this study (Figure 4.4B).

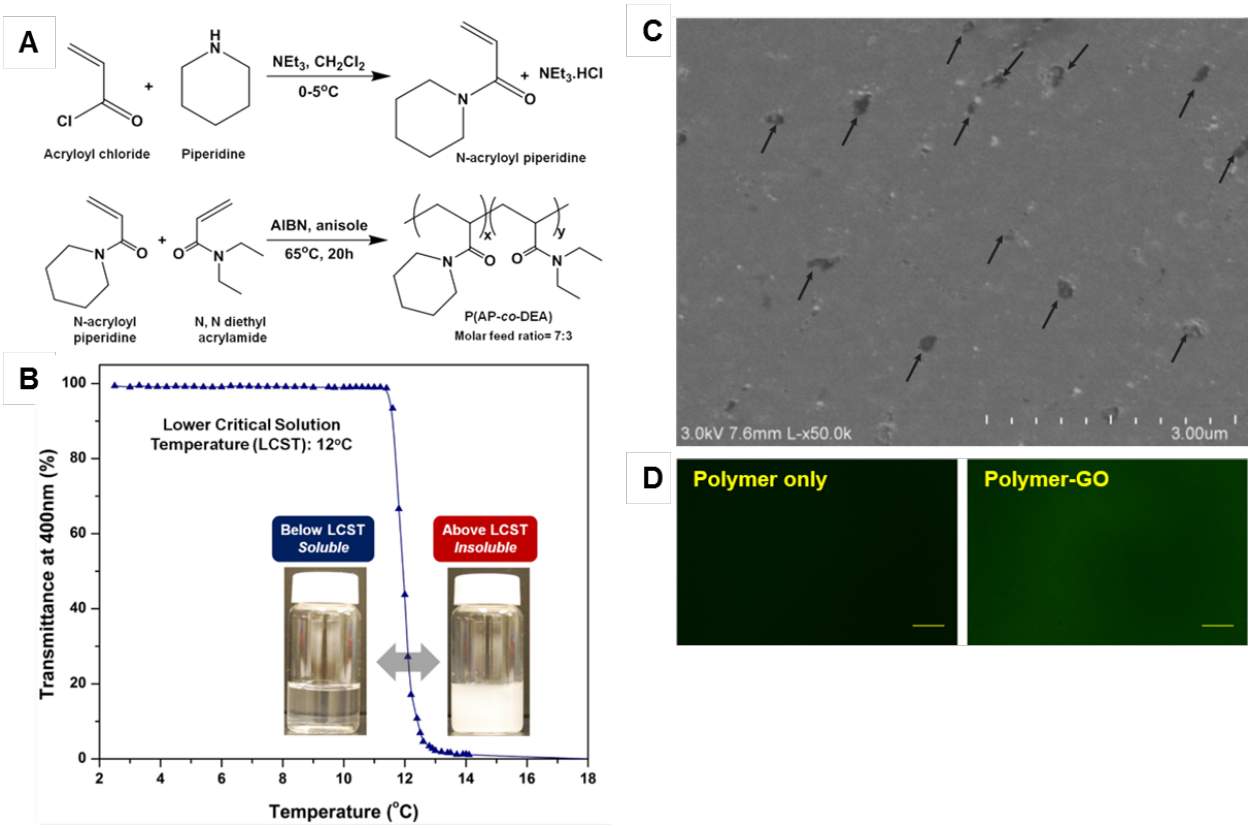

Figure 4.4 Polymer-GO composite
(A) Synthetic scheme for copolymer. (B) UV-vis transmittance vs temperature plots for different polymer batches. (C) SEM image of polymer-GO surface. Arrows indicate GO. (D) Fluorescence images of polymer-only and polymer-GO films. Dye incubation was done at 40°C. Scale bar: 20.0 μm.

4.4.2 Antibody Functionalization Chemistry

GO nanosheets were functionalized with phospholipid-polyethylene-glyco-amine according to an earlier reported method [21]. The polymer-GO nanocomposite films were prepared through drop-casting a DMF solution of polymer and functionalized GO. The drop-cast films were dried at 60°C in oven for 2-3 hours to yield 3-4 μm thick composite film. Figure 4.4C shows the SEM image of Polymer-GO composite surface. The polymer-GO microfluidic devices for cell capture and release were fabricated in two steps (Figure 4.2). Poly(ethylene glycol)

(PEG) is well known to render surfaces non-fouling [153]. The PEG monolayer was necessitated to avoid recapturing of the released CTCs on the glass substrate. In the first step, the polymer-GO composite film was deposited on a patterned and surface modified glass substrate followed by assembly with a PDMS chamber to form a microfluidic device. In the second step, the device was functionalized by immobilizing anti-EpCAM on the surface available GO through a cross-linker and avidin-biotin mediated bio-conjugation, providing cell capture/release functionality.

To show the surface availability of the amine groups from the GO-PEG in polymer-GO composite films, the drop-cast films were incubated with 0.25mM aqueous solution of an amine reactive dye, FSE (5-(and-6)-carboxyfluorescein, succinimidyl ester; Life Technologies (C1311)) for 30 minutes at 40°C and then washed with copious amount of DI water. The dye treated films were then imaged with fluorescence microscope (Olympus BX51 coupled with Olympus DP71 camera and EXFO X-cite Series 120 light source). While polymer-GO composite films showed bright green fluorescence from the surface tethered dye, polymer-only films showed very low to no fluorescence (Figure 4.4D). Though the possibility of physically adsorbed dye molecules cannot be completely ruled out, it is most likely that the dye molecules were primarily tethered to the surface through covalent bonding between the amine groups on film surface and succinimidyl ester groups on the dye, as suggested by large contrast in fluorescence intensity from polymer-GO and polymer-only films. Time dependence of dissolution of polymer-GO composite films in cold water was also determined. Dye treated films were dipped in cold water for different lengths of time and the fluorescence images before and after dipping were compared. Films were dipped in cold water (5°C) for 5, 10, 20, and 30 minutes, and in room temperature water (20°C) for 30 minutes. The beakers with the dipped films were kept on an orbital shaker to weakly simulate conditions in microfluidic devices where the films are

subjected to shearing by the flowing fluids. Figure 4.5 shows the fluorescent images of the films before and after dipping in water at 5°C.

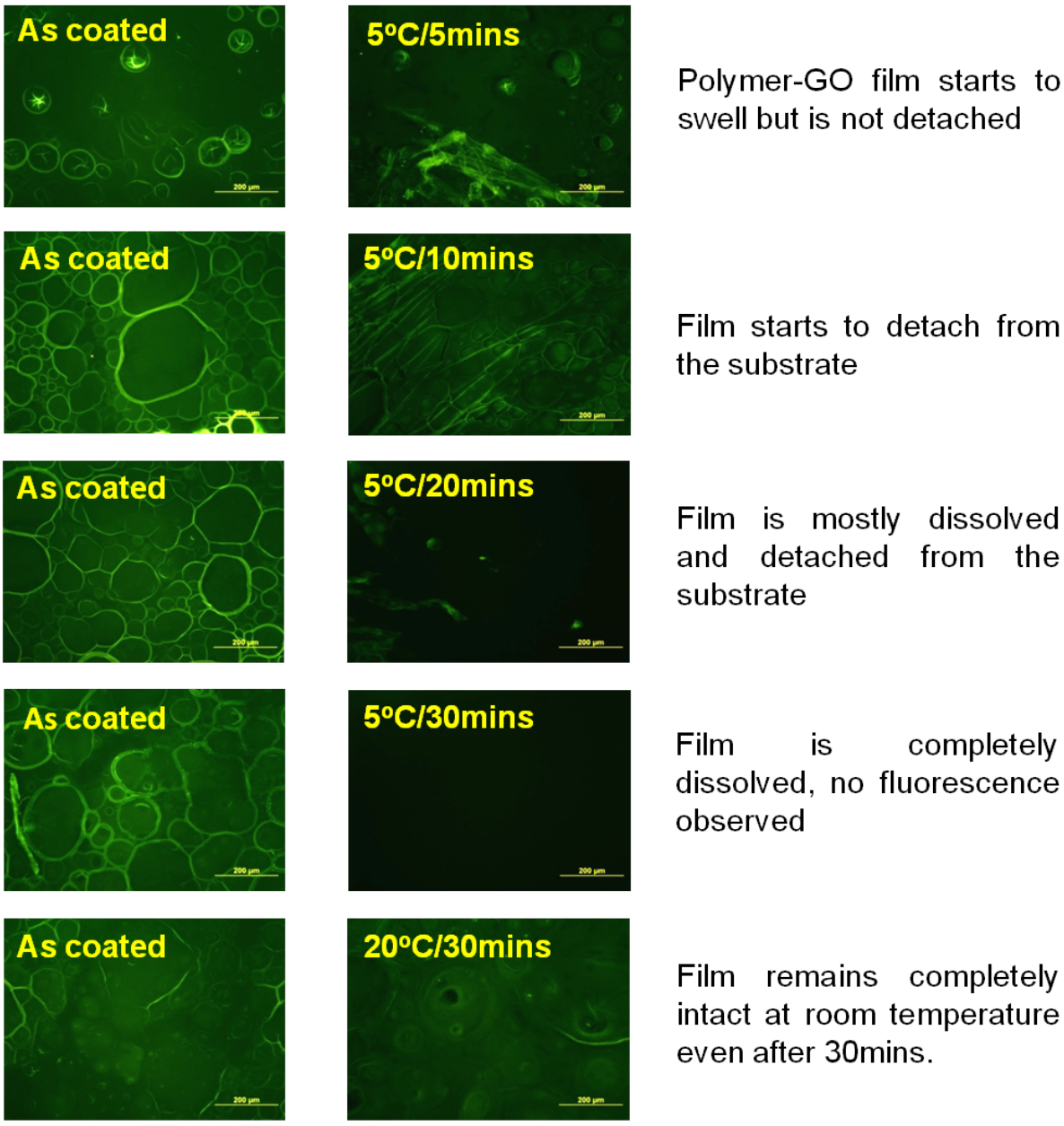

Figure 4.5 Fluorescence microscopy images of polymer-GO films in either cold (5°C) or room temperature (20°C) water.
Fluorescence microscopy images of polymer-GO films incubated with FSE dye before and after being dipped in either cold (5°C) or room temperature (20°C) water for the specified time durations. Scale bar: 200 μm

To verify the steps of the conjugation chemistry, experiments were performed to compare capture by (1) a polymer film lacking GO alone; (2) a polymer film lacking GO with the addition of anti-EpCAM; and (3) the polymer-GO film with full conjugation chemistry. The two control films showed significantly lower levels of capture with the polymer film and the polymer film with antibody capturing at 6.4% and 11.0% the level of the full chemistry, respectively (Figure 4.6A), with the increase in capture of the polymer with antibody condition a likely a result of physically adsorbed anti-EpCAM. This also suggests that very little of the capture antibody on the fully functional device is non-specifically bound.

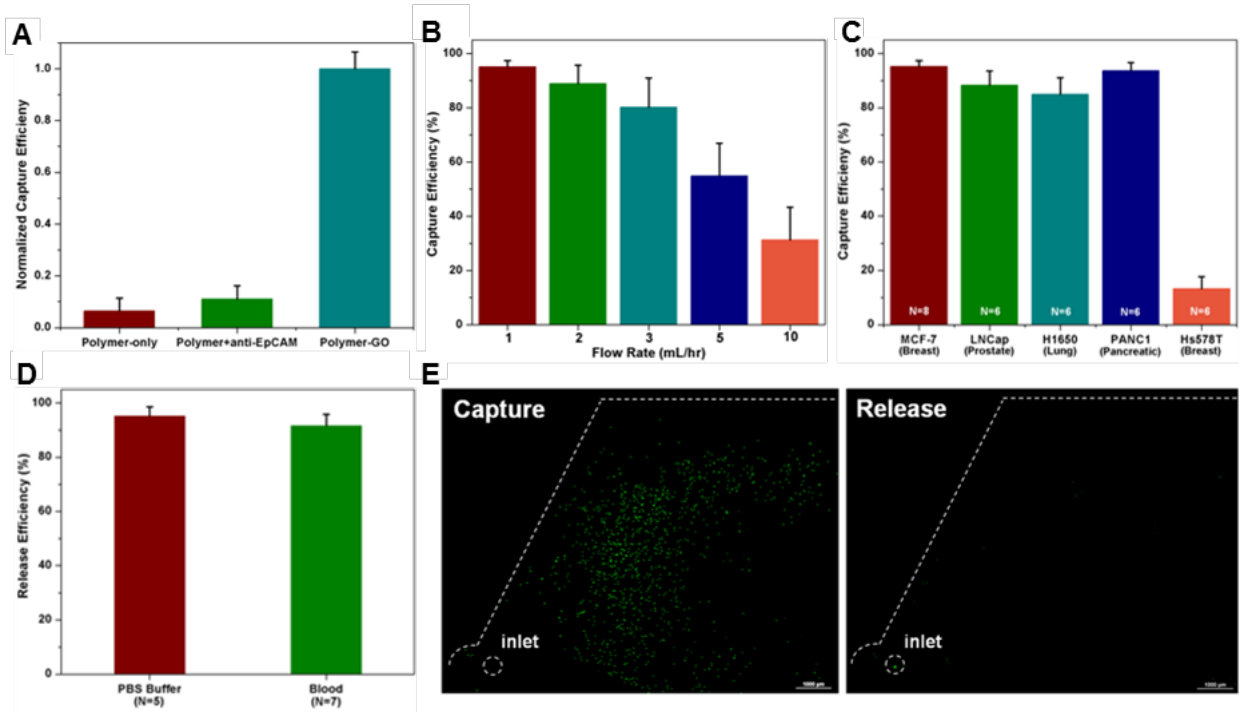

Figure 4.6 Cell Capture and Release Efficiency
(A) Capture efficiency of microfluidic devices featuring only the thermosensitive polymer, the thermosensitive polymer and non-specifically bound anti-EpCAM, and the polymer-GO film with specific conjugation chemistry as normalized by this last condition. (B) Cell capture efficiency of the microfluidic polymer-GO device at various flow rates evaluated using a breast cancer cell line (MCF-7). Error bars show standard deviations (n=6). (C) Capture efficiency of cell lines of varying origin and EpCAM expression levels. MCF-7 (n=8), PANC1, H1650, LNCaP, Hs578T (n=6). (D) Release efficiency of the microfluidic polymer-GO device (MCF-7 cells were spiked into 1 mL of buffer or blood). (E) Fluorescence microscope images of devices after capture and release (MCF-7).

4.4.3 Cell Capture and Release Efficiency

To test the performance of the GO-polymer device for CTC capture, fluorescence labeled human breast cancer cell lines MCF-7 cells (1,000 cells/mL) were spiked into buffer and flowed through the GO-polymer device at different flow rates (1-10 mL/hr). The captured cells in the device and the non-captured cells collected in the waste were then counted. As expected, the capture efficiency decreased with flow rate. We observed that the efficiency rapidly decreased at

flow rates ≥ 5mL/hr. In the 1–3 mL/h range, the average capture efficiency was over 88.2% (n = 6 at each flow rate) (Figure 4.6B) with the highest capture of 95.21% at 1mL/hr. To further investigate the effect of tumor type and EpCAM expression on capture efficiency, three high EpCAM expressing cell lines for various cancer types (MCF-7 breast cancer cells, LNCaP prostate cancer cells, and H1650 lung cancer cells), one low EpCAM expressing cancer-cell line (Panc-1 pancreatic cancer cells), and one EpCAM negative cancer cell lines (Hs578T breast cancer cells) were selected for capture experiments at the flow rate of 1 mL/hr. The cells were fluorescently labeled and spiked into buffer at a concentration of 1000 cells/ml. The results in Figure 4.6C indicate that the anti-EpCAM-coated GO-polymer device achieved high capture efficiency (84.93-95.21%) for EpCAM-positive cancer cells. In contrast, a relatively low number of EpCAM-negative cells (Hs578T) were captured. Furthermore, the device is comparably effective in capturing different tumor cells, indicating the robust sensitivity of the device. After capturing cells on the devices, cell release experiments were carried out by flowing 1 mL PBS through the devices in a room maintained at 5°C at 100 μL/min (Figure 4.6E). Quantification of the cells in the devices before and after release showed an average cell release of 95.21% and 91.56% in buffer and blood experiments, respectively (Figure 4.6D). The released cells are linked with GO nanosheets through the antibody-GO conjugation. Graphene oxide nanosheets have been demonstrated to have good biocompatibility and can enhance cell proliferation [154]. We tested the viability of the released cells by live dead assay, 91.68% of cells remained viable after release (Table 4.3). The high viability of released cells enables further cell expansion and functional experiments.

Table 4.3 Experimental results from Live/Dead assay (MCF-7).

Device	Live cells after release	Dead cells after release	Live/Dead (%)
D1	264	22	92.31
D2	353	7	98.06
D3	174	10	94.57
D4	270	35	88.52
D5	152	27	84.92
Average			91.68

4.4.4 CTC Isolation and Analysis from Clincial Samples

To demonstrate the CTC capture and release in clincial samples using the tunable polymer-GO composite film based device, we processed blood samples obtained from 10 metastatic breast cancer patients and 3 pancreatic cancer patients. Whole blood samples collected into EDTA tubes were processed at a flow rate of 1 mL/hr. Following a washing step, cells were released from the chip and deposited/spun onto glass slides by a cytospin centrifuge. CTCs in these samples were identified as DAPI-positive (shown in blue) nucleated cells staining positive for tumor markers (cytokeratin 7/8, visualized with a secondary antibody tagged with Alexa Fluor 546, shown in red) and negative for leukocyte markers (CD45, visualized with a secondary antibody tagged with Alexa Fluor 488, shown in green) (Figure 4.7A, B). CTCs were successfully recovered from 8 breast cancer patient samples and 2 pancreatic cancer patients

(ranging from 2 to 20 CTCs/mL) (Figure 4.7C). The average number of CTCs recovered from breast samples was 5.6 CTCs/mL and from pancreatic samples was 8.3 CTCs/mL.

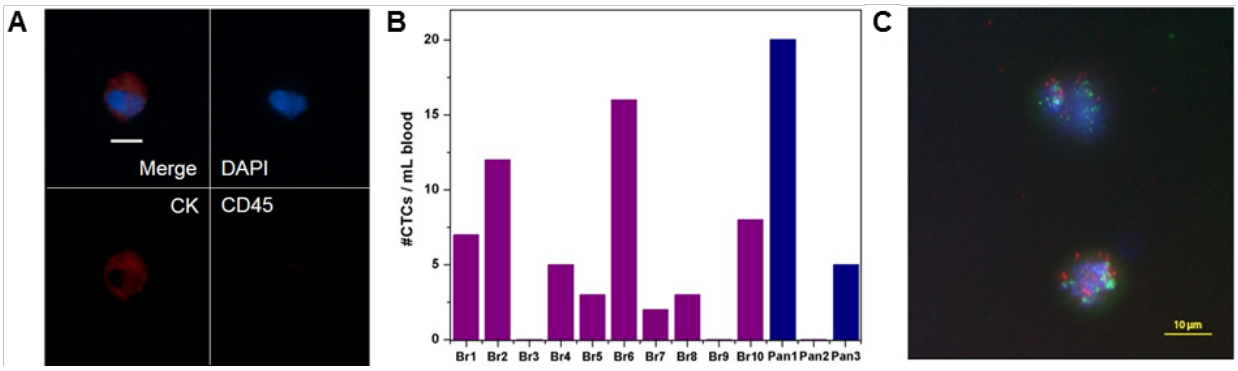

Figure 4.7 CTC isolation and analysis from clinical samples
(A) Fluorescence images of CTCs from breast cancer patient sample. Nucleated cells (blue) staining positive for cytokeratin 7/8 (red) and negative for the white blood cell marker CD45 (green) were enumerated as CTCs. Scale bar = 10 µm. (B) CTC enumeration results from 10 breast cancer patients and 3 pancreatic cancer patients. (C) Fluorescence *in situ* hybridization (FISH) image of CTCs of breast cancer patient sample Br10. HER2 (green)/centromere 17 probe(red).

Released CTCs were viable and structurally intact, and hence could be readily investigated via standard clinical cytopathological and genetic testing. Here, we examined the feasibility of detecting HER2 amplification by fluorescence *in situ* hybridization (FISH). CTCs released from the chip were subsequently made into "cell blocks" by first fixing them with ethanol and then embedding them in Histogel (Thermo Scientific). Blocks were then formalin fixed and stored in 70% ethanol until slide preparation. Blocks were paraffin embedded and sectioned at the University of Michigan Histology Core. FISH was conducted using probes for HER2 (BAC clone RP11-94L15) and chromosome 17 control probe (BAC clone RP11-100E5), revealing HER2 amplification in one breast cancer patient (Figure 4.7D). FISH hybridization and image capture were performed essentially as previously described [155]. One green signal

indicates the presence of one copy of HER2, while one red signal indicates one copy of centromere 17 probe; the multiple green signals in the figure imply HER2 amplification.

The downstream analysis facilitated by the efficient release of captured cells highlights the potential for this device's use in basic and clinical cancer investigation. Through the incorporation of a composite that combines the advantages of a temperature-sensitive modality and sensitive nanomaterial-enabled capture, the polymer-GO film that serves as the basis of this technology overcomes some of the key shortcomings of previous CTC capture technologies (Table 4.2). As evidenced by data obtained from physiologic solutions containing spiked labelled cancer cells from multiple cancers and the processing of primary breast and pancreatic cancer patient blood samples, isolation of these rare cells with this device is highly feasible, completing the first step to unlocking the research opportunities presented by CTCs.

4.5 Conclusion

Compared with other CTC isolation strategies, immunoaffinity based technologies harvest CTCs with high sensitivity and purity [156], but has the drawback of tethering cells within the device. Overcoming this limitation, we are able to collect viable and intact CTCs in suspension after immunocapture, making it ideal for various downstream analysis that requires the high integrity and purity of the targeted cell population, such as genotyping and single cell profiling. This advanced analysis of CTCs could become a 'real-time' indicator to develop personalized therapy, as well as to bring valuable insights into the mechanism underlying cancer metastasis. Due to the low cost and ease of fabrication, this technology is scalable for commercialization. Future study will optimize it for large-scale clinical study and investigate its clinical utility for therapeutic marker discovery, treatment selection, and management.

CHAPTER 5

5 ^{HB}GO chip for High Throughput Circulating Tumor Cell Isolation

5.1 Abstract

To improve the throughput for CTC isolation, we incorporated a herringbone mixer to the existing GO chip. We further optimized the design of the herringbone mixer to maximize the collision of cells with the substrate of microchannels, resulting in a herringbone (HB) GO chip (^{HB}GO chip) for efficient CTC capture at high flow rate. The grooved-herringbone mixer consists of repetitive mixing units, each of which has a set of twelve chevrons staggered asymmetrically with another set of twelve chevrons. The average cell capture efficiency for the unmodified GO Chip dramatically dropped below 70% at 50 and 100 μL/min, and further decreased below 50% at 200 μL/min, whereas the ^{HB}GO Chip maintained a target yield of > 80% up to 200 μL/min with no significant decrease in overall capture efficiency. Moreover, up to a flow rate of 200 μL/min, > 90% of cells were viable, which is equivalent to the cell viability at lower flow rates. We further analyzed the spatial distribution of the cells captured on the chip surface and investigated the correlation between the channel length and flow rates at different capture efficiencies (60%, 70% and 80%). At the flow rate ranging from 50 to 200 μL/min, there is a strong linear relationship between flow rate and the required channel length to achieve a specific capture efficiency.

5.2 Introduction

Metastasis is responsible for over 90% of cancer-associated death. It is widely accepted that the development of metastatic disease is mediated by circulating tumor cells (CTCs) that are shed from the primary tumor and circulate through the bloodstream of cancer patients. Consequently, CTCs holds great potential to act as a biomarker in the area of predicting disease progression, real-time monitoring of tumor status, and identifying novel therapeutic targets. However, CTCs are rare with a frequency of only 1-10 present in one mL of patient blood surrounded by billions of blood cells, which poses significant challenges for CTC isolation and analysis.

Microfluidic technologies have emerged as a solution to isolate CTCs as they provide large surface area-to-volume ratio and high precision flow control. Many microfluidic devices have been developed based on the immune-affinity based capture strategy, which takes advantage of proteins expressed on the cell membrane of CTCs but not on blood cells resulting in a high-purity isolation. Antibodies against antigens of tumor cells, such as the epithelial cellular adhesion molecule (EpCAM), are tethered to the surface of the microfluidic channels to capture CTCs. However, one major drawback of immune-affinity based capture devices is the low throughput, typically ranging from 1 to 3 ml blood per hour, which limits the blood volumes that could be analyzed. Small blood volume used for CTC analysis results in a statistical variability associated with rare event detection [88] and may fail to capture the inherent heterogeneity of CTCs.

We have previously developed a nanomaterial based microfluidic device, the GO chip, which consists of a microfluidic chamber and a substrate coated with graphene oxide (GO) nanosheets where the antibodies are tethered [21]. The throughput of the GO chip for processing

blood samples is only 1mL/hr. This is because that under laminar flow condition within microchannels, cells follow streamlines and have minimal diffusion across the flow channel. Under high flow rates, cells are likely to flow out of the chamber without being in close proximity with the antibodies coated on the substrate of the GO chip (as shown in Figure 5.1A). Therefore, to improve the throughput of the current GO chip, we need to design a structure to disrupt the streamlines and maximize the interactions of cells with the antibody-coated substrate of the microchannels.

Herringbone micromixer, which incorporates arrays of herringbone-like micro-structures, can enhance the transverse flow and generate chaotic mixing in microchannels [188]. The geometries of the herringbone micromixer has been studied to maximize and direct the cell - surface interactions [189]. The incorporation of herringbone structure into several CTC isolation platforms has generated high capture efficiency at a relatively high throughput [19], [79], [157]. However, different from most of the devices in which antibodies are coated on both the bottom and the walls of microchannels, the GO chip needs to be engineered in a way that the flow pattern directs the cells to the substrate where the antibodies are present.

Herein, we optimized the design of the herringbone-mixing channel to maximize the collision of cells with the substrate of microchannels and developed a herringbone GO chip (HBGO chip) for high throughput CTC capture.

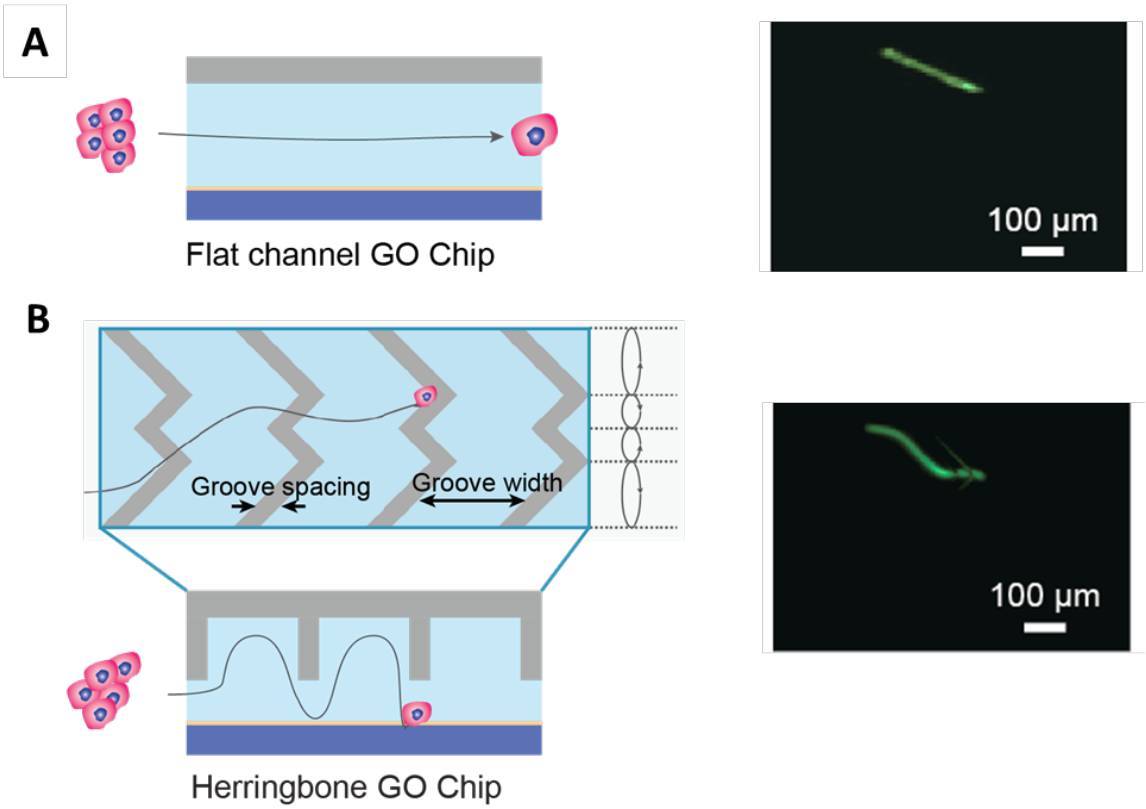

Figure 5.1 Design rationale of the ^{HB}GO-CTC Chip
Schematic illustration and time elapse fluorescent image of the trajectory of cell flowing through the GO chip (A) and the ^{HB}GO chip (B).

5.3 Materials and Methods

5.3.1 Fabrication of System Manifold and ^{HB}GO-CTC Chip

The design of the system manifold was created by CAD software (Solidworks) and fabricated using a high-resolution 3D printer (Projet 3500 Max). An acrylic based resin, M3 crystal, was used for the printing process for its mechanical integrity and biocompatibility. Each component including the pump, heparin injector, power source, and micro controller were placed in the designated compartment and enclosed. The production of the ^{HB}GO-CTC Chip involved two separate processes. First, to fabricate the chip substrate, Cr and Au was evaporated onto a 4-inch silicon dioxide wafer and patterned. The wafer was then diced into individual pieces. Next, to fabricate the PDMS (polydimethylsiloxane) structure, a silicon master mold was created by standard photolithography. Negative photoresist (SU-8 2050, MicroChem) was patterned on a 4 inch bare silicon wafer using two separate masks: one for the main fluidic channel (40 μm height) and the other for the herringbone grooves (60 μm). The height of each layer was measured after each process with a surface profilometer (Veeco Dektak 6M). PDMS pre-polymer mixed with cross linkers at a 10:1 weight ratio was poured onto the mold, degassed, and baked in an oven at 65°C for 24 hours. The cured PDMS structure was then carefully peeled off and cut. At last, two through holes were punched at both ends of the channel to feed and connect tubing.

5.3.2 ^{HB}GO-CTC Chip Assembly and Surface Functionalization

To chemically modify the chip surface, tetrabutyl ammonium hydroxide intercalated GO nanosheets grafted with phospholipid-polyethylene glycol-amine were prepared and assembled on the gold patterned silicone dioxide substrate as described previously [21]. [103]. The substrates and PDMS replicas were subjected to oxygen plasma treatment and bonded to form the final device. N-γ-maleimidobutyryl-oxysuccinimide ester (GMBS) was flowed through the chip using a syringe pump (Harvard apparatus) and incubated for 30 min. The chip was then flushed with 70% ethanol to pre-sterilize the inner chamber wall. Subsequently, neutravidin and biotinylated anti-EpCAM antibody was introduced followed by 3% bovine serum albumin (BSA) to block the remaining binding surface.

5.3.3 Cell Culture and Labeling

Human epithelial breast cancer cell line MCF-7 was purchased from the American Type Culture Collection (ATCC, LGC Standards). MCF-7 cells were cultured at 37°C with 5% CO_2 and maintained by regular passage in complete media consisting of Dulbecco's Modified Eagle's Media (DMEM) with 10% fetal bovine serum (FBS) and 1% penicillin-streptomycin solution (GIBCO®, Life Technology). When cells reached a confluency of 70-80%, they were collected and fluorescently labeled with green cell tracker dye (Invitrogen, CellTracker Green CMFDA, C7025) for cell capture experiments.

5.3.4 Cell Viability Assay

To measure cell viability after processing samples through the ^{HB}GO CTC-Chip, a live/dead viability/cytotoxicity assay kit (GIBCO®, Life Technology) was used. The chip was

washed with 1× PBS (phosphate buffered saline, GIBCO®, Life Technology) after capturing the cells. Subsequently, a live/dead reagent consisting of calcein AM and ethidium homodimer-1 was prepared according to the manufacturer's instruction and applied. Following 30 min incubation, cells were imaged and manually counted under a fluorescent microscope for quantification.

5.4 Results and discussion

5.4.1 Design of ^{HB}GO CTC-Chip

The ^{HB}GO-CTC Chip consists of a 24.5 × 60 mm silicon dioxide substrate with gold patterned thin film layer bonded to a polydimethylsiloxane (PDMS) structure containing four bifurcating microchannels with herringbone grooves embedded on their top surface. Functional GO nanosheets are assembled onto the gold layer presenting high density of anti-EpCAM antibodies on the substrate surface through chemical cross-linkers (Figure 5.2A). The geometry of the herringbone structure has been determined based upon previous designs used for chaotic mixing at low *Re* number (laminar flow). However, in order to maximize the cell to substrate contact frequency, unlike early devices where the interaction mainly takes place near the grooves, several modifications have been applied for optimization.

The grooved-herringbone (HB) mixer consists of repetitive mixing units, each of which has a set of twelve chevrons staggered asymmetrically with another set of twelve chevrons. (Figure 5.2B). The distribution of these points where a vertical drag force is induced by adjacent micro vortexes increased the chance for cells to be directed toward the antibody coated substrate. The dimension of the groove height, width, and spacing was also adjusted to decrease the hydraulic resistance in the groove. This unbalanced resistance between the channel and grooves

increased the overall fluidic circulation by deflecting a significant portion of fluid and cells into the groove, and subsequently, improved the interactions of cells with the channel bottom when cells exit he grooves. Cells flowing through the herringbone moved in a zigzag trajectory until captured which increased its traveling time and distance within the chip (Figure 5.1B). Forbes *et al.* demonstrated that the ratio of the groove width and the groove spacing has a significant effect on the pattern and frequency of particle-surface interaction[191]. The simulation results showed that when the groove width increased to over 3 times of the groove spacing, the hydraulic resistance in the groove decreased significantly, allowing for a large portion of the particles in the fluid to enter and flow along the grooves. Therefore, the groove width was selected to be four times of the groove spacing to maximize the surface contact of the streamlines with the channel bottom for high-performance cell capture (Figure 5.2B). The final dimension of the PDMS structure was as followed: overall height of the main fluidic channel was 40 μm, with a groove height set to 60 μm; the groove pitch and width was 200 and 160 μm respectively and the angle between the chevrons was 45°.

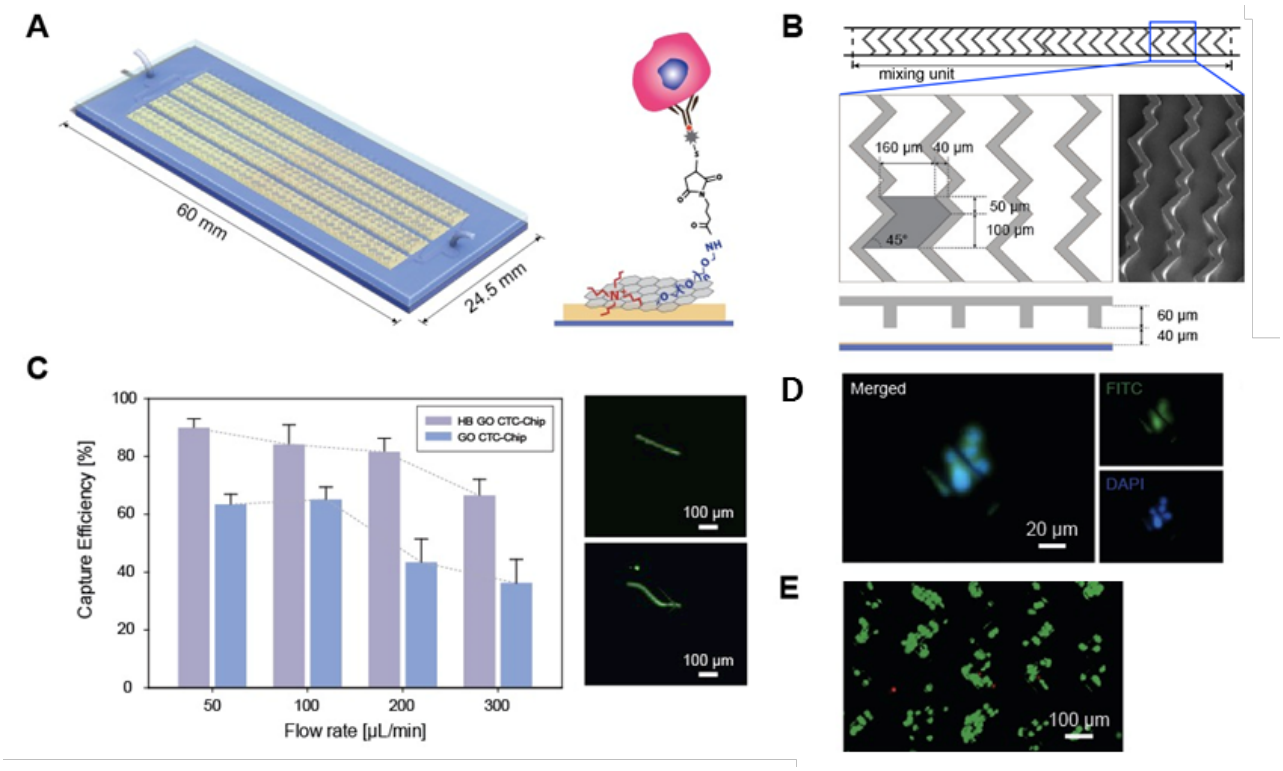

Figure 5.2 Characterization of the ^{HB}GO-CTC Chip
(A) Schematic of the chip demonstrating the device dimension and the surface chemistry. (B), the layout of the herringbone structure with detailed parameters and SEM image illustrating the structure of the herringbone grooves. (C), Comparison of the CTC capture efficiency using the GO-CTC chip and ^{HB}GO-CTC Chip. Time elapse fluorescent image showing the trajectory of cell with in the two chips. (D), Cluster of tumor cells captured on the chip, labeled with green cell tracker dye and stained with a nuclear stain (DAPI). (E), the viability of tumor cells captured on the chip at 200 µL/min using LIVE/DEAD assay, live cells stained with Calcein-AM (green) and dead cells with EthD-1 (red).

5.4.2 Evaluation of ^{HB}GO-CTC Chip by Capture of Cancer Cell Lines

To validate the performance of the ^{HB}GO-CTC Chip for CTC capture at high flow rates, a flat chamber GO-CTC Chip previously reported was used for comparison. Human breast cancer cell-line, MCF-7 cells were labeled with a fluorescent cell-tracker dye and spiked into 5 mL of PBS buffer solution with a concentration of 50-200 cells/mL. After processing the samples, both cells captured on-chip and non-captured cells collected in waste were counted to calculate the capture efficiency. At a flow rate of 1 mL/hr (16.67 μL/min), where most affinity based microfluidic devices operate, the GO chip showed high capture efficiency (mean yield > 90%) [21]. However, at higher flow rate, the average cell capture efficiency for the GO-CTC Chip dramatically dropped below 70% at 50 and 100 μL/min, and further decreased to below 50% at ≥200 μL/min. In contrast, the ^{HB}GO-CTC Chip maintained a target yield of > 80% up to 200 μL/min with no significant decrease in overall capture efficiency which indicates that the herringbone mixer improved cell surface interaction (Figure 5.2C). The drop of capture efficiency of GO chip at high flow rate is due to two reasons: (1) the reduced resident time that the cells flow through the chip; (2) the increased shear force to overcome the cell adhesion force or disrupt adhesion bonds [158]. Whereas, The ^{HB}GO-CTC Chip achieves high capture efficiency up to 200 μL/min because of the improved interactions of cells with the channel bottom and the increased resident time of cells moving in the zigzag trajectory.

In addition, cell viability was assessed at different flow rates to determine the effect of shear force induced by increasing flow rates during the isolation process. Cell viability was one of the critical factors as low viability could adversely affect further downstream analysis of the captured cells. Greater than 90% of cells remained viable at the flow rate of 200 μL/min (Figure 5.2D). Moreover, majority of cell aggregates spiked into buffer to mimic CTC clusters preserved

their shape and were intact upon isolation. However, at 300 μL/min, the high shear stress results in the significant decrease of the cell viability (70%) and the dissociation of cell aggregates.

The spatial distribution of the captured cells along the channel was also analyzed by dividing the flow chamber of the chip into ten areas (the length of each area is 5mm) (Figure 5.3A). At a flow rate of 50 μL/min, a wide spread distribution was observed in the GO Chip, whereas most cells were captured near the inlet of the ^{HB}GO Chip. Over 70% were captured within the first 20% of the device. When the flow rate increased to 300 μL/min, the location of these cells became more scattered along the chip resulting in a mean yield of <70%. We further investigated the correlation between the minimum required length of the channel and the flow rates at different capture efficiencies (60%, 70% and 80%) (Figure 5.3B). At the range of 50 ~ 200 μL/min, a strong linear relationship between the flow rate and the required channel length to achieve a specific capture efficiency was observed (Figure 5.3C). We speculated that the channel length increased linearly in order to compensate for the reduced duration that cells interacts with the substrate per unit length at higher flow rate. However, as the flow rate increased from 100 μL/min to 300 μL/min, the required channel length appeared to increase exponentially to achieve a capture efficiency of 60%, which may be caused by the increased shear disrupting the antigen-antibody bonding, in addition to reduced residue time. These results provide us rationale for optimizing the chip geometry and selecting the proper flow rate. For instance, at the flow rate of 50 μL/min, the channel length could be decreased to 30 mm to achieve 80% capture efficiency while minimizing possible cell damages caused by shear stress. Higher flow rates could be achieved by increasing the width of the channels or by stacking multiple chips together.

As only a few data points are available, the interpretation of graphical data may be adversely affected by random errors in experiments. For future study, the relationship between

channel length and flow rate will be further investigated using a single unit cell of the ^{HB}GO chip, which is 1/4th the width and twice the length of the original chip. Due to the difference in scale, the flow rates tested in the unit cell should be 1/4th of those in the full size ^{HB}GO chip. The capture efficiency and the distribution of captured cells along the chip will be characterized at the flow rate ranges from 10 to 100 µL/min.

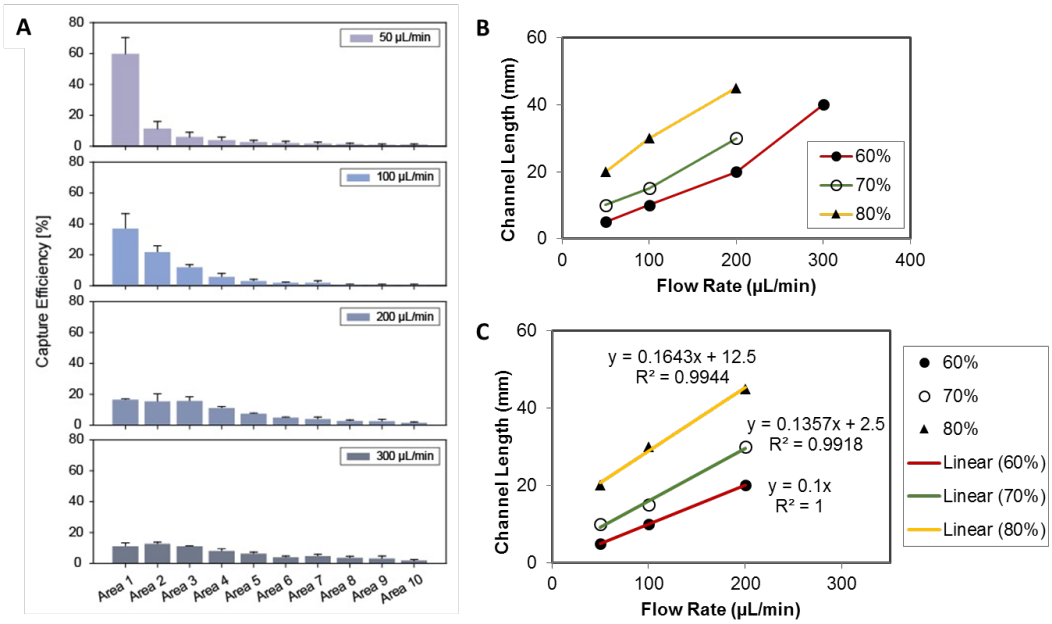

Figure 5.3 The spatial distribution of the cells captured on the ^{HB}GO-CTC Chip
(A), Spatial distribution of the captured CTC captured along the channel. (B), The relationship between the minimum required channel length and the flow rate at different capture efficiencies (60%, 70% and 80%). (C), The linear relationship between the flow rate and the required channel length to achieve a specific capture efficiency (60%, 70% and 80%).

CHAPTER 6

6 Conclusions

6.1 Summary of Research

6.1.1 Monitoring dynamic changes of PD-L1 (+) CTCs during radio(chemo) therapy in NSCLC

The feasibility of monitoring dynamic changes of PD-L1 (+) CTCs is demonstrated among 12 NSCLC patients undergoing radiation or radiochemotherapy. CTCs were detected in all 36 samples (100%), and PD-L1 (+) CTCs were detected in 24 samples (66.7%). After the initiation of radiation or radiochemotherapy, the proportion of PD-L1 (+) CTCs in total CTCs increased significantly, indicating the upregulation of PD-L1 expression in tumor cells during radiation. This validates previous findings in preclinical models that PD-L1 expression in the tumor environment increased after the initiation of radiation, which provides a rationale for the combination of anti-PD-1/PD-L1 immunotherapy and radiation therapy. In addition, patients who were PD-L1 positive (> 5% of CTCs stained with PD-L1) at baseline had shorter PFS time, suggesting that PD-L1 expression in CTCs may have prognostic value among non-metastatic NSCLC patients.

6.1.2 Investigating the potential of CTCs for monitoring tumor status and predicting treatment response in locally advanced pancreatic cancer

CTC isolation and analysis may act as a 'real time' biomarker to monitor treatment response for pancreatic cancer patients. In this study, CTCs were isolated via the GO chip from blood samples taken at different time points during the course of chemotherapy and subsequent radiation therapy among 26 patients with the locally advanced pancreatic cancer. Either the increase of CTC number after chemotherapy or the persistence of high expression of Vimentin in CTCs throughout the treatment course is correlated with poor prognosis. In mRNA profiling of CTCs, the expression levels of three genes, BAX, CHK1 and EZH2, are associated with poor prognosis, which is in line with previous preclinical studies showing that these three genes are involved in drug resistance. This study highlights the clinical utility of assessing the molecular features of CTCs and monitoring the changes of CTCs over the treatment course.

6.1.3 Tunable Thermal-Sensitive Polymer-Graphene Oxide Composite for Efficient Capture and Release of Viable Circulating Tumor Cells

A highly sensitive microfluidic system to capture circulating tumor cells from whole blood of cancer patients is presented. The device incorporates graphene oxide into a thermoresponsive polymer film to serve as the first step of an antibody functionalization chemistry. As the temperature decreases to around 5 °C, the polymer-GO composite detaches from the microfluidic chamber, and subsequently captured cells are released and thus become available for standard clinical cytopathological and genetic testing such as fluorescence in situ hybridization (FISH). Over 90% capture efficiency and release efficiency is achieved. CTCs were successfully recovered from 10 out of 13 samples (ranging from 2 to 20 CTCs/mL). HER2 amplification was detected via FISH analysis from released CTCs from a breast cancer sample.

The downstream analysis facilitated by the efficient release of captured cells highlights the potential for this device's use in basic and clinical cancer investigation.

6.1.4 ^{HB}GO chip for High Throughput Circulating Tumor Cell Isolation

A high throughput immunoaffinity based CTC isolation platform, the ^{HB}GO chip, was developed by incorporating a herringbone mixer into the GO Chip. To generate micro vortices to direct cells toward the bottom of the microchamber, twenty-four chevrons, two sets of twelve staggered asymmetrically, was defined as a single herringbone mixing unit and periodically shifted along the channel axis to place the vertex points with a spacing of 25 μm. The average cell capture efficiency for the unmodified GO Chip dramatically dropped to below 50% at 200 μL/min, while the ^{HB}GO Chip maintained a target yield of > 80% up to 200 μL/min. The correlation between the channel length and flow rates at different capture efficiencies (60%, 70% and 80%) was further investigated. At the range of 50 ~ 200 μL/min, a strong linear relationship between flow rate and the required channel length to achieve a specific capture efficiency was observed.

6.2 Limitations and Future Directions

6.2.1 CTC isolation technologies

In the past two decades, various CTC isolation platforms are developed based on the differences between tumor cells and surrounding blood cells such as varying expression patterns of membrane proteins or physical characteristics. Based on these different design principles, CTC isolation technologies can be categorized into immunoaffinity based isolation and physical properties based isolation [4]. The ultimate goal of CTC isolation is to capture CTC with (1) high

capture efficiency, (2) high purity of CTCs by removing surrounding blood cells, and (3) high throughput for handling large volumes of blood sample, and (4) the feasibility for downstream analysis [159].

Immunoaffinity based technologies isolate CTCs using antibodies against cell surface markers that are expressed by tumor, but not by leukocytes. Anti-Epithelial cell adhesion molecule (EpCAM) is the mostly commonly used antibody as it is universally expressed in cells of solid tumors. The advantage of immunoaffinity based CTC isolation strategy is high purity of the isolated CTCs, which is important for downstream analysis, as contaminating leukocytes will affect the accuracy of the analysis [159]. Moreover, many immunoaffinity based platforms can process whole blood directly without any preprocessing process such as red blood cell lysis which may cause the loss of CTCs.

However, immunoaffinity based isolation also have a few drawbacks. As CTCs may undergo EMT, in which the epithelial markers are down-regulated, isolation based on EpCAM may fail to capture this subgroup of CTCs. The GO Chip (used in Chapter 2 and Chapter 3), an immunoaffinity based approach, incorporates nanomaterial to achieve high antibody coating density of anti-EpCAM and thus enables the isolation of CTCs with low level of EpCAM expression [21]. Moreover, to capture additional CTCs subgroups, cocktails of antibodies (anti-EpCAM, anti-CD133, and anti-EGFR for NSCLC; anti-EpCAM and anti-CD133 for pancreatic cancer) were incorporated in the GO chip.

The GO chip shares another common drawback across most technologies with antibodies attached to a surface: the limitation of post-capture analysis because of the difficulty in releasing viable cells from the capture substrate. To overcome this problem, temperature-sensitive polymer-graphene oxide composite based chip was developed (Chapter 4). Over 90% capture

efficiency and release efficiency is achieved. Released CTCs were viable and structurally intact, enabling subsequent analysis such as standard clinical cytopathological and genetic testing. The polymer-GO nanocomposite films were prepared through drop-casting a DMF solution of polymer and functionalized GO. Drop-casting is a quick and easy method to generate thin films without wasting materials [160]. However, when using drop casting method, differences in evaporation rates across the substrate or concentration fluctuations can result in variations in film thickness and poor uniformity of the internal structure. In a series of experiments, we did observed high variations in the capture and release efficiency of tumor cells when different batches of polymer-GO composite were used. The robustness of the device may be improved by applying different solvents [161] or changing the deposition technique [162].

Another major concern for microfluidic affinity-based devices is the low throughput, which limits the blood volume that could be processed. For instance, in the CTC-chip, when the flow rate increased from 1 to 3 mL/hr, the capture efficiency dropped drastically [10]. This is because of that under high flow rate, the shear force overcomes antibody-antigen affinity interactions [158], [159]. The GO chip currently processes blood sample at 1mL/hr. To reduce the processing time for high volume of blood (5 ~ 10 ml), we developed the ^{HB}GO chip by incorporating a herringbone mixer into the GO chip (Chapter 4). The herringbone structure generates micro vortices to direct cells to the substrate where the antibodies are tethered. By maximizing the cell-antibody collisions, over 90% capture efficiency is achieved at 200 μL/min (12 mL/hr). This device will be further tested with clinical samples from cancer patients to further validate its performance.

6.2.2 Validation of the clinical utility of CTCs

In this thesis, serial blood samples from 26 locally advanced cancer patients and 12 NSCLC patients were analyzed using the GO chips. While CTC counts and their molecular features are correlated with the progression free survival time of patients in this small patient cohort, these findings need further validation with a larger sample size in order to confirm the prognostic value of CTCs. Additionally, in this study with pancreatic cancer (Chapter 2), patients enrolled in the study are on different chemotherapy regimens, which may have distinct effects on the key regulators for drug resistance. Thus the molecular profiling of CTCs should be studied in a group of patients receiving the same treatment regimen to investigate the potential of CTCs for predicting treatment response [163]. Once the correlations are validated, the changes in CTC number and the molecular features of CTCs can be used to create a predictive model for treatment response and tumor progression and can be tested in an independent patient group.

In another study on NSCLC (Chapter 3), because we demonstrated the up-regulation of PD-L1 expression in CTCs during radiation or radiochemotherapy, we suggested that PD-L1 expression in CTCs have the potential to act as a pharmacodynamic marker to guide the combination of anti- PD-1/PD-L1 therapies with radiation. When combination therapies are applied, treatment dose, fraction, timing and sequence need to be carefully planned and monitored to enhance, rather than compromise, the effectiveness of monotherapy [99]. Future efforts should incorporate dynamic monitoring of PD-L1 (+) CTCs in clinical trials with combined therapy for assessing the optimal timing and sequence. For instance, once the increase of PD-L1 (+) CTC number is observed, it may indicate tumor immune escape and can give the guidance as to the optimal time point to start immunotherapy

6.2.3 Genetic analysis of CTCs

The extremely low prevalence of CTCs not only poses a challenge for CTC isolation, but also hinders the molecular analysis of CTCs. Genetic assays have traditionally been used to analyze tissue fragments or large number of cells. RT-PCR has been used to detect tumor-associated antigens in the peripheral blood and the sensitivity could be as high as one CTC per 10^5 or 10^6 leukocytes [164] . However, the sensitivity of detection and accuracy varies, depending on the tumor type and the choice of genes of interest. In this thesis, CTCs were first isolated by the GO chip and then analyzed for mRNA profiling via a RT-PCR protocol suitable for detecting the expression of low-abundance mRNAs.

However, although the purity of CTCs isolated via the GO chip is much higher than via other conventional methods [21], the enriched cell population still contains a surplus of leukocytes. Therefore, the genetic analysis of CTCs may be masked by signals from the contaminating leukocytes and result in false negatives. To overcome this challenge, the single cell profiling of CTCs has been established for different genetic analysis methods such as transcriptome analysis and whole-genome sequencing [165], [166]. Moreover, single cell analysis can address the heterogeneity of CTCs, which may be shed from distinct subclones within the tumor or from primary and/or different metastatic sites. The polymer-GO chip reported in Chapter 3 enables the release of CTCs after isolation, and the collected cell solution can be readily processed for single cell profiling using platforms such as C1 machine from Fluidigm.

6.2.4 Developing an in-vivo CTC isolation system

One major drawback of the existing immunoaffinity based CTC isolation technologies is the low throughput, which typically ranges from 1 ~ 3 ml blood per hour [159]. Because only a limited blood volume can be processed in practice, a low number of CTCs are captured, which

may not be sufficient for downstream analysis. Furthermore, the small number of CTCs may not accurately reflect the spectrum of tumor cell heterogeneity and may lead to statistical variability. In order to harvest a sufficient number of CTCs in peripheral blood, we envisioned developing an in-vivo CTC isolation system that can be worn on patients and continuously collect CTCs directly from the peripheral vein via a dual lumen catheter. Using this system, blood can be routed at a define flow rate (over 0.2 mL/min) through the CTC capture device for several hours, permitting the screening of large blood volumes for improved probability of detection and statistical accuracy of the analysis. One major challenge of building such system is the development of a CTC isolation device which achieves efficient cell capture at high flow rate.

In chapter 4, we presented the ^{HB}GO chip, which is developed on the basis of the GO chip and achieved an over 10-fold increase in throughput. In addition to shortening the processing time of blood samples for in-vitro CTC isolation, the ^{HB}GO chip provides unique advantages to realize the in-vivo CTC isolation. The ^{HB}GO chip is a great fit for in-vivo CTC isolation for the following reasons: (1) it achieve high capture efficiency (>80%) at high flow rate (up to 200 μL/hr); (2) it can process whole blood at a high flow rate without any preprocessing step or infusion of any solution; (3) the device has low chance of clogging; (4) the device is portable. Therefore, the ^{HB}GO chip can be incorporate into an indwelling catheter system for in-vivo CTC isolation.

To achieve continuous blood sampling for CTC isolation, this system is designed to consist of a CTC capture module (the ^{HB}GO chip), peristaltic pump for continuous blood sampling from the peripheral vein through a dual-lumen catheter, a microcontroller to manage the flow rate, and a heparin injector to prevent blood clot formation during operation. Future

study will focus on the integration of the system and the safety of the cannulization and apheresis. This system could be tested in living vertebrate animal (such as experimental dogs).

6.3 Concluding remarks

This work highlights the clinical utility of CTCs as a potential biomarker to predict and monitor the treatment response and outcome in pancreatic cancer and NSCLC. The nanomaterial based microfluidic devices introduced here utilize various strategies to capture CTC with high sensitivity and can be applied in CTC studies for various cancer types. Ultimately, these studies hold the potential to help improve personalized therapy for cancer patients and identify promising therapeutic targets.

BIBLIOGRAPHY

[1] P. Mehlen and A. Puisieux, "Metastasis: a question of life or death," *Nat. Rev. Cancer*, vol. 6, no. 6, pp. 449–458, Jun. 2006.

[2] K. Pantel and M. R. Speicher, "The biology of circulating tumor cells," *Oncogene*, vol. 35, no. 10, pp. 1216–1224, Mar. 2016.

[3] C. Alix-Panabières and K. Pantel, "Circulating Tumor Cells: Liquid Biopsy of Cancer," *Clinical Chemistry*, vol. 59, no. 1, pp. 110–118, Jan. 2013.

[4] M. Kozminsky, Y. Wang, and S. Nagrath, "The incorporation of microfluidics into circulating tumor cell isolation for clinical applications," *Current Opinion in Chemical Engineering*, vol. 11, pp. 59–66, Feb. 2016.

[5] W. J. Allard, J. Matera, M. C. Miller, M. Repollet, M. C. Connelly, C. Rao, A. G. J. Tibbe, J. W. Uhr, and L. W. M. M. Terstappen, "Tumor Cells Circulate in the Peripheral Blood of All Major Carcinomas but not in Healthy Subjects or Patients With Nonmalignant Diseases," *Clin Cancer Res*, vol. 10, no. 20, pp. 6897–6904, Oct. 2004.

[6] M. G. Krebs, J.M. Hou, T. H. Ward, F. H. Blackhall, and C. Dive, "Circulating tumour cells: their utility in cancer management and predicting outcomes," *Therapeutic Advances in Medical Oncology*, vol. 2, no. 6, pp. 351–365, Aug. 2010.

[7] D. A. Smirnov, D. R. Zweitzig, B. W. Foulk, M. C. Miller, G. V. Doyle, K. J. Pienta, N. J. Meropol, L. M. Weiner, S. J. Cohen, J. G. Moreno, M. C. Connelly, L. W. M. M. Terstappen, and S. M. O'Hara, "Global Gene Expression Profiling of Circulating Tumor Cells," *Cancer Res*, vol. 65, no. 12, pp. 4993–4997, Jun. 2005.

[8] J. den Toonder, "Circulating tumor cells: the Grand Challenge," *Lab on a Chip*, vol. 11, no. 3, pp. 375–377, 2011.

[9] B. J. Green, T. Saberi Safaei, A. Mepham, M. Labib, R. M. Mohamadi, and S. O. Kelley, "Beyond the Capture of Circulating Tumor Cells: Next-Generation Devices and Materials," *Angew. Chem. Int. Ed. Engl.*, vol. 55, no. 4, pp. 1252–1265, Jan. 2016.

[10] S. Nagrath, L. V. Sequist, S. Maheswaran, D. W. Bell, D. Irimia, L. Ulkus, M. R. Smith, E. L. Kwak, S. Digumarthy, A. Muzikansky, P. Ryan, U. J. Balis, R. G. Tompkins, D. A. Haber, and M. Toner, "Isolation of rare circulating tumour cells in cancer patients by microchip technology," *Nature*, vol. 450, no. 7173, pp. 1235–1239, Dec. 2007.

[11] E. K. Sackmann, A. L. Fulton, and D. J. Beebe, "The present and future role of microfluidics in biomedical research," *Nature*, vol. 507, no. 7491, pp. 181–189, Mar. 2014.

[12] K.-A. Hyun and H.-I. Jung, "Advances and critical concerns with the microfluidic enrichments of circulating tumor cells," *Lab on a Chip*, vol. 14, no. 1, pp. 45–56, 2014.

[13] S. Maheswaran, L. V. Sequist, S. Nagrath, L. Ulkus, B. Brannigan, C. V. Collura, E. Inserra, S. Diederichs, A. J. Iafrate, D. W. Bell, S. Digumarthy, A. Muzikansky, D. Irimia, J. Settleman, R. G. Tompkins, T. J. Lynch, M. Toner, and D. A. Haber, "Detection of Mutations in EGFR in Circulating Lung-Cancer Cells," *N Engl J Med,* vol. 359, no. 4, pp. 366–377, Jul. 2009.

[14] J. P. Gleghorn, E. D. Pratt, D. Denning, H. Liu, N. H. Bander, S. T. Tagawa, D. M. Nanus, P. A. Giannakakou, and B. J. Kirby, "Capture of circulating tumor cells from whole blood of prostate cancer patients using geometrically enhanced differential immunocapture (GEDI) and a prostate-specific antibody," *Lab on a Chip*, vol. 10, no. 1, pp. 27–29, Jan. 2010.

[15] G. Galletti, M. S. Sung, L. T. Vahdat, M. A. Shah, S. M. Santana, G. Altavilla, B. J. Kirby, and P. Giannakakou, "Isolation of breast cancer and gastric cancer circulating tumor cells by use of an anti HER2-based microfluidic device," *Lab on a Chip*, vol. 14, no. 1, pp. 147–156, 2014.

[16] A. A. Adams, P. I. Okagbare, J. Feng, M. L. Hupert, D. Patterson, J. Göttert, R. L. McCarley, D. Nikitopoulos, M. C. Murphy, and S. A. Soper, "Highly Efficient Circulating Tumor Cell Isolation from Whole Blood and Label-Free Enumeration Using Polymer-Based Microfluidics with an Integrated Conductivity Sensor," *J. Am. Chem. Soc.*, vol. 130, no. 27, pp. 8633–8641, Jun. 2008.

[17] M. L. Hupert, J. M. Jackson, H. Wang, M. A. Witek, J. Kamande, M. I. Milowsky, Y. E. Whang, and S. A. Soper, "Arrays of high-aspect ratio microchannels for high-throughput isolation of circulating tumor cells (CTCs)," *Microsyst Technol*, vol. 20, no. 10, pp. 1815–1825, 2014.

[18] Z. Ke, M. Lin, J.-F. Chen, J.-S. Choi, Y. Zhang, A. Fong, A.J. Liang, S.-F. Chen, Q. Li, W. Fang, P. Zhang, M. A. Garcia, T. Lee, M. Song, H.-A. Lin, H. Zhao, S. C. Luo, S. Hou, H. H. Yu, and H.-R. Tseng, "Programming Thermoresponsiveness of NanoVelcro Substrates Enables Effective Purification of Circulating Tumor Cells in Lung Cancer Patients," *ACS Nano*, vol. 9, no. 1, pp. 62–70, Dec. 2014.

[19] S. L. Stott, C. H. Hsu, D. I. Tsukrov, and M. Yu, "Isolation of circulating tumor cells using a microvortex-generating herringbone-chip," *Proc. Natl. Acad. Sci. U.S.A.*, 2010.

[20] V. Murlidhar, M. Zeinali, S. Grabauskiene, M. Ghannad Rezaie, M. S. Wicha, D. M. Simeone, N. Ramnath, R. M. Reddy, and S. Nagrath, "A Radial Flow Microfluidic Device for Ultra-High-Throughput Affinity-Based Isolation of Circulating Tumor Cells," *Small*, vol. 10, no. 23, pp. 4895–4904, Dec. 2014.

[21] H. J. Yoon, T. H. Kim, Z. Zhang, E. Azizi, T. M. Pham, C. Paoletti, J. Lin, N. Ramnath, M. S. Wicha, D. F. Hayes, D. M. Simeone, and S. Nagrath, "Sensitive capture of circulating tumour cells by functionalized graphene oxide nanosheets," *Nat Nanotechnol*, vol. 8, no. 10, pp. 735–741, Oct. 2013.

[22] B. P. Casavant, L. N. Strotman, J. J. Tokar, S. M. Thiede, A. M. Traynor, J. S. Ferguson, J. M. Lang, and D. J. Beebe, "Paired diagnostic and pharmacodynamic analysis of rare non-small cell lung cancer cells enabled by the VerIFAST platform," *Lab on a Chip*, vol. 14, no. 1, pp. 99–105, Nov. 2013.

[23] H. J. Yoon, M. Kozminsky, and S. Nagrath, "Emerging Role of Nanomaterials in Circulating Tumor Cell Isolation and Analysis," *ACS Nano*, vol. 8, no. 3, pp. 1995–2017, Mar. 2014.

[24] P. Pinzani, B. Salvadori, L. Simi, S. Bianchi, V. Distante, L. Cataliotti, M. Pazzagli, and C. Orlando, "Isolation by size of epithelial tumor cells in peripheral blood of patients with breast cancer: correlation with real-time reverse transcriptase–polymerase chain reaction results and feasibility of molecular analysis by laser microdissection," *Human Pathology*, vol. 37, no. 6, pp. 711–718, Jun. 2006.

[25] V. J. Hofman, M. I. Ilie, C. Bonnetaud, E. Selva, E. Long, T. Molina, J. M. Vignaud, J.-F. Flejou, S. Lantuejoul, E. Piaton, C. Butori, N. Mourad, M. Poudenx, P. Bahadoran, S. Sibon, N. Guevara, J. Santini, N. Vénissac, J. Mouroux, P. Vielh, and P. M. Hofman, "Cytopathologic Detection of Circulating Tumor Cells Using the Isolation by Size of Epithelial Tumor Cell MethodPromises and Pitfalls," *Am J Clin Pathol*, vol. 135, no. 1, pp. 146–156, Jan. 2011.

[26] M.-D. Zhou, S. Hao, A. J. Williams, R. A. Harouaka, B. Schrand, S. Rawal, Z. Ao, R. Brenneman, E. Gilboa, B. Lu, S. Wang, J. Zhu, R. Datar, R. Cote, Y.-C. Tai, and S.-Y. Zheng, "Separable Bilayer Microfiltration Device for Viable Label-free Enrichment of Circulating Tumour Cells," *Sci Rep*, vol. 4, p. 7392, Dec. 2014.

[27] R. A. Harouaka, M.-D. Zhou, Y.-T. Yeh, W. J. Khan, A. Das, X. Liu, C. C. Christ, D. T. Dicker, T. S. Baney, J. T. Kaifi, C. P. Belani, C. I. Truica, W. S. El-Deiry, J. P. Allerton, and S.-Y. Zheng, "Flexible Micro Spring Array Device for High-Throughput Enrichment of Viable Circulating Tumor Cells," *Clinical Chemistry*, vol. 60, no. 2, pp. 323–333, Feb. 2014.

[28] L. R. Huang, E. C. Cox, R. H. Austin, and J. C. Sturm, "Continuous Particle Separation Through Deterministic Lateral Displacement," *Science*, vol. 304, no. 5673, pp. 987–990, May 2004.

[29] E. Sollier, D. E. Go, J. Che, D. R. Gossett, S. O'Byrne, W. M. Weaver, N. Kummer, M. Rettig, J. Goldman, N. Nickols, S. McCloskey, R. P. Kulkarni, and D. Di Carlo, "Size-selective collection of circulating tumor cells using Vortex technology," *Lab on a Chip*, vol. 14, no. 1, pp. 63–77, 2014.

[30] M. E. Warkiani, G. Guan, K. B. Luan, W. C. Lee, A. A. S. Bhagat, P. K. Chaudhuri, D. S.-W. Tan, W.-T. Lim, S. C. Lee, P. C. Y. Chen, C. T. Lim, and J. Han, "Slanted spiral microfluidics for the ultra-fast, label-free isolation of circulating tumor cells," *Lab on a Chip*, vol. 14, no. 1, pp. 128–137, 2014.

[31] J. Sun, M. Li, C. Liu, Y. Zhang, D. Liu, W. Liu, G. Hu, and X. Jiang, "Double spiral microchannel for label-free tumor cell separation and enrichment," *Lab on a Chip*, vol. 12, no. 20, pp. 3952–3960, 2012.

[32] T. H. Kim, H. J. Yoon, P. Stella, and S. Nagrath, "Cascaded spiral microfluidic device for deterministic and high purity continuous separation of circulating tumor cells," *Biomicrofluidics*, vol. 8, no. 6, p. 064117, Dec. 2014.

[33] H. W. Hou, M. E. Warkiani, B. L. Khoo, Z. R. Li, R. A. Soo, D. S.-W. Tan, W.-T. Lim, J. Han, A. A. S. Bhagat, and C. T. Lim, "Isolation and retrieval of circulating tumor cells using centrifugal forces," *Sci Rep*, vol. 3, p. 1259, Feb. 2013.

[34] B. L. Khoo, M. E. Warkiani, D. S.-W. Tan, A. A. S. Bhagat, D. Irwin, D. P. Lau, A. S. T. Lim, K. H. Lim, S. S. Krisna, W.-T. Lim, Y. S. Yap, S. C. Lee, R. A. Soo, J. Han, and C. T. Lim, "Clinical Validation of an Ultra High-Throughput Spiral Microfluidics for the Detection and Enrichment of Viable Circulating Tumor Cells," *PLoS ONE*, vol. 9, no. 7, p. e99409, Jul. 2014.

[35] V. Gupta, I. Jafferji, M. Garza, V. O. Melnikova, D. K. Hasegawa, R. Pethig, and D. W.

Davis, “ApoStream™, a new dielectrophoretic device for antibody independent isolation and recovery of viable cancer cells from blood,” *Biomicrofluidics*, vol. 6, no. 2, p. 024133, Jun. 2012.

[36] P. Li, Z. Mao, Z. Peng, L. Zhou, Y. Chen, P.-H. Huang, C. I. Truica, J. J. Drabick, W. S. El-Deiry, M. Dao, S. Suresh, and T. J. Huang, “Acoustic separation of circulating tumor cells.,” *Proc. Natl. Acad. Sci. U.S.A.*, vol. 112, no. 16, pp. 4970–4975, Apr. 2015.

[37] X. Ding, Z. Peng, S.-C. S. Lin, M. Geri, S. Li, P. Li, Y. Chen, M. Dao, S. Suresh, and T. J. Huang, “Cell separation using tilted-angle standing surface acoustic waves.,” *Proc. Natl. Acad. Sci. U.S.A.*, vol. 111, no. 36, pp. 12992–12997, Sep. 2014.

[38] D. Vergara, P. Simeone, J. Franck, M. Trerotola, A. Giudetti, L. Capobianco, A. Tinelli, C. Bellomo, I. Fournier, A. Gaballo, S. Alberti, M. Salzet, and M. Maffia, “Translating epithelial mesenchymal transition markers into the clinic: Novel insights from proteomics,” *EuPA Open Proteomics*, vol. 10, pp. 31–41, Mar. 2016.

[39] J. H. Tsai and J. Yang, “Epithelial-mesenchymal plasticity in carcinoma metastasis.,” *Genes Dev.*, vol. 27, no. 20, pp. 2192–2206, Oct. 2013.

[40] S. J. Grille, A. Bellacosa, J. Upson, A. J. Klein-Szanto, F. van Roy, W. Lee-Kwon, M. Donowitz, P. N. Tsichlis, and L. Larue, “The Protein Kinase Akt Induces Epithelial Mesenchymal Transition and Promotes Enhanced Motility and Invasiveness of Squamous Cell Carcinoma Lines,” *Cancer Res*, vol. 63, no. 9, pp. 2172–2178, May 2003.

[41] X. Zheng, J. L. Carstens, J. Kim, M. Scheible, J. Kaye, H. Sugimoto, C.-C. Wu, V. S. LeBleu, and R. Kalluri, “Epithelial-to-mesenchymal transition is dispensable for metastasis but induces chemoresistance in pancreatic cancer,” *Nature*, vol. 527, no. 7579, pp. 525–530, Nov. 2015.

[42] S. A. Mani, W. Guo, M.-J. Liao, E. N. Eaton, A. Ayyanan, A. Y. Zhou, M. Brooks, F. Reinhard, C. C. Zhang, M. Shipitsin, L. L. Campbell, K. Polyak, C. Brisken, J. Yang, and R. A. Weinberg, “The Epithelial-Mesenchymal Transition Generates Cells with Properties of Stem Cells,” *Cell*, vol. 133, no. 4, pp. 704–715, May 2008.

[43] S. Heerboth, G. Housman, M. Leary, M. Longacre, S. Byler, K. Lapinska, A. Willbanks, and S. Sarkar, “EMT and tumor metastasis,” *Clinical and Translational Medicine 2015 4:1*, vol. 4, no. 1, p. 6, Feb. 2015.

[44] J. P. Sleeman and J.-P. Thiery, “SnapShot: The Epithelial-Mesenchymal Transition,” *Cell*, vol. 145, no. 1, pp. 162–162.e1, Apr. 2011.

[45] Y. Li, C. Q. Chen, Y. L. He, S. R. Cai, D. J. Yang, W. L. He, J. B. Xu, and W. H. Zan, “Abnormal expression of E-cadherin in tumor cells is associated with poor prognosis of gastric carcinoma,” *J Surg Oncol.*, vol. 106, no. 3, pp. 304–310, Sep. 2012.

[46] L. Hui, S. Zhang, X. Dong, D. Tian, Z. Cui, and X. Qiu, “Prognostic Significance of Twist and N-Cadherin Expression in NSCLC,” *PLoS ONE*, vol. 8, no. 4, p. e62171, Apr. 2013.

[47] B. Aktas, M. Tewes, T. Fehm, S. Hauch, R. Kimmig, and S. Kasimir-Bauer, “Stem cell and epithelial-mesenchymal transition markers are frequently overexpressed in circulating tumor cells of metastatic breast cancer patients,” *Breast Cancer Res.*, vol. 11, no. 4, p. R46, Jul. 2009.

[48] A. J. Armstrong, M. S. Marengo, S. Oltean, G. Kemeny, R. L. Bitting, J. D. Turnbull, C. I.

Herold, P. K. Marcom, D. J. George, and M. A. Garcia-Blanco, “Circulating tumor cells from patients with advanced prostate and breast cancer display both epithelial and mesenchymal markers,” *Mol. Cancer Res.*, vol. 9, no. 8, pp. 997–1007, Aug. 2011.

[49] S. Wu, S. Liu, Z. Liu, J. Huang, X. Pu, J. Li, D. Yang, H. Deng, N. Yang, and J. Xu, “Classification of Circulating Tumor Cells by Epithelial-Mesenchymal Transition Markers,” *PLoS ONE*, vol. 10, no. 4, p. e0123976, Apr. 2015.

[50] A. Lecharpentier, P. Vielh, P. Perez-Moreno, D. Planchard, J. C. Soria, and F. Farace, “Detection of circulating tumour cells with a hybrid (epithelial/mesenchymal) phenotype in patients with metastatic non-small cell lung cancer,” *British Journal of Cancer*, vol. 105, no. 9, pp. 1338–1341, Oct. 2011.

[51] M. Yu, A. Bardia, B. S. Wittner, S. L. Stott, M. E. Smas, D. T. Ting, S. J. Isakoff, J. C. Ciciliano, M. N. Wells, A. M. Shah, K. F. Concannon, M. C. Donaldson, L. V. Sequist, E. Brachtel, D. Sgroi, J. Baselga, S. Ramaswamy, M. Toner, D. A. Haber, and S. Maheswaran, “Circulating breast tumor cells exhibit dynamic changes in epithelial and mesenchymal composition,” *Science*, vol. 339, no. 6119, pp. 580–584, Feb. 2013.

[52] D. T. Ting, B. S. Wittner, M. Ligorio, N. Vincent Jordan, A. M. Shah, D. T. Miyamoto, N. Aceto, F. Bersani, B. W. Brannigan, K. Xega, J. C. Ciciliano, H. Zhu, O. C. MacKenzie, J. Trautwein, K. S. Arora, M. Shahid, H. L. Ellis, N. Qu, N. Bardeesy, M. N. Rivera, V. Deshpande, C. R. Ferrone, R. Kapur, S. Ramaswamy, T. Shioda, M. Toner, S. Maheswaran, and D. A. Haber, “Single-Cell RNA Sequencing Identifies Extracellular Matrix Gene Expression by Pancreatic Circulating Tumor Cells,” *Cell Reports*, vol. 8, no. 6, pp. 1905–1918, Sep. 2014.

[53] Z. Ao, S. H. Shah, L. M. Machlin, R. Parajuli, P. C. Miller, S. Rawal, A. J. Williams, R. J. Cote, M. E. Lippman, R. H. Datar, and D. El-Ashry, “Identification of Cancer-Associated Fibroblasts in Circulating Blood from Patients with Metastatic Breast Cancer.,” *Cancer Res*, vol. 75, no. 22, pp. 4681–4687, Nov. 2015.

[54] E. H. Cho, M. Wendel, M. Luttgen, and C. Yoshioka, “Characterization of circulating tumor cell aggregates identified in patients with epithelial tumors,” *Phys. Biol.,* vol. 9, no. 1, 016001, Feb. 2012.

[55] M. G. Krebs, J.-M. Hou, R. Sloane, L. Lancashire, L. Priest, D. Nonaka, T. H. Ward, A. Backen, G. Clack, A. Hughes, M. Ranson, F. H. Blackhall, and C. Dive, “Analysis of Circulating Tumor Cells in Patients with Non-small Cell Lung Cancer Using Epithelial Marker-Dependent and -Independent Approaches,” *Journal of Thoracic Oncology*, vol. 7, no. 2, pp. 306–315, Feb. 2012.

[56] N. Aceto, A. Bardia, D. T. Miyamoto, M. C. Donaldson, B. S. Wittner, J. A. Spencer, M. Yu, A. Pely, A. Engstrom, H. Zhu, B. W. Brannigan, R. Kapur, S. L. Stott, T. Shioda, S. Ramaswamy, D. T. Ting, C. P. Lin, M. Toner, D. A. Haber, and S. Maheswaran, “Circulating Tumor Cell Clusters Are Oligoclonal Precursors of Breast Cancer Metastasis,” *Cell*, vol. 158, no. 5, pp. 1110–1122, Aug. 2014.

[57] M. C. Chang, Y. T. Chang, J. Y. Chen, Y. M. Jeng, C. Y. Yang, Y. W. Tien, S. H. Yang, H. L. Chen, T. Y. Liang, C. F. Wang, E. Y. H. P. Lee, Y. C. Chang, and W. H. Lee, “Clinical Significance of Circulating Tumor Microemboli as a Prognostic Marker in Patients with Pancreatic Ductal Adenocarcinoma,” *Clinical Chemistry*, vol. 62, no. 3, pp. 505–513, Feb. 2016.

[58] J.-M. Hou, M. G. Krebs, L. Lancashire, R. Sloane, A. Backen, R. K. Swain, L. J. C. Priest, A. Greystoke, C. Zhou, K. Morris, T. Ward, F. H. Blackhall, and C. Dive, "Clinical Significance and Molecular Characteristics of Circulating Tumor Cells and Circulating Tumor Microemboli in Patients With Small-Cell Lung Cancer," *Journal of Clinical Oncology*, vol. 30, no. 5, pp. 525–532, Sep. 2016.

[59] Y. Hong, F. Fang, and Q. Zhang, "Circulating tumor cell clusters: What we know and what we expect (Review)," *Int. J. Oncol.*, Vol. 49, pp. 2206-2216, Oct. 2016.

[60] D. Sharma, K. E. Brummel Ziedins, B. A. Bouchard, and C. E. Holmes, "Platelets in Tumor Progression: A Host Factor That Offers Multiple Potential Targets in the Treatment of Cancer," *Journal of Cellular Physiology*, vol. 229, no. 8, pp. 1005–1015, Aug. 2014.

[61] L. Borsig, R. Wong, R. O. Hynes, N. M. Varki, and A. Varki, "Synergistic effects of L- and P-selectin in facilitating tumor metastasis can involve non-mucin ligands and implicate leukocytes as enhancers of metastasis," *Proc. Natl. Acad. Sci. U.S.A.*, vol. 99, no. 4, pp. 2193–2198, Feb. 2002.

[62] Q. Liu, Q. Liao, and Y. Zhao, "Myeloid-derived suppressor cells (MDSC) facilitate distant metastasis of malignancies by shielding circulating tumor cells (CTC) from immune surveillance," *Med. Hypotheses*, vol. 87, pp. 34–39, Feb. 2016.

[63] M. Labelle, S. Begum, and R. O. Hynes, "Direct Signaling between Platelets and Cancer Cells Induces an Epithelial-Mesenchymal-Like Transition and Promotes Metastasis," *Cancer Cell*, vol. 20, no. 5, pp. 576–590, Nov. 2011.

[64] D. G. Duda, A. M. M. J. Duyverman, M. Kohno, M. Snuderl, E. J. A. Steller, D. Fukumura, and R. K. Jain, "Malignant cells facilitate lung metastasis by bringing their own soil," *Proc. Natl. Acad. Sci. U.S.A.*, vol. 107, no. 50, pp. 21677–21682, Dec. 2010.

[65] L. A. Torre, F. Bray, R. L. Siegel, J. Ferlay, J. Lortet Tieulent, and A. Jemal, "Global cancer statistics, 2012," *CA: A Cancer Journal for Clinicians*, vol. 65, no. 2, pp. 87–108, Mar. 2015.

[66] N. Yu, J. Zhou, F. Cui, and X. Tang, "Circulating Tumor Cells in Lung Cancer: Detection Methods and Clinical Applications," *Lung*, vol. 193, no. 2, pp. 157–171, 2015.

[67] Z. Zhang, N. Ramnath, and S. Nagrath, "Current Status of CTCs as Liquid Biopsy in Lung Cancer and Future Directions," *Frontiers in Oncology*, vol. 5, no. 1, p. 9, 2015.

[68] V. Hofman, M. I. Ilie, E. Long, E. Selva, C. Bonnetaud, T. Molina, N. Vénissac, J. Mouroux, P. Vielh, and P. Hofman, "Detection of circulating tumor cells as a prognostic factor in patients undergoing radical surgery for non-small-cell lung carcinoma: comparison of the efficacy of the CellSearch Assay™ and the isolation by size of epithelial tumor cell method," *International journal of cancer*, vol. 129, no. 7, pp. 1651–1660, Oct. 2011.

[69] Z. Mu, C. Wang, Z. Ye, L. Austin, J. Civan, T. Hyslop, J. P. Palazzo, R. Jaslow, B. Li, R. E. Myers, J. Jiang, J. Xing, H. Yang, and M. Cristofanilli, "Prospective assessment of the prognostic value of circulating tumor cells and their clusters in patients with advanced-stage breast cancer," *Breast Cancer Res. Treat.*, vol. 154, no. 3, pp. 563–571, Nov. 2015.

[70] E. A. Punnoose, S. Atwal, W. Liu, R. Raja, B. M. Fine, B. G. M. Hughes, R. J. Hicks, G. M. Hampton, L. C. Amler, A. Pirzkall, and M. R. Lackner, "Evaluation of Circulating

Tumor Cells and Circulating Tumor DNA in Non–Small Cell Lung Cancer: Association with Clinical Endpoints in a Phase II Clinical Trial of Pertuzumab and Erlotinib," *Clin Cancer Res*, vol. 18, no. 8, pp. 2391–2401, Apr. 2012.

[71] M. G. Krebs, R. Sloane, L. Priest, L. Lancashire, J.-M. Hou, A. Greystoke, T. H. Ward, R. Ferraldeschi, A. Hughes, G. Clack, M. Ranson, C. Dive, and F. H. Blackhall, "Evaluation and Prognostic Significance of Circulating Tumor Cells in Patients With Non–Small-Cell Lung Cancer," *Journal of Clinical Oncology*, vol. 29, no. 12, pp. 1556–1563, Sep. 2016.

[72] L. Muinelo-Romay, M. Vieito, A. Abalo, M. Nocelo, F. Barón, U. Anido, E. Brozos, F. Vázquez, S. Aguín, M. Abal, and R. López, "Evaluation of Circulating Tumor Cells and Related Events as Prognostic Factors and Surrogate Biomarkers in Advanced NSCLC Patients Receiving First-Line Systemic Treatment," *Cancers 2014, Vol. 6, Pages 153-165*, vol. 6, no. 1, pp. 153–165, Jan. 2014.

[73] M. Ilie, V. Hofman, E. Long-Mira, E. Selva, J. M. Vignaud, B. Padovani, J. Mouroux, C.-H. Marquette, and P. Hofman, "'Sentinel' Circulating Tumor Cells Allow Early Diagnosis of Lung Cancer in Patients with Chronic Obstructive Pulmonary Disease," *PLoS ONE*, vol. 9, no. 10, p. e111597, Oct. 2014.

[74] A. Fiorelli, M. Accardo, E. Carelli, D. Angioletti, M. Santini, and M. Di Domenico, "Circulating Tumor Cells in Diagnosing Lung Cancer: Clinical and Morphologic Analysis," *The Annals of Thoracic Surgery*, vol. 99, no. 6, pp. 1899–1905, Jun. 2015.

[75] R. Vijayalakshmi and A. Krishnamurthy, "Targetable 'Driver' Mutations in Non Small Cell Lung Cancer," *Indian J Surg Oncol*, vol. 2, no. 3, pp. 178–188, 2011.

[76] S. Maheswaran, L. V. Sequist, S. Nagrath, L. Ulkus, B. Brannigan, C. V. Collura, E. Inserra, S. Diederichs, A. J. Iafrate, D. W. Bell, S. Digumarthy, A. Muzikansky, D. Irimia, J. Settleman, R. G. Tompkins, T. J. Lynch, M. Toner, and D. A. Haber, "Detection of Mutations in EGFR in Circulating Lung-Cancer Cells," *N Engl J Med,* vol. 359, no. 4, pp. 366–377, Jul. 2009.

[77] F. Breitenbuecher, S. Hoffarth, K. Worm, D. Cortes-Incio, T. C. Gauler, J. Köhler, T. Herold, K. W. Schmid, L. Freitag, S. Kasper, and M. Schuler, "Development of a Highly Sensitive and Specific Method for Detection of Circulating Tumor Cells Harboring Somatic Mutations in Non-Small-Cell Lung Cancer Patients," *PLoS ONE*, vol. 9, no. 1, p. e85350, Jan. 2014.

[78] E. Pailler, J. Adam, A. Barthélémy, M. Oulhen, N. Auger, A. Valent, I. Borget, D. Planchard, M. Taylor, F. André, J.-C. Soria, P. Vielh, B. Besse, and F. Farace, "Detection of Circulating Tumor Cells Harboring a Unique ALK Rearrangement in ALK-Positive Non–Small-Cell Lung Cancer," *Journal of Clinical Oncology*, vol. 31, no. 18, pp. 2273–2281, Sep. 2016.

[79] W. He, D. Xu, Z. Wang, X. Xiang, B. Tang, S. Li, M. Hou, Y. Zhang, J.-F. Chen, M. Lin, L. Wang, S. Hou, H.-R. Tseng, M. Kuang, and Z.-F. Ke, "Detecting ALK-rearrangement of CTC enriched by nanovelcro chip in advanced NSCLC patients.," *Oncotarget*, Mar. 2016.

[80] R. L. Siegel, K. D. Miller, and A. Jemal, "Cancer statistics, 2016," *CA: A Cancer Journal for Clinicians*, vol. 66, no. 1, pp. 7–30, Jan. 2016.

[81] B. Agarwal, A. M. Correa, and L. Ho, "Survival in Pancreatic Carcinoma Based on Tumor Size," *Pancreas*, vol. 36, no. 1, pp. e15–e20, Jan. 2008.

[82] G. H. Sakorafas and M. G. Sarr, "Pancreatic cancer after surgery for chronic

pancreatitis," *Digestive and Liver Disease*, vol. 35, no. 7, pp. 482–485, Jul. 2003.
[83] A. D. Rhim, E. T. Mirek, N. M. Aiello, A. Maitra, J. M. Bailey, F. McAllister, M. Reichert, G. L. Beatty, A. K. Rustgi, R. H. Vonderheide, S. D. Leach, and B. Z. Stanger, "EMT and Dissemination Precede Pancreatic Tumor Formation," *Cell*, vol. 148, no. 1, pp. 349–361, Jan. 2012.
[84] A. D. Rhim, F. I. Thege, S. M. Santana, T. B. Lannin, T. N. Saha, S. Tsai, L. R. Maggs, M. L. Kochman, G. G. Ginsberg, J. G. Lieb, V. Chandrasekhara, J. A. Drebin, N. Ahmad, Y. X. Yang, B. J. Kirby, and B. Z. Stanger, "Detection of Circulating Pancreas Epithelial Cells in Patients With Pancreatic Cystic Lesions," *Gastroenterology*, vol. 146, no. 3, pp. 647–651, Mar. 2014.
[85] J. L. Cameron and J. He, "Two Thousand Consecutive Pancreaticoduodenectomies," *Journal of the American College of Surgeons*, vol. 220, no. 4, pp. 530–536, Apr. 2015.
[86] J. S. Ankeny, C. M. Court, S. Hou, Q. Li, M. Song, D. Wu, J. F. Chen, T. Lee, M. Lin, S. Sho, M. M. Rochefort, M. D. Girgis, J. Yao, Z. A. Wainberg, V. R. Muthusamy, R. R. Watson, T. R. Donahue, O. J. Hines, H. A. Reber, T. G. Graeber, H. R. Tseng, and J. S. Tomlinson, "Circulating tumour cells as a biomarker for diagnosis and staging in pancreatic cancer," *British Journal of Cancer*, vol. 114, no. 12, pp. 1367–1375, Jun. 2016.
[87] L. Han, W. Chen, and Q. Zhao, "Prognostic value of circulating tumor cells in patients with pancreatic cancer: a meta-analysis," *Tumor Biology*, vol. 35, no. 3, pp. 2473–2480, Nov. 2013.
[88] F.-M. Kong, R. K. Ten Haken, M. J. Schipper, M. A. Sullivan, M. Chen, C. Lopez, G. P. Kalemkerian, and J. A. Hayman, "High-dose radiation improved local tumor control and overall survival in patients with inoperable/unresectable non–small-cell lung cancer: Long-term results of a radiation dose escalation study," *Int. J. Radiation Oncology Biol. Phys.*, vol. 63, no. 2, pp. 324–333, Oct. 2005.
[89] M. Chen, J. A. Hayman, R. K. Ten Haken, D. Tatro, S. Fernando, and F.-M. Kong, "Long-term results of high-dose conformal radiotherapy for patients with medically inoperable T1–3N0 non–small-cell lung cancer: Is low incidence of regional failure due to incidental nodal irradiation?," *Int. J. Radiation Oncology Biol. Phys.*, vol. 64, no. 1, pp. 120–126, Jan. 2006.
[90] J. J. Beitler, E. A. Badine, D. El-Sayah, D. Makara, P. Friscia, P. Silverman, and T. Terjanian, "Stereotactic body radiation therapy for nonmetastatic lung cancer: An analysis of 75 patients treated over 5 years," *Int. J. Radiation Oncology Biol. Phys.,* vol. 65, no. 1, pp. 100–106, May 2006.
[91] D. M. Pardoll, "The blockade of immune checkpoints in cancer immunotherapy," *Nat. Rev. Cancer*, vol. 12, no. 4, pp. 252–264, Apr. 2012.
[92] S. P. Patel and R. Kurzrock, "PD-L1 Expression as a Predictive Biomarker in Cancer Immunotherapy," *Mol Cancer Ther*, vol. 14, no. 4, pp. 847–856, Apr. 2015.
[93] S. L. Topalian, F. S. Hodi, J. R. Brahmer, S. N. Gettinger, D. C. Smith, D. F. McDermott, J. D. Powderly, R. D. Carvajal, J. A. Sosman, M. B. Atkins, P. D. Leming, D. R. Spigel, S. J. Antonia, L. Horn, C. G. Drake, D. M. Pardoll, L. Chen, W. H. Sharfman, R. A. Anders, J. M. Taube, T. L. McMiller, H. Xu, A. J. Korman, M. Jure-Kunkel, S. Agrawal, D. McDonald, G. D. Kollia, A. Gupta, J. M. Wigginton, and M. Sznol, "Safety, activity, and immune correlates of anti-PD-1 antibody in cancer," *N. Engl. J. Med.*, vol. 366, no. 26, pp. 2443–2454, Jun. 2012.

[94] N. A. Rizvi, J. Mazières, D. Planchard, T. E. Stinchcombe, G. K. Dy, S. J. Antonia, L. Horn, H. Lena, E. Minenza, B. Mennecier, G. A. Otterson, L. T. Campos, D. R. Gandara, B. P. Levy, S. G. Nair, G. Zalcman, J. Wolf, P.-J. Souquet, E. Baldini, F. Cappuzzo, C. Chouaid, A. Dowlati, R. Sanborn, A. Lopez-Chavez, C. Grohe, R. M. Huber, C. T. Harbison, C. Baudelet, B. J. Lestini, and S. S. Ramalingam, "Activity and safety of nivolumab, an anti-PD-1 immune checkpoint inhibitor, for patients with advanced, refractory squamous non-small-cell lung cancer (CheckMate 063): a phase 2, single-arm trial," *Lancet Oncol.*, vol. 16, no. 3, pp. 257–265, Mar. 2015.

[95] J. R. Brahmer, S. S. Tykodi, L. Q. M. Chow, W.-J. Hwu, S. L. Topalian, P. Hwu, C. G. Drake, L. H. Camacho, J. Kauh, K. Odunsi, H. C. Pitot, O. Hamid, S. Bhatia, R. Martins, K. Eaton, S. Chen, T. M. Salay, S. Alaparthy, J. F. Grosso, A. J. Korman, S. M. Parker, S. Agrawal, S. M. Goldberg, D. M. Pardoll, A. Gupta, and J. M. Wigginton, "Safety and activity of anti-PD-L1 antibody in patients with advanced cancer," *N. Engl. J. Med.*, vol. 366, no. 26, pp. 2455–2465, Jun. 2012.

[96] A. D. Le, S. K. Alzghari, G. W. Jean, and N. M. La-Beck, "Update on targeted therapies for advanced non-small cell lung cancer: nivolumab in context," *Therapeutics and Clinical Risk Management*, vol. 13, pp. 223–236, 2017.

[97] V. K. Anagnostou and J. R. Brahmer, "Cancer immunotherapy: a future paradigm shift in the treatment of non-small cell lung cancer," *Clin Cancer Res*, vol. 21, no. 5, pp. 976–984, Mar. 2015.

[98] S. Gettinger and R. S. Herbst, "B7-H1/PD-1 blockade therapy in non-small cell lung cancer: current status and future direction," *Cancer J*, vol. 20, no. 4, pp. 281–289, Jul. 2014.

[99] J. Kang, S. Demaria, and S. Formenti, "Current clinical trials testing the combination of immunotherapy with radiotherapy," *Journal for ImmunoTherapy of Cancer 2016 4:1*, vol. 4, no. 1, p. 51, Sep. 2016.

[100] L. Deng, H. Liang, B. Burnette, M. Beckett, T. Darga, R. R. Weichselbaum, and Y.-X. Fu, "Irradiation and anti–PD-L1 treatment synergistically promote antitumor immunity in mice," *J. Clin. Invest.*, vol. 124, no. 2, pp. 687–695, Feb. 2014.

[101] S. J. Dovedi, A. L. Adlard, G. Lipowska-Bhalla, C. McKenna, S. Jones, E. J. Cheadle, I. J. Stratford, E. Poon, M. Morrow, R. Stewart, H. Jones, R. W. Wilkinson, J. Honeychurch, and T. M. Illidge, "Acquired Resistance to Fractionated Radiotherapy Can Be Overcome by Concurrent PD-L1 Blockade," *Cancer Res*, vol. 74, no. 19, pp. 5458–5468, Sep. 2014.

[102] O. Juan, J. Vidal, R. Gisbert, J. Muñoz, S. Maciá, and J. Gómez-Codina, "Prognostic significance of circulating tumor cells in advanced non-small cell lung cancer patients treated with docetaxel and gemcitabine," *Clin Transl Oncol*, vol. 16, no. 7, pp. 637–643, Jul. 2014.

[103] H. J. Yoon, A. Shanker, Y. Wang, M. Kozminsky, Q. Jin, N. Palanisamy, M. L. Burness, E. Azizi, D. M. Simeone, M. S. Wicha, J. Kim, and S. Nagrath, "Tunable Thermal-Sensitive Polymer-Graphene Oxide Composite for Efficient Capture and Release of Viable Circulating Tumor Cells," *Advanced Materials*, vol. 28, no. 24, pp. 4891–4897, Jun. 2016.

[104] M. N. McCall, H. R. McMurray, H. Land, and A. Almudevar, "On non-detects in qPCR data," *Bioinformatics*, vol. 30, no. 16, pp. 2310–2316, Aug. 2014.

[105] X. Meng, Z. Huang, F. Teng, L. Xing, and J. Yu, "Predictive biomarkers in PD-1/PD-

L1 checkpoint blockade immunotherapy," *Cancer Treat. Rev.*, vol. 41, no. 10, pp. 868–876, Dec. 2015.

[106] K. J. Lastwika, W. Wilson, Q. K. Li, J. Norris, H. Xu, S. R. Ghazarian, H. Kitagawa, S. Kawabata, J. M. Taube, S. Yao, L. N. Liu, J. J. Gills, and P. A. Dennis, "Control of PD-L1 Expression by Oncogenic Activation of the AKT-mTOR Pathway in Non-Small Cell Lung Cancer," *Cancer Res*, vol. 76, no. 2, pp. 227–238, Jan. 2016.

[107] M. Mazel, W. Jacot, K. Pantel, K. Bartkowiak, D. Topart, L. Cayrefourcq, D. Rossille, T. Maudelonde, T. Fest, and C. Alix-Panabières, "Frequent expression of PD-L1 on circulating breast cancer cells," *Mol Oncol*, vol. 9, no. 9, pp. 1773–1782, Nov. 2015.

[108] C. Nicolazzo, C. Raimondi, M. Mancini, S. Caponnetto, A. Gradilone, O. Gandini, M. Mastromartino, G. del Bene, A. Prete, F. Longo, E. Cortesi, and P. Gazzaniga, "Monitoring PD-L1 positive circulating tumor cells in non-small cell lung cancer patients treated with the PD-1 inhibitor Nivolumab," *Sci Rep*, vol. 6, no. 1, p. 2604, 2016.

[109] C.-Y. Yang, M.-W. Lin, Y.-L. Chang, C.-T. Wu, and P.-C. Yang, "Programmed cell death-ligand 1 expression in surgically resected stage I pulmonary adenocarcinoma and its correlation with driver mutations and clinical outcomes," *European Journal of Cancer*, vol. 50, no. 7, pp. 1361–1369, May 2014.

[110] W. A. Cooper, T. Tran, R. E. Vilain, J. Madore, C. I. Selinger, M. Kohonen-Corish, P. Yip, B. Yu, S. A. O'Toole, B. C. McCaughan, J. H. Yearley, L. G. Horvath, S. Kao, M. Boyer, and R. A. Scolyer, "PD-L1 expression is a favorable prognostic factor in early stage non-small cell carcinoma," *Lung Cancer*, vol. 89, no. 2, pp. 181–188, Aug. 2015.

[111] Y.-B. Chen, C.-Y. Mu, and J.-A. Huang, "Clinical significance of programmed death-1 ligand-1 expression in patients with non-small cell lung cancer: a 5-year-follow-up study.," *Tumori*, vol. 98, no. 6, pp. 751–755, Nov. 2012.

[112] H. M. Elzawahry, M. M. Saber, N. M. Mokhtar, A. A. Zeeneldin, Y. M. Ismail, and N. H. Alieldin, "Role of Ki67 in predicting resistance to adjuvant tamoxifen in postmenopausal breast cancer patients," *J Egypt Natl Canc Inst*, vol. 25, no. 4, pp. 181–191, Dec. 2013.

[113] H. Itamochi, J. Kigawa, and N. Terakawa, "Mechanisms of chemoresistance and poor prognosis in ovarian clear cell carcinoma," *Cancer Sci.*,vol. 99, no. 4, pp. 653–658, Apr. 2008.

[114] C. R. Lindsay, S. Le Moulec, F. Billiot, Y. Loriot, M. Ngo-Camus, P. Vielh, K. Fizazi, C. Massard, and F. Farace, "Vimentin and Ki67 expression in circulating tumour cells derived from castrate-resistant prostate cancer," vol. 16, no. 1, p. 518, Feb. 2016.

[115] A. Durrans, D. Gao, R. Gupta, K. R. Fischer, H. Choi, T. El Rayes, S. Ryu, A. Nasar, C. F. Spinelli, W. Andrews, O. Elemento, D. Nolan, B. Stiles, S. Rafii, N. Narula, R. Davuluri, N. K. Altorki, and V. Mittal, "Identification of Reprogrammed Myeloid Cell Transcriptomes in NSCLC," *PLoS ONE*, vol. 10, no. 6, p. e0129123, Jun. 2015.

[116] C.-Y. Liu, Y.-M. Wang, C.-L. Wang, P.-H. Feng, H.-W. Ko, Y.-H. Liu, Y.-C. Wu, Y. Chu, F.-T. Chung, C.-H. Kuo, K.-Y. Lee, S.-M. Lin, H.-C. Lin, C.-H. Wang, C.-T. Yu, and H.-P. Kuo, "Population alterations of l-arginase- and inducible nitric oxide synthase-expressed CD11b+/CD14−/CD15+/CD33+ myeloid-derived suppressor cells and CD8+ T lymphocytes in patients with advanced-stage non-small cell lung cancer," *J. Cancer Res. Clin. Oncol.*, vol. 136, no. 1, pp. 35–45, Jul. 2009.

[117] F. C. Bidard, F. Huguet, C. Louvet, L. Mineur, O. Bouche, B. Chibaudel, P. Artru, F. Desseigne, J. B. Bachet, C. Mathiot, J. Y. Pierga, and P. Hammel, "Circulating tumor cells in locally advanced pancreatic adenocarcinoma: the ancillary CirCe 07 study to the LAP 07 trial," *Ann Oncol*, vol. 24, no. 8, pp. 2057–2061, Jul. 2013.
[118] A. Ivashkevich, C. E. Redon, A. J. Nakamura, R. F. Martin, and O. A. Martin, "Use of the γ-H2AX assay to monitor DNA damage and repair in translational cancer research," *Cancer Letters*, vol. 327, no. 1, pp. 123–133, Dec. 2012.
[119] A. Avan, F. Crea, E. Paolicchi, N. Funel, E. Galvani, V. E. Marquez, R. J. Honeywell, R. Danesi, G. J. Peters, and E. Giovannetti, "Molecular Mechanisms Involved in the Synergistic Interaction of the EZH2 Inhibitor 3-Deazaneplanocin A with Gemcitabine in Pancreatic Cancer Cells," *Mol Cancer Ther*, vol. 11, no. 8, pp. 1735–1746, Aug. 2012.
[120] M. L. Brongersma, N. J. Halas, and P. Nordlander, "Plasmon-induced hot carrier science and technology," *Nat Nanotechnol*, vol. 10, no. 1, pp. 25–34, Jan. 2015.
[121] P. Paterlini-Brechot and N. L. Benali, "Circulating tumor cells (CTC) detection: Clinical impact and future directions," *Cancer Letters*, vol. 253, no. 2, pp. 180–204, Aug. 2007.
[122] C. Alix-Panabières and K. Pantel, "Challenges in circulating tumour cell research," *Nat. Rev. Cancer*, vol. 14, no. 9, pp. 623–631, Sep. 2014.
[123] Z. Zhang and S. Nagrath, "Microfluidics and cancer: are we there yet?," *Biomed Microdevices*, vol. 15, no. 4, pp. 595–609, 2013.
[124] L. Wang, W. Asghar, U. Demirci, and Y. Wan, "Nanostructured substrates for isolation of circulating tumor cells," *Nano Today*, vol. 8, no. 4, pp. 374–387, Aug. 2013.
[125] X. Sun, Z. Liu, K. Welsher, J. T. Robinson, A. Goodwin, S. Zaric, and H. Dai, "Nano-graphene oxide for cellular imaging and drug delivery," *Nano Res.*, vol. 1, no. 3, pp. 203–212, 2008.
[126] J. H. Jung, D. S. Cheon, F. Liu, K. B. Lee, and T. S. Seo, "A Graphene Oxide Based Immuno-biosensor for Pathogen Detection," *Angew. Chem. Int. Ed. Engl.*, vol. 49, no. 33, pp. 5708–5711, Aug. 2010.
[127] L. Feng, Y. Chen, J. Ren, and X. Qu, "A graphene functionalized electrochemical aptasensor for selective label-free detection of cancer cells," *Biomaterials*, vol. 32, no. 11, pp. 2930–2937, Apr. 2011.
[128] M. Nitschke, S. Gramm, T. Götze, M. Valtink, J. Drichel, B. Voit, K. Engelmann, and C. Werner, "Thermo-responsive poly(NiPAAm-co-DEGMA) substrates for gentle harvest of human corneal endothelial cell sheets," *Journal of Biomedical Materials Research Part A*, vol. 80, no. 4, pp. 1003–1010, Mar. 2007.
[129] R. A. Stile and K. E Healy, "Thermo-Responsive Peptide-Modified Hydrogels for Tissue Regeneration," *Biomacromolecules*, vol. 2, no. 1, pp. 185–194, Feb. 2001.
[130] D. Cunliffe, C. A. Smart, J. Tsibouklis, S. Young, C. Alexander, and E. N. Vulfson, "Bacterial adsorption to thermoresponsive polymer surfaces," *Biotechnology Letters*, vol. 22, no. 2, pp. 141–145, 2000.
[131] D. L. Huber, R. P. Manginell, M. A. Samara, B.-I. Kim, and B. C. Bunker, "Programmed Adsorption and Release of Proteins in a Microfluidic Device," *Science*, vol. 301, no. 5631, pp. 352–354, Jul. 2003.
[132] S. Hou, H. Zhao, L. Zhao, Q. Shen, K. S. Wei, D. Y. Suh, A. Nakao, M. A. Garcia, M. Song,

T. Lee, B. Xiong, S. C. Luo, H.-R. Tseng, and H. H. Yu, "Capture and Stimulated Release of Circulating Tumor Cells on Polymer-Grafted Silicon Nanostructures," *Advanced Materials*, vol. 25, no. 11, pp. 1547–1551, Mar. 2013.

[133] A. Hatch, G. Hansmann, and S. K. Murthy, "Engineered Alginate Hydrogels for Effective Microfluidic Capture and Release of Endothelial Progenitor Cells from Whole Blood," *Langmuir: the ACS journal of surfaces and colloids*, vol. 27, no. 7, pp. 4257–4264, Apr. 2011.

[134] A. M. Shah, M. Yu, Z. Nakamura, J. Ciciliano, M. Ulman, K. Kotz, S. L. Stott, S. Maheswaran, D. A. Haber, and M. Toner, "A Biopolymer System for Cell Recovery from Microfluidic Cell Capture Devices," *Anal. Chem.*, vol. 84, no. 8, pp. 3682–3688, Apr. 2012.

[135] H. Liu, X. Liu, J. Meng, P. Zhang, G. Yang, B. Su, K. Sun, L. Chen, D. Han, S. Wang, and L. Jiang, "Hydrophobic Interaction-Mediated Capture and Release of Cancer Cells on Thermoresponsive Nanostructured Surfaces," *Advanced Materials*, vol. 25, no. 6, pp. 922–927, Feb. 2013.

[136] T. K. Das and S. Prusty, "Graphene-Based Polymer Composites and Their Applications," *Polymer-Plastics Technology and Engineering*, vol. 52, no. 4, pp. 319–331, Feb. 2013.

[137] Q. Wu, Y. Xu, Z. Yao, A. Liu, and G. Shi, "Supercapacitors Based on Flexible Graphene/Polyaniline Nanofiber Composite Films," *ACS Nano*, vol. 4, no. 4, pp. 1963–1970, Mar. 2010.

[138] X. D. Zhuang, Y. Chen, G. Liu, P. P. Li, C. X. Zhu, E. T. Kang, K. G. Noeh, B. Zhang, J. H. Zhu, and Y. X. Li, "Conjugated-Polymer-Functionalized Graphene Oxide: Synthesis and Nonvolatile Rewritable Memory Effect," *Advanced Materials*, vol. 22, no. 15, pp. 1731–1735, Apr. 2010.

[139] N. G. Sahoo, H. Bao, Y. Pan, M. Pal, M. Kakran, H. K. F. Cheng, L. Li, and L. P. Tan, "Functionalized carbon nanomaterials as nanocarriers for loading and delivery of a poorly water-soluble anticancer drug: a comparative study," *Chemical Communications*, vol. 47, no. 18, pp. 5235–5237, 2011.

[140] H. Kim, R. Namgung, K. Singha, I.-K. Oh, and W. J. Kim, "Graphene Oxide–Polyethylenimine Nanoconstruct as a Gene Delivery Vector and Bioimaging Tool," *Bioconjugate Chem.*, vol. 22, no. 12, pp. 2558–2567, Nov. 2011.

[141] S. H. Hu, Y. W. Chen, W. T. Hung, I. W. Chen, and S. Y. Chen, "Quantum-Dot-Tagged Reduced Graphene Oxide Nanocomposites for Bright Fluorescence Bioimaging and Photothermal Therapy Monitored In Situ," *Advanced Materials*, vol. 24, no. 13, pp. 1748–1754, Apr. 2012.

[142] S. Kumar, S. Raj, E. Kolanthai, A. K. Sood, S. Sampath, and K. Chatterjee, "Chemical Functionalization of Graphene To Augment Stem Cell Osteogenesis and Inhibit Biofilm Formation on Polymer Composites for Orthopedic Applications," *ACS Appl. Mater. Interfaces*, vol. 7, no. 5, pp. 3237–3252, Jan. 2015.

[143] B. Chaudhuri, D. Bhadra, L. Moroni, and K. Pramanik, "Myoblast differentiation of human mesenchymal stem cells on graphene oxide and electrospun graphene oxide–polymer composite fibrous meshes: importance of graphene oxide conductivity and dielectric constant on their biocompatibility," *Biofabrication*, vol. 7, no. 1, p. 015009, Mar. 2015.

[144] S. Thampi, V. Muthuvijayan, and R. Parameswaran, "Mechanical characterization

of high-performance graphene oxide incorporated aligned fibroporous poly(carbonate urethane) membrane for potential biomedical applications," *Journal of Applied Polymer Science*, vol. 132, no. 16, 48109, Apr. 2015.

[145] H. R. Pant, P. Pokharel, M. K. Joshi, S. Adhikari, H. J. Kim, C. H. Park, and C. S. Kim, "Processing and characterization of electrospun graphene oxide/polyurethane composite nanofibers for stent coating," *Chemical Engineering Journal*, vol. 270, pp. 336–342, Jun. 2015.

[146] Yun Suk Jo, André J van der Vlies, Jay Gantz, Sasa Antonijevic, Davide Demurtas, A. Diana Velluto, Jeffrey A Hubbell, "RAFT Homo- and Copolymerization of N-Acryloyl-morpholine, Piperidine, and Azocane and Their Self-Assembled Structures," *Macromolecules*, vol. 41, no. 4, pp. 1140–1150, Feb. 2008.

[147] L. Zhang, L. D. Ridgway, M. D. Wetzel, J. Ngo, W. Yin, D. Kumar, J. C. Goodman, M. D. Groves, and D. Marchetti, "The Identification and Characterization of Breast Cancer CTCs Competent for Brain Metastasis," *Science Translational Medicine*, vol. 5, no. 180, pp. 180ra48–180ra48, Apr. 2013.

[148] G. Vona, A. Sabile, M. Louha, V. Sitruk, S. Romana, K. Schütze, F. Capron, D. Franco, M. Pazzagli, M. Vekemans, B. Lacour, C. Bréchot, and P. Paterlini-Brechot, "Isolation by Size of Epithelial Tumor Cells," *The American Journal of Pathology*, vol. 156, no. 1, pp. 57–63, Jan. 2000.

[149] A. H. Talasaz, A. A. Powell, D. E. Huber, J. G. Berbee, K.-H. Roh, W. Yu, W. Xiao, M. M. Davis, R. F. Pease, M. N. Mindrinos, S. S. Jeffrey, and R. W. Davis, "Isolating highly enriched populations of circulating epithelial cells and other rare cells from blood using a magnetic sweeper device.," *Proc. Natl. Acad. Sci. U.S.A.*, vol. 106, no. 10, pp. 3970–3975, Mar. 2009.

[150] C. Ruiz, J. Li, M. S. Luttgen, A. Kolatkar, J. T. Kendall, E. Flores, Z. Topp, W. E. Samlowski, E. McClay, K. Bethel, S. Ferrone, J. Hicks, and P. Kuhn, "Limited genomic heterogeneity of circulating melanoma cells in advanced stage patients," *Phys. Biol.*, vol. 12, no. 1, p. 016008, Feb. 2015.

[151] S. Riethdorf, H. Fritsche, V. Müller, T. Rau, C. Schindlbeck, B. Rack, W. Janni, C. Coith, K. Beck, F. Jänicke, S. Jackson, T. Gornet, M. Cristofanilli, and K. Pantel, "Detection of Circulating Tumor Cells in Peripheral Blood of Patients with Metastatic Breast Cancer: A Validation Study of the CellSearch System," *Clin Cancer Res*, vol. 13, no. 3, pp. 920–928, Feb. 2007.

[152] K. Hoshino, M. Taniguchi, T. Kitao, S. Morohashi, and T. Sasakura, "Preparation of a new thermo-responsive adsorbent with maltose as a ligand and its application to affinity precipitation," *Biotechnology and Bioengineering*, vol. 60, no. 5, pp. 568–579, Dec. 1998.

[153] Francesca Cecchet, Benoît De Meersman, Sophie Demoustier-Champagne, A. Bernard Nysten, and A. M. Jonas, "One Step Growth of Protein Antifouling Surfaces: Monolayers of Poly(ethylene oxide) (PEO) Derivatives on Oxidized and Hydrogen-Passivated Silicon Surfaces," *Langmuir*, vol. 22, no. 3, pp. 1173–1181, Jan. 2006.

[154] Y. Chang, S.-T. Yang, J.-H. Liu, E. Dong, Y. Wang, A. Cao, Y. Liu, and H. Wang, "In vitro toxicity evaluation of graphene oxide on A549 cells," *Toxicology Letters*, vol. 200, no. 3, pp. 201–210, Feb. 2011.

[155] S. Ithimakin, K. C. Day, F. Malik, Q. Zen, S. J. Dawsey, T. F. Bersano-Begey, A. A.

Quraishi, K. W. Ignatoski, S. Daignault, A. Davis, C. L. Hall, N. Palanisamy, A. N. Heath, N. Tawakkol, T. K. Luther, S. G. Clouthier, W. A. Chadwick, M. L. Day, C. G. Kleer, D. G. Thomas, D. F. Hayes, H. Korkaya, and M. S. Wicha, "HER2 Drives Luminal Breast Cancer Stem Cells in the Absence of HER2 Amplification: Implications for Efficacy of Adjuvant Trastuzumab," *Cancer Res*, vol. 73, no. 5, pp. 1635–1646, Mar. 2013.

[156] S. K. Arya, B. Lim, and A. R. A. Rahman, "Enrichment, detection and clinical significance of circulating tumor cells," *Lab on a Chip*, vol. 13, no. 11, pp. 1995–2027, 2013.

[157] W. Sheng, O. O. Ogunwobi, T. Chen, J. Zhang, T. J. George, C. Liu, and Z. H. Fan, "Capture, release and culture of circulating tumor cells from pancreatic cancer patients using an enhanced mixing chip," *Lab Chip*, vol. 14, no. 1, pp. 89–98, 2014.

[158] G. Simone, G. Perozziello, E. Battista, F. De Angelis, P. Candeloro, F. Gentile, N. Malara, A. Manz, E. Carbone, P. Netti, and E. Di Fabrizio, "Cell rolling and adhesion on surfaces in shear flow. A model for an antibody-based microfluidic screening system," *Microelectronic Engineering*, vol. 98, pp. 668–671, Oct. 2012.

[159] V. Murlidhar, L. Rivera-Báez, and S. Nagrath, "Affinity Versus Label-Free Isolation of Circulating Tumor Cells: Who Wins?," *Small*, vol. 12, no. 33, pp. 4450–4463, Sep. 2016.

[160] H. N. Tsao and K. Müllen, "Improving polymer transistor performance via morphology control.," *Chem Soc Rev*, vol. 39, no. 7, pp. 2372–2386, Jul. 2010.

[161] G. Bussetti, S. Trabattoni, S. Uttiya, A. Sassella, M. Riva, A. Picone, A. Brambilla, L. Duò, F. Ciccacci, and M. Finazzi, "Controlling drop-casting deposition of 2D Pt-octaethyl porphyrin layers on graphite," *Synthetic Metals*, vol. 195, pp. 201–207, Sep. 2014.

[162] K. Norrman, A. Ghanbari-Siahkali, and N. B. Larsen, "6 Studies of spin-coated polymer films," *Annu. Rep. Prog. Chem., Sect. C: Phys. Chem.*, vol. 101, no. 0, pp. 174–201, Oct. 2005.

[163] C. N. A. M. Oldenhuis, S. F. Oosting, J. A. Gietema, and E. G. E. de Vries, "Prognostic versus predictive value of biomarkers in oncology," *European Journal of Cancer*, vol. 44, no. 7, pp. 946–953, May 2008.

[164] X. Tong, L. Yang, J. C. Lang, M. Zborowski, and J. J. Chalmers, "Application of immunomagnetic cell enrichment in combination with RT-PCR for the detection of rare circulating head and neck tumor cells in human peripheral blood," *Cytometry Part B: Clinical Cytometry*, vol. 72, no. 5, pp. 310–323, Sep. 2007.

[165] E. Heitzer, M. Auer, C. Gasch, M. Pichler, P. Ulz, E. M. Hoffmann, S. Lax, J. Waldispuehl-Geigl, O. Mauermann, C. Lackner, G. Höfler, F. Eisner, H. Sill, H. Samonigg, K. Pantel, S. Riethdorf, T. Bauernhofer, J. B. Geigl, and M. R. Speicher, "Complex tumor genomes inferred from single circulating tumor cells by array-CGH and next-generation sequencing.," *Cancer Res*, vol. 73, no. 10, pp. 2965–2975, May 2013.

[166] D. Ramsköld, S. Luo, Y.-C. Wang, R. Li, Q. Deng, O. R. Faridani, G. A. Daniels, I. Khrebtukova, J. F. Loring, L. C. Laurent, G. P. Schroth, and R. Sandberg, "Full-length mRNA-Seq from single-cell levels of RNA and individual circulating tumor cells," *Nature Biotechnology*, vol. 30, no. 8, pp. 777–782, Aug. 2012.